MECHANISMS UNDERLYING DOPAMINERGIC MODULATION OF STRIATAL FIRING AND LEARNING

by

Sriraman Damodaran
A Dissertation
Submitted to the
Graduate Faculty
of
George Mason University
in Partial Fulfillment of
The Requirements for the Degree
of
Doctor of Philosophy
Neuroscience

Committee:

_____	Dr. Kim Blackwell, Dissertation Director
_____	Dr. Dietmar Plenz, Committee Member
_____	Dr. John R. Cressman, Committee Member
_____	Dr. Giorgio Ascoli, Committee Member
_____	Dr. Kenneth A. De Jong, Interim Director, Krasnow Institute for Advanced Studies
_____	Dr. Donna M. Fox, Associate Dean for Student and Academic Affairs, College of Science
_____	Dr. Peggy Agouris, Dean, College of Science

Date:_____ Spring Semester 2015
George Mason University
Fairfax, VA

Mechanisms Underlying Dopaminergic Modulation of Striatal Firing and Learning

A Dissertation submitted in partial fulfillment of the requirements for the degree of Doctor of Philosophy at George Mason University

by

Sriraman Damodaran
Bachelor of Science
Purdue University, 2007

Director: Kim Blackwell, Professor
Department of Neuroscience

Spring Semester 2015
George Mason University
Fairfax, VA

DEDICATION

To Amma, Appa, Rag and Aditi who always supported, Coby who kept me honest, and my thatha Dr. T. Rangarajan who set the example.

ACKNOWLEDGEMENTS

I would like to thank first and foremost my advisor Dr. Avrama Blackwell. You have always prioritized the growth and maturation of your students and lab members. You would rather be seen as a villain than have us repeat our mistakes. Your kindness and nurturing qualities are often taken for granted but I know that if not for your sincerity and honesty I would not have the confidence in my abilities and knowledge in neuroscience.

Many heartfelt thanks to my committee members Dr. Girogio Ascoli, Dr. Dietmar Plenz, and Dr. Rob Cressman for their invaluable advice, perspective, and support. I'd like to especially thank Dr. Ascoli, who has taught me valuable lessons about Science and ways in which we can be productive and useful to the scientific community.

I have also made some dear friends during my time in the CEN lab. I'd like to thank Sarah Hawes, Rebekah Evans, Rodrigo, Asia, Zbyszek and Andrew for their constant support. In particular, I would like to thank Sarah who has not only been a good friend but someone who through her hard work, perseverance and insights has repeatedly inspired me to dig a little deeper.

To my family and friends, your constant disappointment in me not having graduated after so many years has been as good a motivator as any. To Thatha, who has been the reason for many of the opportunities that my cousins and I take for granted. You have also been an incredible example of perseverance and will power to all in your family. To Rag, if not for your support throughout, especially when I broke my ankle and was broke, things would be very different. To my parents, who have only thought of what is best for my brother and me as long as I have known them. Even when they didn't understand why someone wouldn't just live comfortably as a rich engineer rather than living as a poor grad student they never wavered in their support. And finally to Dr. Coby Nordman, who allowed me to express in an unfiltered and crazed manner my passions in science, frustrations over inefficiencies and ideas about my scientific future in a way that no other person could have done. You helped make this process rich, fun, competitive and effortless.

TABLE OF CONTENTS

Page

List of Tables viviii

List of Figures ix

List of Abbreviations and Symbols x

Abstract xi

Chapter One: Striatal Cellular Models 1

- Striatum in Disease and Health 1
- Cell classes in the striatum 2
- Simple MSN Models 4
- Complex MSN Models 4
- Interneuron Models 6
- Striatal Network Models 8
- Conclusion 9
- Contributions 10

Chapter Two: Synchronized firing of fast-spining interneurons is critical to maintain balanced firing between direct and indirect pathway neurons of the striatum 11

- Abstract 11
- Introduction 12
- Materials and Methods 14
  - D1 and D2 MSN models 14
  - FSI network 15
  - Striatal network 16
  - Extrinsic Synaptic Input 17
  - Analysis of spikes 19
  - Electrophysiology for Model Tuning 20
- Results 21

Changes in channel properties between D1 and D2 MSNs are sufficient to reporoduce electrophysiological dichotomy 21
Network inhibition balances excitability between D1 and D2 MSNs 26
Inputs from FSIs are responsible for striatal balance 29
Synchronization of FSIs by gap junctions is critical for striatal balance 34
Direct modulation of intrinsic channels is sufficirnt to disrupt striatal balance 35
Discussion 38
FSI inhibition produces striatal balance by reducting D2 MSN activity 38
Desynchronization of FSIs is sufficient to distupt striatal balance 40
Functional Implications of Dopamine 42
Contributions 45
Chapter Three: Desychronization of fast spiking interneurons reduces β-band oscillations and imbalance in firing in the dopamine-depleted striatum 47
Abstract 47
Introduction 48
Materials and Methods 50
Striatal network 50
Intrinsic Synaptic Inputs. 51
Extrinsic Synaptic Input. 53
Dopamine depletion – Cellular changes. 54
Dopamine depletion – Circuit changes. 54
Analysis of spikes. 55
Results 57
Implementation of Dopamine Depletion changes. 58
Emergent β-band oscillations and striatal imbalance sensitive to level of cortical input correlation 61
Reduction of LI results in largest change in β-band power in response to high cortical input correlation 65
Blocking gap junctions restores MSN oscillations and firing during dopamine depletion. 68
Striatal network responds quickly to increases in cortical correlation 73
Discussion 74
Firing imbalance between D1 and D2 MSNs accompanies changes to β-band oscillations 74

Interneuron contribution to striatal β-band oscillations 75
Gap junctions as a target to restore basal ganglia oscillations and balance 77
Contributions 80
Chapter Four: Calcium dynamics predicts direction of synaptic plasticity in striatal spiny projection neurons 81
Introduction 81
Materials and Methods 82
MSN morphology. 83
Ionic channels. 83
Calcium dynamics. 84
Plasticity rule. 85
STDP protocols 86
Simulation 87
Results 87
Ca^{2+} transient activity replicates measurements in spines of MSNs. 89
Synaptic weight change in MSNs predicted by Ca^{2+} transient activity for several STDP paradigms 90
Sensitivity of calcium to spike timing. 94
Calcium-based rule not sufficient to explain all dopamine-depletion changes to cortico-striatal plasticity 97
Discussion 99
Amplitude, duration and location of calcium are critical 100
Interactions of Dopamine and Calcium in Synaptic Plaicity 101
Contributions 104
References 105

LIST OF TABLES

Table Page
Table 1 Computational Models of striatal neurons. 9
Table 2 Modulation of Channel Conductances. 24
Table 3 Differences between MSN-MSN and FSI-MSN synapse properties. 29
Table 4 Balance in firing for different network conditions. 61
Table 5 α-band power for different conditions. 71

LIST OF FIGURES

Figure Page
Figure 1 Differences in intrinsic channel properties are sufficient to describe the dichotomy in excitability between D1 and D2 MSNs 22
Figure 2 Model of striatal network with 1000 MSNs and 49 FSIs 25
Figure 3 Contribution of FSI-MSN and MSN-MSN synapses to striatal balance 30
Figure 4 Contributions of FSI-FSI interactions on balance of firing between D1 and D2 MSNs. 33
Figure 5 Effects of modulating channel properties and their interaction with inhibitory input on affecting striatal balance. 35
Figure 6 Summary of conditions that produce Parkinsonian imbalance and conditions that restore striatal balance 37
Figure 7 Differences in cellular and circuit properties between control and dopamine depletion conditions. 57
Figure 8 Emergence of β-band oscillations in dopamine-depleted striatal network model 60
Figure 9 Contribution of network, cell properties and GABAergic decay constant to power of β-band oscillations. 64
Figure 10 Blocking gap junctions compensates for weak decorrelation by LI during dopamine depletion. 67
Figure 11 Contribution of striatum to abnormal oscillatory activity experimentally observed in Parkinson's Disease. 72
Figure 12 Validation of calcium response in dendrite and dendritic spine 90
Figure 13 Calcium transients and plasticity rule in response to a single pairing of three different STDP protocols. 93
Figure 14 Two threshold plasticity rule and change in synaptic weight over time. 96
Figure 15 Contribution of NMDARs to corticostriatal STDP. 99
Figure 16 The effect of chronic dopamine depletion on calcium transients and on Synaptic weight. 100

LIST OF ABBREVIATIONS AND SYMBOLS

α-Amino-3-hydroxy-5-methyl-4-isoxazolepropionic acid ..... AMPA
Acetylcholinergic ..... ACh
Action potential ..... AP
AMPA receptor ..... AMPAR
Artificial cerebrospinal fluid ..... aCSF
current-frequency ..... IF
current-voltage IV
Delayed rectifying potassium channel ..... Kdr
Excitatory post-synaptic current ..... EPSC
Excitatory post-synaptic potential ..... EPSP
Fast potassium A channel ..... KaF
Fast sodium channel ..... NaF
Fast spiking interneuron ..... FSI
Gamma-aminobutyric acid ..... GABA
High frequency stimulation ..... HFS
Beta ..... β
Inhibitory post-synaptic potential ..... IPSP
Inwardly rectifying potassium channel ..... Kir
Long term depression ..... LTD
Long term potentiation ..... LTP
Low frequency stimulation ..... LFS
Low voltage activated ..... LVA
Medium spiny neuron ..... MSN
Micro ..... μ
N-methyl-D-aspartate ..... NMDA
NMDA receptor ..... NMDAR
Nucleus Accumbens ..... N. Acc.
Resistant persistent potassium channel ..... Krp
Slow potassium A channel ..... KaS
Small conductance potassium channel ..... SK
Spike timing dependent plasticity ..... STDP
Striatal enriched protein phosphatase ..... STEP
Timing dependent LTP ..... tLTP
Timing interval ..... Δt
Voltage gated calcium channel ..... VGCC

ABSTRACT

Mechanisms Underlying Dopaminergic Modulation of Striatal Firing and Learning

Sriraman Damodaran, Ph.D.

George Mason University, 2015

Dissertation Director: Dr. Kim Blackwell

This dissertation investigates the mechanisms underlying the changes in firing, oscillations and synaptic plasticity after dopamine depletion in order to identify potential therapeutic targets for Parkinson's disease. Dopamine depletion leads to an imbalance in the activation of the two classes of MSNs and aberrant oscillations in β-band frequencies observed in the basal ganglia output nuclei. Therefore, understanding the mechanisms underlying balanced firing in the control condition, and mechanisms controlling oscillations and synchrony in the dopamine depleted condition, can help us understand how to restore normal activity in Parkinson's disease. In order to investigate these mechanisms, we used a detailed computational model of striatal medium spiny neurons (MSN), and a striatal network model consisting of MSNs and fast spiking interneurons (FSI). I first investigate the mechanisms that modulate striatal firing by analyzing the firing frequency of direct (D1 MSN) and indirect (D2 MSN) pathway neurons in response to excitatory synaptic input in a network of 1049 neurons. I show that though

D2 MSNs are significantly more excitable than D1 MSN in response to current injection both neuron classes fire at similar frequencies in the network. Simulations also reveal that the synchronized firing of FSIs is critical in producing this balance and the removal of gap junctions between FSIs was sufficient to eliminate the balance in firing. I extend this work by investigating whether the striatum can be the source of the aberrant β-band oscillations observed in the basal ganglia output nuclei after dopamine depletion. I modeled the dopamine depleted striatal network by implementing changes to cellular and network properties that have been reported to occur after dopamine depletion. Simulations reveal that these changes are sufficient to produce increased β-band oscillations and imbalanced firing in the MSNs. Simulations also reveal that reducing the synchronicity between FSIs by blocking gap junctions is sufficient to restore oscillations and balance in firing in the dopamine depleted network to control levels. I then begin to investigate learning by the striatal network in response to realistic *in vivo* input by developing a calcium-based synaptic plasticity rule to investigate mechanisms whereby dopamine contributes to cortico-striatal plasticity. The plasticity rule is implemented in a MSN with sophisticated model of calcium diffusion, buffering, and pump extrusion, tuned to match experimentally reported post-synaptic calcium dynamics during timed plasticity protocols. Using this model I show that a calcium-based plasticity rule is sufficient to predict the direction of plasticity in both D1 and D2 MSNs in response to several different STDP protocols. In conclusion, this dissertation presents insights about striatal physiology that helps us better understand diseased states involving the basal ganglia, and that will potentially lead to novel therapeutic targets.

CHAPTER ONE: STRIATAL CELLULAR MODELS

Striatal Function in Disease and Health

The striatum is the main input structure of the Basal Ganglia, and is implicated in habit learning, addiction, and neuropathologies such as Parkinson's Disease and Huntington's Disease. Parkinson's Disease is a motor dysfunction caused by degeneration of dopaminergic neurons that project strongly to the striatum. Huntington's disease is another motor dysfunction caused by degeneration of a subset of the neurons in the striatum. Experiments in both humans and animals have demonstrated that normal habit learning involves the striatum, and in particular changes in striatal neural activity are observed consequent to cortical glutamatergic activity (in response to environmental stimuli or motor activity) and dopamine release in response to reward.

Motor dysfunction in Parkinson's disease is linked to aberrant oscillations in the globus pallidus (the output structure of the basal ganglia) and imbalanced activation of the direct and indirect pathways. The direct pathway is comprised of striatal medium spiny neurons (MSNs) that express dopamine D1 receptors (D1 MSNs) and projects to both the Substantia Nigra pars reticulata (SNr) and the internal segment of the globus pallidus. The indirect pathway is comprised of MSNs that express dopamine D2 receptors (D2 MSNs) and projects to the external segment of the globus pallidus. Studies report synchrony and oscillations within the cortex (Goldberg et al., 2002), the striatum (Courtemanche et al., 2003; Costa et al., 2006), and between the cortex and striatum

(Costa et al., 2006) following dopamine depletion. These observations are consistent with the hypothesis that the striatum is the source of the aberrant activity; however, the closed feedback loop of the basal ganglia could be generating striatal oscillations. The limited knowledge on how changes to the striatum propagate through the striatal circuit to produce oscillations and changes to firing is due to the technical difficulty in experimentally isolating the effects of different GABAergic inputs *in vivo*. Computational modeling can therefore provide key insights into striatal physiology that can potentially lead to new therapeutic targets for diseased states.

Several computational models of the striatal network with simple single neuron models (Alexander and Wickens, 1993; Humphries et al., 2009; Yim et al., 2011) have been developed to address some of these questions. Though these studies provide key insights to striatal physiology, the lack of detailed biophysics in the component single neuron models makes it difficult for these network models to provide experimentally testable predictions about key mechanisms underlying these diseases. Thus, large-scale network models need to include single neuron models with specific channels and synapses that can be experimentally targeted in experiments.

Cell classes in the striatum

The projection neurons of the striatum are the medium spiny neurons (MSNs) which make up the majority (90-95%) of the neurons. MSNs are further subdivided into two classes: those with dopamine D1 receptors, which co-release substance P and dynorphin, and those with dopamine D2 receptors, which co-release mu-opiods. Three other classes of interneurons have been extensively studied: the GABAergic fast spiking

interneurons (FSIs) which are connected by gap junctions, the GABergic neuropeptide Y positive (NPY) interneurons which also produce nitrous oxide, and the acetylcholinergic (ACh) interneurons, also called the tonically active neuron because of its spontaneous and regular firing pattern. More recently it has been possible to characterize a set of tyrosine hydroxylase expressing neurons using transgenic expression systems. These neurons exhibit four different firing patterns, but their role in striatal circuits remains to be elucidated. The GABAergic interneurons are in a position to modulate the timing and pattern of firing of the projection neurons of the striatum. In addition, their interconnections via both chemical and electrical synapses may play a role in synchronization. The acetylcholinergic neurons modulate dopamine release from the substantia nigra, and modulate striatal neuron properties through pre- and post-synaptic metabotropic receptors.

One of the compelling questions about striatal function is the role of the D1 versus D2 MSNs. The prevalent theory regarding Parkinson's disease is that dopamine increases excitability of D1 MSNs and decreases excitability of D2 MSNs. This leads to overactivity of the D2 MSNs which tend to inhibit motor movement. Thus, some striatal models have been developed to evaluate which characteristics of MSNs can explain the difference between D1 and D2 neurons and the effect of dopamine. Both neuron classes exhibit a characteristic bi-modal membrane potential distribution during anesthesia and sleep, known as up-states and down-states. Though the significance of this activity is still unclear, several models have investigated which neuron mechanisms underlie this activity. Both normal habit learning and the overly strong habit learning of drug addiction

likely involve synaptic plasticity of the MSNs, thus several models have investigated the control of calcium concentration during synaptic and neuronal activity, which are essential for synaptic plasticity.

Simple MSN Models

Some models contain only a subset of cellular components and attempt to reproduce a specific cellular phenomenon. The purpose of these types of models is to explain cellular behavior using the smallest possible subset of mechanisms. This has the dual advantage of minimizing the number of free parameters and also demonstrating that specific channels/interactions are required. It has the disadvantage of being unable to demonstrate possible alternative mechanisms which might explain the data just as well. An example of this approach is Gruber et al. (2003) which uses two potassium channels and one calcium channel to test whether the known effects of dopamine on these channels affects membrane bi-stability. Another model (Koos et al. 2004) represents the complete morphology, but contains no voltage-dependent channels. This model shows that morphological characteristics, such as electrotonic distance, can account for the difference in amplitude of inhibitory post-synaptic potentials (IPSPs) produced by FSIs compared to MSNs.

Complex MSN Models

Another class of striatal models includes the complex models. These contain a large number of cellular features, and attempt to reproduce many characteristics of voltage and/or calcium waveforms. The advantage of this approach is being able to isolate specific channels or morphological characteristics within the context of many

cellular characteristics to demonstrate the necessity or sufficiency of a mechanism in replicating an experimental finding. These models can often be re-used to explain new data with minimal change. The disadvantage of this approach is having numerous free parameters, and the complexity can sometimes hinder the ability to illuminate concepts.

The first complete MSN model (Wolf et al. 2005) used the NEURON simulation software to model a neuron from the ventral striatum (also called the nucleus accumbens). It contains two sodium channels, six potassium channels, and six calcium channels, as well as synaptic channels (NMDA, AMPA, GABA). This model replicates many of the characteristics of MSNs such as the long delay to action potential at rheobase and the low frequency of spiking. The model was used to test the effects of the NMDA/AMPA ratio on entrainment to oscillation (Wolf et al., 2005) and later to test the effects of dopamine modulation on synaptic integration (Moyer et al.2007). The inwardly rectifying potassium current (Kir) was re-tuned (Steephen and Manchanda, 2009) and implemented in this model to investigate the role of inactivating Kir in MSN excitability. This model was adapted by Spiga et al. (2010), who added morphology based on a digital reconstruction of an MSN and tested the effects of spine loss and AMPA current reduction on AP frequency during simulated upstates.

Several other complex models of dorsal striatal MSNs have been developed. A NEURON model MSN by (Gertler et al. 2008) has one sodium channel, one calcium channel, five potassium channels and synaptic channels (AMPA). The model was used to test the contribution of morphological differences between D1 and D2 MSNs in describing their different electrophysiological characteristics. This model was adapted by

(Plotkin et al. 2011) to test the ability of distal dendrites to evoke sustained somatic depolarizations. A similar model, by the same group (Day et al., 2008) was used to investigate the back propagation of the action potential into MSN dendrites.

Another NEURON model MSN by Flores-Barrera et al. (2009) has one sodium channel, two calcium channels, and five potassium channels as well as synaptic channels (NMDA,AMPA, GABA). This model is used to test whether GABAergic input, which is depolarizing below its reversal potential (roughly -60mV), plays a role in maintaining the depolarization of an MSN during a cortico-striatal upstate.

The most recent models (Evans et al., 2012, 2013) use the GENESIS simulation software to model a dorsal striatum MSN containing one sodium channel, six potassium channels, five calcium channels, and four different NMDA receptor types as well as AMPA receptors. This model is used to test whether the NMDA receptor subtypes, based on the four GluN2 subunits, differentially affect the calcium influx into spines during closely-timed pairings of pre and post-synaptic activity (spike timing dependent plasticity protocols).

Interneuron Models

Most striatal models focus on the spiny projection neurons, but there are several models of striatal interneurons.

The first complete model of a fast spiking interneuron (FSI) (Hellgren Kotaleski et al. 2006) contains three potassium channels, one sodium channel and synaptic channels (AMPA, GABA). This model replicated the observed spike latency and high firing frequency of striatal FSIs. This model was used to investigate how upstate firing of FSIs

is controlled by transient potassium currents and the contribution of these channels to enhancing signal detection. This model was further used to construct a network model (Hjorth et al. 2009) that investigated the contribution of gap junctions in FSI sensitivity to coincident input from the cortex. This network model was further modified and connected to a network of MSNs (Damodaran et al., 2014), to investigate the contribution of synchronized firing of FSIs on balanced firing between D1 and D2 MSNs in the striatum.

Several simple models of acetylcholinergic neurons (ACh) have been developed. The goal of most of these models is to explain mechanisms underlying the rhythmic firing and burst firing observed in these neurons. Two models demonstrate two different set of currents which can explain membrane potential oscillations in these models. The first model (Wilson 2005) demonstrates that Kir, HCN (Hyperpolarization-activated and cyclic nucleotide-gated channel) and leak conductance in a single compartment could explain membrane potential oscillations in the voltage range of -80 to – 60 mV. A second model investigates yet a different mechanism responsible for a slower time course of oscillations. This model (Wilson and Goldberg 2006) is implemented in XPPAUT and is also a single compartment. It contains an L type calcium channel, high voltage activated potassium channel, leak current, a calcium dependent potassium current, and calcium concentration calculated using a single time constant of decay. Simulations investigated why the slow afterhyperpolarization (sAHP) is activated by long depolarizations (even of small amplitude) but not activated by brief ones. Another model of ACh neurons (Goldberg et al., 2009) was used to investigate the role of calcium channel colocalization

in mediating slow and fast after hyperpolarizations. This model had a single electrical compartment that was subdivided into multiple concentric calcium compartments coupled by diffusion. Several calcium binding proteins enabled the model to demonstrate that the transient calcium influx produced by an action potential preferentially binds to SK channels, whereas the lower but more prolonged calcium influx produced by subthreshold depolarization preferentially binds to the slower, higher affinity binding proteins.

Striatal Network Models

Similar to the variation in single neuron models network models can also be differentiated based on the level of complexity, being largely dependent on the complexity of the single neurons used in the network. An example of a striatal network model with simple neurons is Humphries et al. (2009) that used Izhikevich neurons to show that, with realistic *in vivo* background input, small assemblies of synchronized MSNs spontaneously appear. The model contains 1400 neurons (1359 MSNs and 41 FSIs) and uses a detailed model of striatal anatomy.

The first complex striatal network model is a recent model that uses GENESIS simulation software to model a section of the dorsal striatum using detailed MSN (Evans et al., 2012) and FSI (Kotaleski et al., 2006; Hjorth et al., 2009) single neuron models and detailed striatal anatomy of both the MSN and FSI networks (Damodaran et al., In Press., 2014). These studies found that blocking gap junctions between fast-spiking interneurons after dopamine depletion was sufficient to restore striatal firing and oscillations to control levels. This striatal network model will be explained in detail in the next two chapters.

Conclusion

There are several models of striatal neurons that contain cellular detail. These models vary in complexity, morphology, and active channels. Each model is configured to test a specific aspect of striatal physiology as efficiently and accurately as possible, and therefore both the simple and the complex models are valuable. With the increasing power of computers and tools for parameter optimization, the accuracy and efficiency of complex models is likely to increase.

Table 1 Computational Models of striatal neurons

Citation	Cell type	Simple/complex	Software	Available modelDB
Gruber et al. 2003	MSN	Simple	NEURON	Yes
Moyer et al. 2007; Wolf et al. 2005	MSN, N. Acc.	Complex	NEURON	Yes
Steephen and Manchanda 2009	MSN, N. Acc.	Complex	NEURON	Yes
Spiga et al. 2010	MSN, N. Acc.	Complex	NEURON	Yes
Koos et al. 2004	MSN	Simple	NEURON	No
Gertler et al. 2008	MSN	Complex	NEURON	No
Day et al. 2008	MSN	Complex	NEURON	No
Flores-Barrera et al. 2009	MSN	Complex	NEURON	No
Evans et al. 2012	MSN	Complex	Genesis	Yes
Humphries et al., 2009	MSN, FSI	Simple	MATLAB	Yes
Damodaran et al. 2014	MSN, FSI	Complex	Genesis	Yes
Hellgren Kotaleski et al. 2006	FSI	Complex	Genesis	Yes
Wilson 2005	ACh	Simple	XPPAUT	No
Wilson and Goldberg 2006	ACh	Simple	XPPAUT	No
Goldberg et al. 2009	ACh	Simple	XPPAUT	No

Contributions

Wrote chapter: Sriraman Damodaran, Rebekah C. Evans, Kim T. Blackwell

Edited chapter: Sriraman Damodaran, Rebekah C. Evans, Kim T. Blackwell

Modified from:

Damodaran S, Evans RC, Blackwell KT (2013) Striatal models: Cellular Detail, *Encyclopedia of Computational Neuroscience*. *SpringerReference*. Eds. Dieter Jaeger and Ranu Jung.

CHAPTER TWO: SYNCHRONIZED FIRING OF FAST-SPIKING INTERNEURONS IS CRITICAL TO MAINTAIN BALANCED FIRING BETWEEN DIRECT AND INDIRECT PATHWAY NEURONS OF THE STRIATUM

Abstract

The inhibitory circuits of the striatum are known to be critical for motor function, yet their contributions to Parkinsonian motor deficits are not clear. Altered firing in the globus pallidus suggests that striatal medium spiny neurons (MSN) of the direct (D1 MSN) and indirect pathway (D2 MSN) are imbalanced during dopamine depletion. Both MSN classes receive inhibitory input from each other and from inhibitory interneurons within the striatum, specifically the fast-spiking interneurons (FSI). To investigate the role of inhibition in maintaining striatal balance, we developed a biologically-realistic striatal network model consisting of multi-compartmental neuron models: 500 D1 MSNs, 500 D2 MSNs and 49 FSIs. The D1 and D2 MSN models are differentiated based on published experiments of individual channel modulations by dopamine, with D2 MSNs being more excitable than D1 MSNs. Despite this difference in response to current injection, in the network D1 and D2 MSNs fire at similar frequencies in response to excitatory synaptic input. Simulations further reveal that inhibition from FSIs connected by gap junctions is critical to produce balanced firing. Though gap junctions produce only a small increase in synchronization between FSIs, removing these connections resulted in significant firing differences between D1 and D2 MSNs, and balanced firing

was restored by providing synchronized cortical input to the FSIs. Together these findings suggest that desynchronization of FSI firing is sufficient to alter balanced firing between D1 and D2 MSNs.

INTRODUCTION

Dopamine depletion leads to an imbalance in the activation of the direct and indirect pathways of the striatum (Albin et al., 1989; DeLong, 1990; Hikosaka et al., 2000; Obeso et al., 2004; Mallet et al., 2006). The direct pathway is comprised of striatal medium spiny neurons (MSNs) that express dopamine D1 receptors (D1 MSNs) and projects to both the Substantia Nigra pars reticulata (SNr) and the internal segment of the globus pallidus. The indirect pathway is comprised of MSNs that express dopamine D2 receptors (D2 MSNs) and projects to the external segment of the globus pallidus. The two populations of MSNs differ in their intrinsic excitability with D2 MSNs more responsive to somatic current injection (Gertler et al., 2008b). Inhibitory circuits of the striatal network, including feedback inhibition from other MSNs and feedforward inhibition from fast-spiking interneurons (FSIs), modulate this excitability (Koós and Tepper, 1999; Plenz, 2003). The contributions of these circuits to maintaining balanced firing between D1 and D2 MSNs in the network (Mallet et al., 2006; Cui et al., 2013) are not clear.

A strong source of GABAergic inhibition to MSNs is feedforward inhibition from the parvalbumin-positive (PV+) fast-spiking interneurons (Koós and Tepper, 1999). FSIs receive convergent input from multiple cortical regions (Ramanathan et al., 2002) and are interconnected by gap junctions that increase synchronicity of FSI firing (Traub et al.,

2001; Hjorth et al., 2009b). Each FSI in turn projects to over 100 MSNs (Kita et al., 1990; Bennett and Bolam, 1994) and therefore synchronous activation of FSIs can have wide-spread effects. Dopamine depletion reduces the immediate-early gene response of PV+ neurons in the striatum (Trevitt et al., 2005) and therefore loss of dopamine might release MSNs from normal FSI inhibition, thus affecting the activation of the direct and indirect pathways. The effect of synchronicity of FSI firing, specifically the modulation of gap junctions, on MSN output and its contribution to striatal balance is not known.

Another source of GABAergic inhibition to MSNs is feedback inhibition from other MSNs. One of the differences between MSN and FSI input to MSNs is in their strength of inhibition (Koós and Tepper, 1999). Multiple factors contribute to this difference in strength, including the increased level of synchronization between FSIs, and the more proximal distribution of FSI synapses. Since it is difficult to investigate the effects of MSN inhibition experimentally, a realistic network model of the striatum is a plausible alternative approach.

In this paper, a computational model of the striatal network, consisting of multi-compartmental models of 1000 MSNs and 49 FSIs, was used to identify the inhibitory mechanisms critical for striatal balance. Simulation experiments show that network interactions produced balanced firing, which is disrupted with selective removal of FSI input but not with removal of MSN input. The balancing effect of FSI inhibition is disrupted when gap junctions between FSIs are removed, suggesting that the base level of synchronization that these connections provide could be critical for FSIs to balance striatal firing.

MATERIALS AND METHODS

Ethics Statement

All animal handling and procedures were in accordance with the National Institutes of Health animal welfare guidelines and were approved by the George Mason University institutional animal care and use committee (IACUC).

D1 and D2 MSN models

D1 and D2 MSN models were generated by modifying a previously published MSN model (Evans et al., 2012b). The morphology of both MSN models was the same as this previous model except with the spines removed (to improve computational efficiency), and consisted of 189-compartments with 4 primary dendrites which divide into 8 secondary and then 16 tertiary dendrites. Each primary dendrite was 20 μm long, secondary dendrites were 24 μm and tertiary dendrites were comprised of 11 compartments, each 36 μm long. The kinetics of the channels included in the model were identical to the previous model (Evans et al., 2012b). D1 and D2 MSN models were created by changing the maximal conductance of intrinsic and synaptic channels from values used for our previous MSN model (Table 2), based on experimental data measuring the effect of D1 or D2 receptor agonists, as summarized in (Nicola et al., 2000; Moyer et al., 2007b). The maximal conductances of the AMPA and NMDA receptors of both MSN classes were additionally adjusted to maintain the NMDA/AMPA ratio of 2.75/1 measured in cortico-striatal terminals from dorsal striatum of adult animals (Ding et al., 2008), as used previously (Evans et al., 2012b). Note that this value is

considerably greater than the NMDA/AMPA ratio measured in the striatum from other striatal regions (ventral -0.22; Popescu et al., 2007) or from younger animals (~1.0; Logan et al., 2007).

For simulations that investigate the contribution of morphology differences between D1 and D2 MSNs in explaining differences in excitability, the number of primary dendrites for D1 MSNs was increased from 4 to 6 based on reconstructions of these neurons (Gertler et al., 2008b). The intrinsic channel properties of both MSN classes were set to match those of a D2 MSN for these simulations since this produced F-I curves that matched experimental results most accurately.

FSI network

A previously published FSI network model was used (Hjorth et al., 2009b) and extended to include chemical synapses, as seen experimentally (Gittis et al., 2010). Each FSI in this network consisted of 127 compartments with a soma and 2 primary dendrites, which divide into 4 secondary and 8 tertiary dendrites. The channels incorporated in this model included a fast-sodium channel (NaF), Kv3.1, Kv1.3 and an A-type (transient) potassium channel (KA)(Kotaleski et al., 2006b). The gap junction connections between the FSIs were modeled as resistive elements between the primary dendrites, with a conductance of 0.5nS, coupling coefficient of 25% and probability of gap junction connection between nearby FSIs of 0.3 (Koós and Tepper, 1999; Galarreta and Hestrin, 2002; Hjorth et al., 2009b). Chemical synapses were GABAergic, chloride permeable channels (rise time constant, 1.33 ms; decay time constant, 4 ms; reversal potential, -60 mV; maximal conductance, 1 nS; (Gittis et al., 2010)). The probability of chemical synapse connection

between FSIs was 0.58 (Gittis et al., 2010) and was independent of the probability of gap junction connection.

Striatal network

The striatal network consisted of 1000 MSNs (500 D1 MSNs and 500 D2 MSNs) and 49 FSIs (Fig 2A). The MSN:FSI ratio was based on experimental observations; each MSN receives input from 55% of nearby striatal FSIs (Tecuapetla et al., 2007), and between 4-27 converge on the same MSN (Koós and Tepper, 1999). Based on these estimates the 49 neuron FSI network corresponded to the FSI network seen by 1000 postsynaptic MSNs. Though the percentage of FSIs is slightly larger than observed experimentally, a smaller number of FSIs would have incorrectly produced homogenous FSI input to each MSN in the network model. A heterogeneous network of neurons was generated by changing the A-type (transient) potassium channel conductance (both MSNs and FSIs) and NMDA channel conductance (MSN only) by $\pm$10%. The range of activity of MSNs used in the network, in response to current injections, was within the range of experimentally observed responses (Fig 2B; electrophysiology methods described below). The distance between each MSN soma in the model was 25 μm both in the x-axis and the y-axis based on experimental observations (Tunstall et al., 2002), resulting in a 775x775 μm^2 grid**.** At each grid location, the assignment of either D1 or D2 MSNs was random with probability=0.5.

The probabilities of connection of MSN-MSN and FSI-MSN synapses were modeled using a distance-based exponential function, tuned to match experimentally

observed probabilities of connections (Plenz, 2003; Taverna et al., 2008; Gittis et al., 2010; Planert et al., 2010):

$P(x) = e^{\frac{-((x_2-x_1)^2+(y_2-y_1)^2)}{f}}$ where f=95 μm^2. FSIs were connected to MSNs with GABAergic synapses (rise time constant, 0.25ms; decay time constant, 3.65ms; reversal potential, -60mV; maximal conductance, 8.4nS; (Gittis et al., 2010)) whereas the GABAergic synapses between MSNs had a maximal conductance of 0.75 nS with the same rise and decay times (Koos et al., 2004b). Note that GABAergic synapses in MSNs are depolarizing due to the hyperpolarized (-80 to -90 mV) resting membrane potential of mature MSNs (Wilson and Kawaguchi, 1996), coupled with GABA responses which reverse between -60 and -50 mV (Kita, 1996; Tunstall et al., 2002; Mercuri et al., 1991). The FSI-MSN synapses also were more proximal than MSN-MSN synapses (Oorschot et al., 2010). The probability and strength of connection of MSN-MSN and FSI-MSN synapses in the network model were independent of the type of pre- or post- synaptic MSN (Planert et al., 2010). The transmission delays were distance-based using a conduction velocity of 0.8 m/s for both FSI and MSN synapses (Wilson, 1986; Wilson et al., 1990; Tepper and Lee, 2007).

Extrinsic Synaptic Input

Excitatory input to the striatum comes primarily from the cortex and thalamus. We simulated this glutamatergic input as Poisson distributed spike trains with a minimum time between spikes of 100 μs. Both MSN classes in this model have 360 AMPA and NMDA synapses and 227 GABA synapses. Note that each Poisson train represents activity from more than one cortical neuron, and each synapse represents the population

of synapses in a single isopotential compartment. Thus the 100 μs minimum interspike interval is to prevent more than 1 spike per time step to each MSN. Each synaptic channel in the MSN model receives an input of 10 Hz during the upstate which results in a total input of ~ 800 synaptic inputs per second and 1/20 of this input during down states (Blackwell et al., 2003). Each FSI model has 127 AMPA synapses and 93 GABA synapses, resulting in a total AMPA input of 282 Hz and GABA input of 207 Hz when 2 Hz input is provided to each synapse (Kotaleski et al., 2006b). To introduce correlations within both the MSN and FSI input, each spike from the set of spike trains was assigned to more than one synapse, with probability P=1/n, where $n = N - \sqrt{c(N-1)}$, N=number of synapses, and c=0.5 (Hjorth et al., 2009b). For each neuron, starting from a single mother spike train per neuron, spike trains for each synapse were created by assigning the spike to that synapse if a uniform random number was greater than P. This produced a mean number of synapses activated by each spike of 1.4 for the control simulations. To introduce between-neuron input correlation, an additional shared set of input spikes was generated. The between-neuron input correlation was then adjusted by changing the fraction of input each neuron received from this shared pool (as opposed to the spike trains that were unique to each neuron). Unless otherwise stated, 30% of all excitatory synaptic input to either the FSI or MSN populations was shared; with FSIs and MSNs each having their own sets of shared inputs. This base level of between-neuron correlation was incorporated based on studies that report correlation among the cortical input to the striatum (Krüger and Aiple, 1988; Ts'o and Gilbert, 1988; Stern et al., 1998). For the case where synchronized cortical input was provided to FSIs to compensate for

lack of gap junctions, the correlation value was doubled for FSI inputs only.

The model was implemented in GENESIS (Bower and Beeman, 2007) and simulations used a time step of 100 μs. The simulation time was 2 seconds with five 0.2 s duration upstates separated by 0.2 s duration downstates. Each upstate used a different set of cortical input spikes and thus was an independent observation of the network response. Each network simulation experiment took three weeks to run. The cortico-striatal Poisson spike trains were generated using MATLAB (version 2007b, MathWorks). The simulation and output processing software along with the files used for the simulations are freely available from the authors' website (http://krasnow.gmu.edu/CENlab/) and modelDB (http://senselab.med.yale.edu/ModelDB/)

Analysis of spikes

Mean firing frequency during upstates was plotted by averaging across neurons of the same class using 10 ms time bins. The firing frequency was expressed as mean $\pm$ S.D of values obtained from five different upstates. To investigate the contribution of gap junctions on synchronization, cross-correlograms were constructed for each directly coupled neuron pair in the FSI network, and then averaged over the network (Hjorth et al., 2009b). Cross-correlograms also were constructed for directly coupled MSN pairs. Correlation was corrected for firing frequency by subtracting the shuffled cross-correlograms for the same network condition. Statistical analyses were performed using SAS. When only two groups were being compared, the procedure TTEST was used. When more than two groups were compared, one-way analysis of variance was

performed using the GLM procedure with network condition as the independent variable and difference between D1 and D2 MSN frequencies as the dependent variable. Each of the five upstates was considered as an independent replication and $p<0.05$ was considered significant. Post-hoc analyses used Bonferonni correction for multiple comparisons with $p<0.01$ considered significant.

Electrophysiology for Model Tuning

Patch clamp recordings were performed to obtain a range of responses of MSNs to somatic current injection (Fig 1B). C57B6 male and female mice (at least 20 days old) were anesthetized with isoflurane and decapitated. Brains were quickly extracted and placed in oxygenated ice-cold slicing solution (in mM: KCL 2.8, Dextrose 10, $NaHCO_3$ 26.2, NaH_2PO_4 1.25, $CaCl_2$ 0.5, Mg_2SO_4 7, Sucrose 210). Hemicoronal slices from both hemispheres were cut 350 µm thick using a vibratome (Leica VT 1000S). Slices were immediately placed in an incubation chamber containing artificial cerebrospinal fluid (aCSF) (in mM: NaCl 126, NaH_2PO_4 1.25, KCl 2.8, $CaCl_2$ 2, Mg_2SO_4 1, $NaHCO_3$ 26.2, Dextrose 11) for 30 minutes at 33°C, then removed to room temperature (21-24°C) for at least 90 more minutes before use.

A single hemislice was transferred to a submersion recording chamber (ALA Science) gravity-perfused with oxygenated aCSF containing 50 µM picrotoxin. Temperature was maintained at 30-32°C (ALA Science) and was monitored with an external thermister. Whole cell patch clamp recordings were obtained from neurons under visual guidance using infrared differential interference contrast imaging (Zeiss Axioskop2 FS plus). Pipettes were pulled from borosilicate glass on a laser pipette puller

(Sutter P-2000) and fire-polished (Narishige MF-830) to a resistance of 3-7 MΩ. Pipettes were filled with a potassium based internal solution (in mM: K-gluconate 132, KCl 10, NaCl 8, HEPES 10, Mg-ATP 3.56, Na-GTP 0.38, EGTA 0.1, Biocytin 0.77) for all recordings. Intracellular signals were collected in current clamp and filtered at 3 kHz using an Axoclamp2B amplifier (Axon instruments), and sampled at 10-20 kHz using an ITC-16 (Instrutech) and Pulse v8.80 (HEKA Electronik). Series resistance (6-30 MΩ) was manually compensated.

RESULTS

Changes in channel properties between D1 and D2 MSNs are sufficient to reproduce electrophysiological dichotomy

Development of a network model of D1 and D2 MSNs required single neuron models which have similar intrinsic excitability to that seen experimentally (Gertler et al., 2008b). Differences in morphology or intrinsic channel properties (Nicola et al., 2000; Moyer et al., 2007b) have been proposed to explain the observation that D2 MSNs are more excitable than D1 MSNs (Kreitzer and Malenka, 2007; Gertler et al., 2008b). We simulated the response to current injection in D1 and D2 MSNs created two different ways, and compared these responses to experimental measurements.

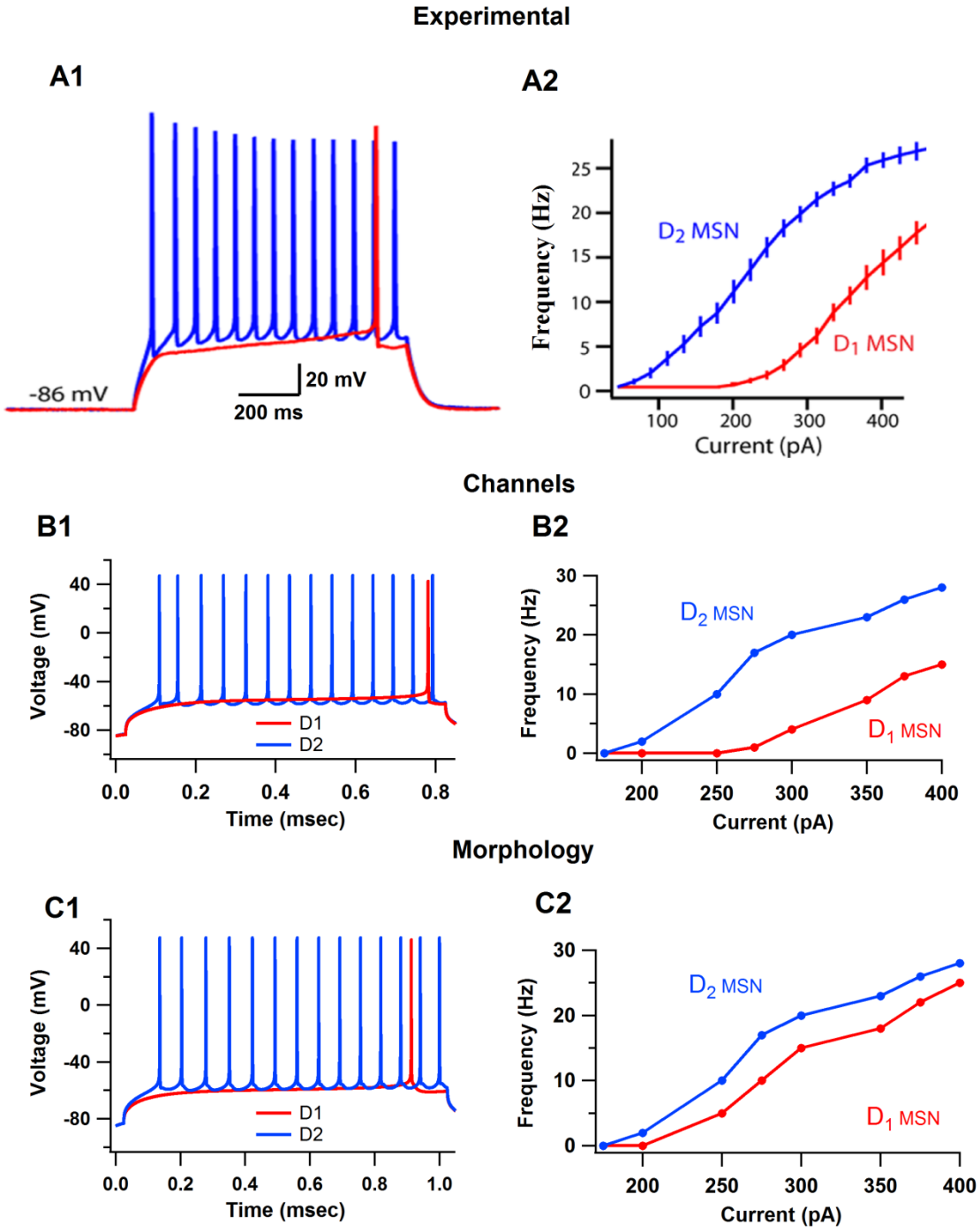
Experimental
A1
A2
-86 mV
20 mV
200 ms
Frequency (Hz)
D2 MSN
D1 MSN
Current (pA)
Channels
B1
B2
Voltage (mV)
D1
D2
Time (msec)
Frequency (Hz)
D2 MSN
D1 MSN
Current (pA)
Morphology
C1
C2
Voltage (mV)
D1
D2
Time (msec)
Frequency (Hz)
D2 MSN
D1 MSN
Current (pA)

Figure 1. **Differences in intrinsic channel properties are sufficient to describe the dichotomy in excitability between D1 and D2 MSNs.**
A. Experimental observations of responses of D1 and D2 MSNs to current injection. Adopted from (Gertler et al., 2008b) with permission from the authors and Journal of Neuroscience. **A1.** D1 MSNs have significantly higher rheobase current (median, 270 pA, n=35) than D2 MSNs (median, 130pA, n=31). **A2.** F-I plot of D1 and D2 MSNs demonstrate higher intrinsic excitability in D2 MSNs. **B.** Models of D1 and D2 MSNs constructed with differences in intrinsic excitability reproduce electrophysiological dichotomy. The intrinsic channels with different properties are the L-type calcium channels, fast-sodium channels, A-type potassium channels and inward-rectifying potassium channels. **B1.** D1 and D2 MSN models have rheobase current of 275 pA and 155pA**,** respectively. **B2.** F-I plot of these models reproduce experimentally observed differences in spiking activity. **C.** Simulations suggest that models of D1 and D2 MSNs differentiated based solely on morphological differences do not replicate dichotomy in spiking activity. **C1.** D1 MSN models constructed with six primary dendrites and D2 MSN models constructed with four primary dendrites have rheobase currents of 210 pA and 160 pA, respectively. **C2.** The F-I plot of these MSN models does not replicate the dichotomy of D1 and D2 MSN excitability seen experimentally.

We first evaluated whether the larger number of primary dendrites in D1 MSNs (Gertler et al., 2008b) could explain the difference in D1 and D2 MSN excitability. The morphology of both MSN classes was modeled the same except for the number of primary dendrites, with the D1 MSNs having six and the D2 MSNs having four (Gertler et al., 2008b). The intrinsic channel properties were the same between both MSN models (see Methods). In response to current injection, the D1 MSN model had significantly greater rheobase current than the D2 MSN model (D1 MSN, 210 pA; D2 MSN, 160 pA; Fig 1C1). These results match experimental observations (Fig 1A; Gertler et al., 2008)**.** However, the shape of the F-I curve **(**Fig 1C2**)** did not match experiments and thus spiking activity differences were not accurately modeled by morphological differences alone.

Since anatomical differences were not sufficient to accurately describe electrophysiological differences between the D1 and D2 MSNs, the contribution of intrinsic channel differences alone in describing the excitability difference was investigated. The morphology of both neuron models was made the same, with each

MSN model containing four primary dendrites. The channel properties were changed based on studies that measured the effects of D1 and D2 agonists on intrinsic and synaptic channels of both types of MSNs (Table 2) (Nicola et al., 2000; Moyer et al., 2007b). The differences between D1 and D2 MSN excitability in response to current injection, including the F-I curve, were replicated using these MSN models (Fig 1B). The rheobase current for D1 MSNs was 275pA and for D2 MSNs was 155pA. Intrinsic channel differences between D1 and D2 MSNs were thus sufficient to describe the dichotomy between D1 and D2 MSN spiking activity. This suggests that differences in excitability between D1 and D2 MSNs measured in identified neurons may be due to basal levels of dopamine present in the slice. These models (same morphology, differences in channels) were used for the remainder of the study.

Table 2: Modulation of Channel Conductances

Channels	D1	D2
Fast Sodium Channel (NaF)	95	110
Slow A-type Potassium Channel (KAs)	No Change	110
Inward-rectifying Potassium channel (KIR)	125	No Change
L-type Calcium (CaL1.2)	200	No Change
L-type Calcium (CaL1.3)	No Change	75
NMDA (synaptic)	130	No Change
AMPA (synaptic)	No Change	80

Numbers represent % of the conductance value reported in Evans et al. (2012).

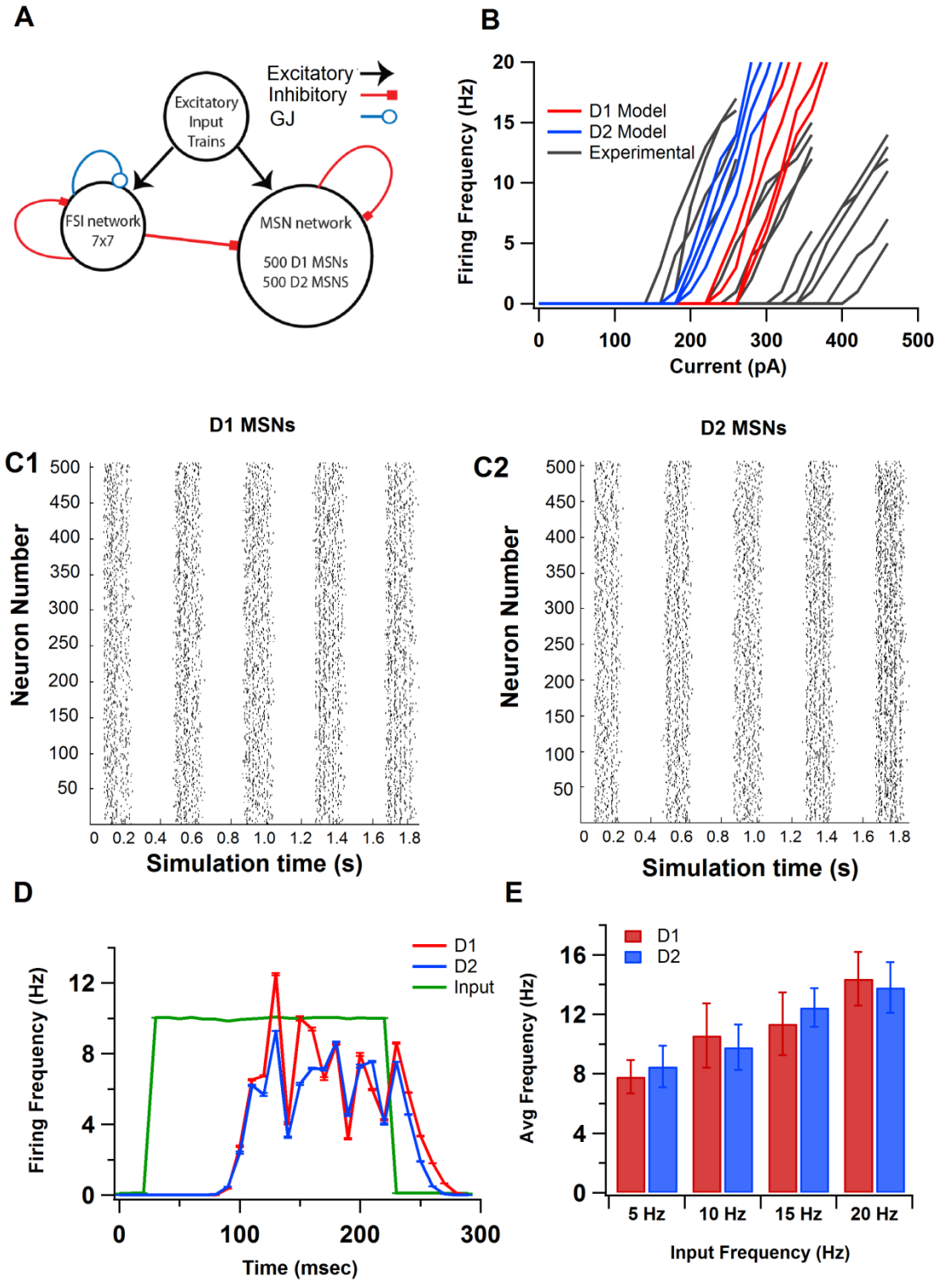
A
Excitatory
Inhibitory
GJ
Excitatory Input Trains
FSI network 7x7
MSN network
500 D1 MSNs
500 D2 MSNS
B
Firing Frequency (Hz)
D1 Model
D2 Model
Experimental
Current (pA)
C1
D1 MSNs
Neuron Number
Simulation time (s)
C2
D2 MSNs
Neuron Number
Simulation time (s)
D
Firing Frequency (Hz)
D1
D2
Input
Time (msec)
E
Avg Frequency (Hz)
D1
D2
5 Hz
10 Hz
15 Hz
20 Hz
Input Frequency (Hz)

Figure 2. **Model of striatal network with 1000 MSNs and 49 FSIs.**
A. Schematic of network model with MSNs receiving inhibitory input from FSIs and other MSNs. Roughly equal numbers of D1 and D2 MSNs are randomly distributed on a regular grid. FSIs receive input from other FSIs through both GABAergic synapses and gap junction (GJ) connections. Excitatory input to both MSNs and FSIs is provided by simulated Poisson trains. **B.** Heterogeneous distribution of MSNs was generated by changing A-type potassium channel and NMDA channel conductances by ±10%. The range of responses of these D1 and D2 MSN model neurons to somatic current injection was within the range of responses seen experimentally. **C.** Raster plots of D1 (**C1**) and D2 (**C2**) MSNs in response to synaptic input in the striatal network. **D.** Firing frequencies of D1 and D2 MSN populations during the upstate, calculated from rasters in (**C**) by averaging across the neurons within a class and across upstates. Excitatory synaptic input (green) is illustrated to show latency of MSN firing with respect to input. Both MSN classes have similar firing frequencies (D1 MSNs: 10.77±0.60 Hz; D2 MSNs: 9.59± 0.13 Hz). **E.** D1 and D2 MSNs have balanced firing frequencies across a range of cortical input frequencies.

Network inhibition balances excitability between D1 and D2 MSNs

In order to investigate the mechanisms that balance activation of the direct and indirect pathways, a striatal network model was developed. We used 500 each of the D1 and D2 MSN models, together with 49 FSIs to create the network **(**Fig 2A**)**. A heterogeneous network of these neurons was created using small random changes (within ±10% of original value) in A-type potassium channel and NMDA channel conductance, and this produced a range in rheobase current comparable to that observed experimental on unidentified MSNs (Fig 2B). The probability of connections between MSNs was determined using an exponential distance-based function that matched the probabilities and strength of connections seen experimentally (see Methods; Koós and Tepper, 1999; Taverna et al., 2008). The probability of FSI-MSN connections also was described using the exponential distance-based function, but these connections were made stronger and more proximal than the MSN inputs (Gittis et al., 2010; Planert et al., 2010). The network (MSNs and FSIs) was activated with excitatory input from Poisson trains that represented cortical input and simulated up and down states **(**Fig 2C**),** as seen in organotypic co-cultures and in anesthetized animals. For the simulations that explored single neuron differences, that were described in the previous section, synaptic channels were not

included; however, for all network simulations, the synaptic channels of the MSN classes differed between D1 and D2 models as measured experimentally in response to dopamine agonists (Table 1; Nicola et al., 2000).

Figure 2D shows the firing rates of D1 and D2 MSNs, averaged across neurons and upstates, in response to cortical input and network inhibition. Both MSN classes had similar firing rates when connected in this network (D1 MSN: 10.77$\pm$2.16 Hz; D2 MSN: 9.59$\pm$1.53 Hz), representing balanced firing. These results, that D1 and D2 MSNs fire at similar frequencies in the network, is consistent with two *in vivo* studies: one in anesthetized rats (Mallet et al., 2006), and another in awake behaving mice where spike frequencies were measured between tasks (Cui et al., 2013). Therefore, the imbalance in D1 and D2 MSN firing rates in response to current injection is overcome in the presence of synaptic excitation and inhibition in the network. This balanced firing was observed for a range of cortical input frequencies (Fig 2E).

Two different variations on inhibitory connectivity were evaluated to verify that the balanced network output does not depend on the specific connectivity results implemented. Some studies have reported slight imbalances in connectivity between D1 and D2 MSNs (Tunstall et al., 2002; Taverna et al., 2008), specifically the higher occurrence of presynaptic D2 MSNs as compared to presynaptic D1 MSNs (Taverna et al., 2008). In order to confirm that the balanced network output was independent of these changes to MSN-MSN connectivity, simulations were repeated in a network with a higher probability of connection from presynaptic D2 MSNs (twice that of presynaptic D1 MSNs), and with stronger connections from presynaptic D2 MSNs (double the

strength of connections from presynaptic D1 MSNs). This did not produce significant differences in the firing rates of either MSN class nor in the balance produced in the network between the two MSN classes (D1 MSN: 11.66±3.36 Hz; D2 MSN: 10.06±3.12 Hz; p=0.153). Another possible variation in network connectivity is based on differences in connectivity between FSIs and MSNs. Experimental studies have reported both similar (Planert et al., 2010) and different probabilities of connections (Gittis et al., 2010) from FSI input to the two MSN classes. To confirm that the function of FSI-MSN synapses in balancing firing is independent of differences in connectivity, simulations were repeated with FSI connections to D1 MSNs 15% higher than FSI connections to D2 MSNs (Gittis et al., 2010). These changes did not produce significant changes in the firing rates of either MSN class in the intact network and was similar to that seen in the control condition (D1 MSNs: 10.16±2.35 Hz; D2 MSNs: 9.72±1.31 Hz; p=0.204). This suggests that the effects of FSI inhibition to striatal balance are independent of slight differences in connectivity from FSIs to the two MSN classes.

In order for network inhibition to balance firing, the intrinsic channels of the MSNs had to be differentially modulated between the MSN classes. When the differential intrinsic excitability of MSNs was produced through a difference in morphology alone (e.g. Fig 1C), the two MSN classes were imbalanced even in the presence of network inhibition and differences in synaptic channels (D1 MSN: 2.82±0.12 Hz, D2 MSN: 11.65±0.18 Hz; p<0.01). The network also was imbalanced in the presence of synaptic modulation (Table 2) but not intrinsic channel modulation (D1 MSN: 4.84±1.73 Hz; D2 MSN: 14.35±3.61 Hz). This suggests that intrinsic channel differences might allow D1

and D2 MSNs to be influenced differently by network inhibition. The interaction between network inhibition and intrinsic channels was investigated later in the study.

Table 3: Differences between MSN-MSN and FSI-MSN synapse properties

Synapse property	MSN-MSN	FSI-MSN
GABA g_{max}	0.75 nS	8.4 nS
Latency to fire (observed)	75 ms	10 ms
Distribution	Distal	Proximal

Inputs from FSIs are responsible for striatal balance

The contributions of the two main inhibitory circuits of the striatum to balanced MSN firing were studied next. These circuits are the local feedforward inhibition from FSIs to MSNs and the more numerous but weaker feedback inhibitory connections from MSNs to other MSNs. The differences in properties of MSN-MSN and FSI-MSN connections in our model are listed in Table 3. Both types of synaptic inhibition were removed separately to observe their specific roles on MSN firing. Since MSN-MSN synapses were more widespread, two approaches were used to investigate the effect of their removal. In one simulation, removal of MSN-MSN synapses was followed by a replacement of ~30% of those GABAergic inputs with Poisson distributed input trains that had the same latency and frequency of MSN inputs as seen during the control condition. This was done to maintain the same number of GABAergic input as the FSI removal condition and to

prevent a large increase in overall MSN firing from masking the specific effects that feedback inhibition had on the two MSN classes.

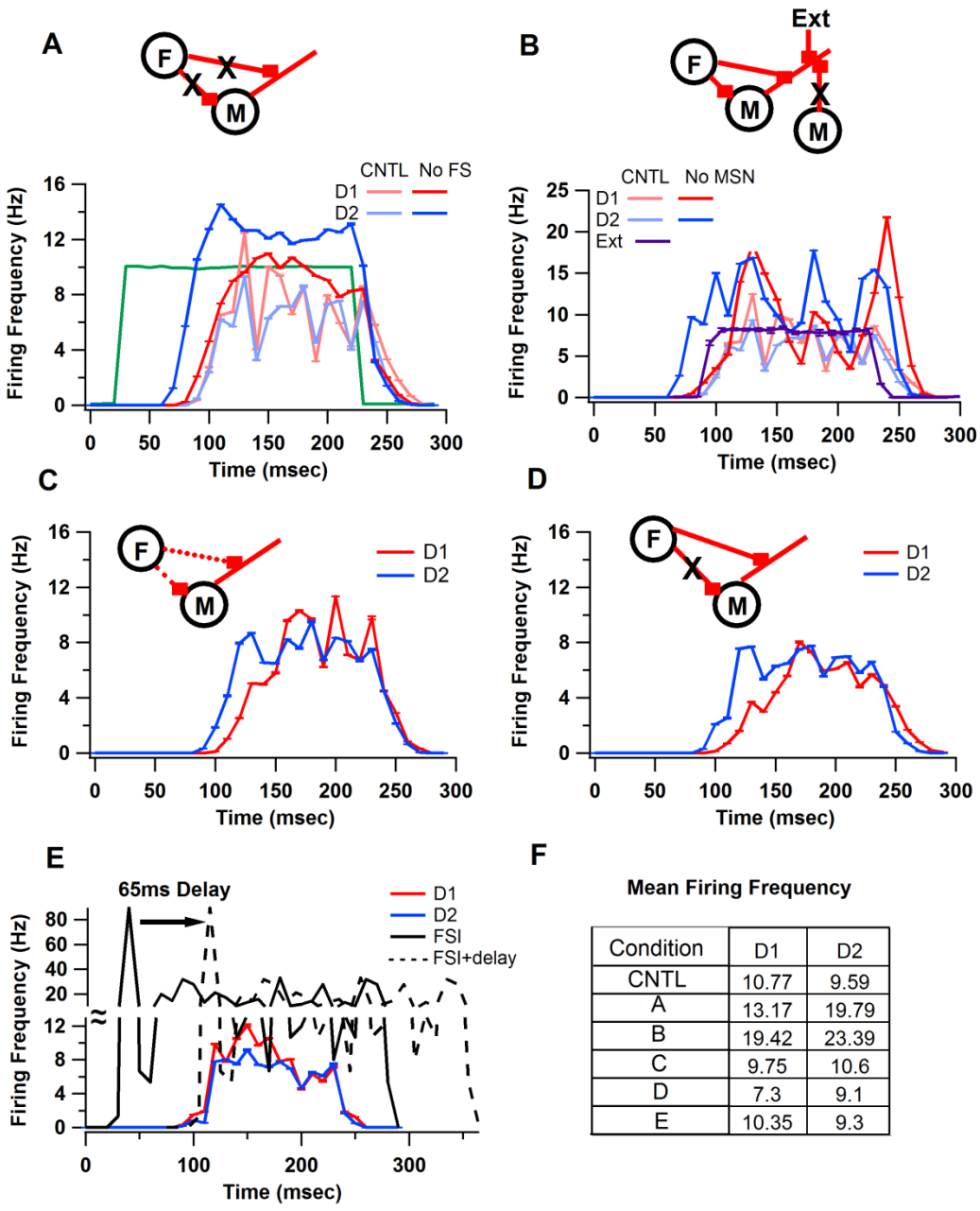

Condition	D1	D2
CNTL	10.77	9.59
A	13.17	19.79
B	19.42	23.39
C	9.75	10.6
D	7.3	9.1
E	10.35	9.3

Figure 3. Contribution of FSI-MSN and MSN-MSN synapses to striatal balance.
A. Removing FSI inhibition (F) to MSNs introduces a 40% imbalance in firing between D1 and D2 MSNs. **B.** Removing MSN-MSN synapses (M) and replacing those GABAergic synapses with extrinsic input trains (Ext) that keep the overall inhibition similar to control level results in a large increase in firing frequency, but only 18%

difference between D1 and D2 MSN firing frequencies. **C.** Reducing the weight (dashed lines) of FSI-MSN synapses to the level of MSN-MSN synapses (8.4 nS to 0.75nS) produced slight changes (9%) to firing differences between D1 and D2 MSNs. **D.** Removing proximal FSI-MSN synapses and making FSI-MSN synapses as distal as MSN-MSN synapses also did not disrupt balance of firing. **E.** A delay of 65ms was added to FSI-MSN synaptic connections to identify the contribution of early FSI firing on disrupting balance in firing. This resulted in a 10% difference in firing between the MSN classes. All percent differences are calculated as difference divided by mean. **F.** Table of mean firing frequencies and % differences between D1 and D2 MSNs for the control condition and for the conditions represented by the respective panels.

Simulations revealed that FSIs are more significant for balanced firing than MSNs. Removing FSI-MSN input resulted in increased firing in both MSNs but produced even higher firing frequencies in D2 MSNs as compared to D1 MSNs **(**D1:13.17$\pm$5.96 Hz; D2:19.79$\pm$5.31 Hz**;** Fig 3A).

In contrast to FSI removal, replacing the feedback inputs between MSNs produced a smaller change in the balance of firing between D1 and D2 MSNs (18% vs 40% during FSI block) despite a greater overall increase in firing frequency (Fig 3B;D1:19.42$\pm$3.99 Hz; D2:23.29$\pm$3.36 Hz). Removing MSN-MSN synapses but not replacing any of those inputs with Poisson trains also produced the same effect; i.e., a smaller change in the balance of firing between the two MSN classes as compared to FSI removal (D1:26.91$\pm$3.93 Hz; D2:23.98$\pm$3.78 Hz). GLM reveals that the differences in D1 and D2 MSN firing for the control (fully intact network), no FSI-MSN and no MSN-MSN groups were significantly different from each other ($F(3,19)=109.24$, $p<0.05$). Post-hoc tests (Bonferroni correction for paired comparisons) show that difference in firing for FSI-MSN removal > difference for MSN replacement ~= difference for MSN removal > control ($p<0.01$). These results suggest that FSI inhibition is more important for producing balanced firing than is MSN inhibition.

To identify the properties of FSI-MSN synaptic connections that elicit differential responses from D1 and D2 MSNs, simulations were repeated with each property (conductance, proximity, latency) individually changed to match that of MSN-MSN synapses (see Table 3). FSI-MSN synapses with the conductance of MSN-MSN synapses produced a slight imbalance, but only during the beginning of the upstate, with the D2 MSNs firing more than the D1 MSNs (Fig 3C). A lack of proximal FSI-MSN synapses also produced a slight imbalance in the beginning of the upstate, again with the D2 MSNs firing more than the D1 MSNs (Fig 3D). Removing early FSI inhibition (adding a latency in FSI firing such that synaptic input from FSI arrives at a similar time as synaptic input from MSNs) did not produce any significant difference in striatal balance during the entire upstate (Fig 3E). GLM shows that all of these groups are significantly different from the no FSI-MSN group ($F(3,19)=751.56$, $p<0.05$). In summary, an isolated modulation of any one of these properties was not sufficient to reproduce the imbalance seen during the FSI block condition.

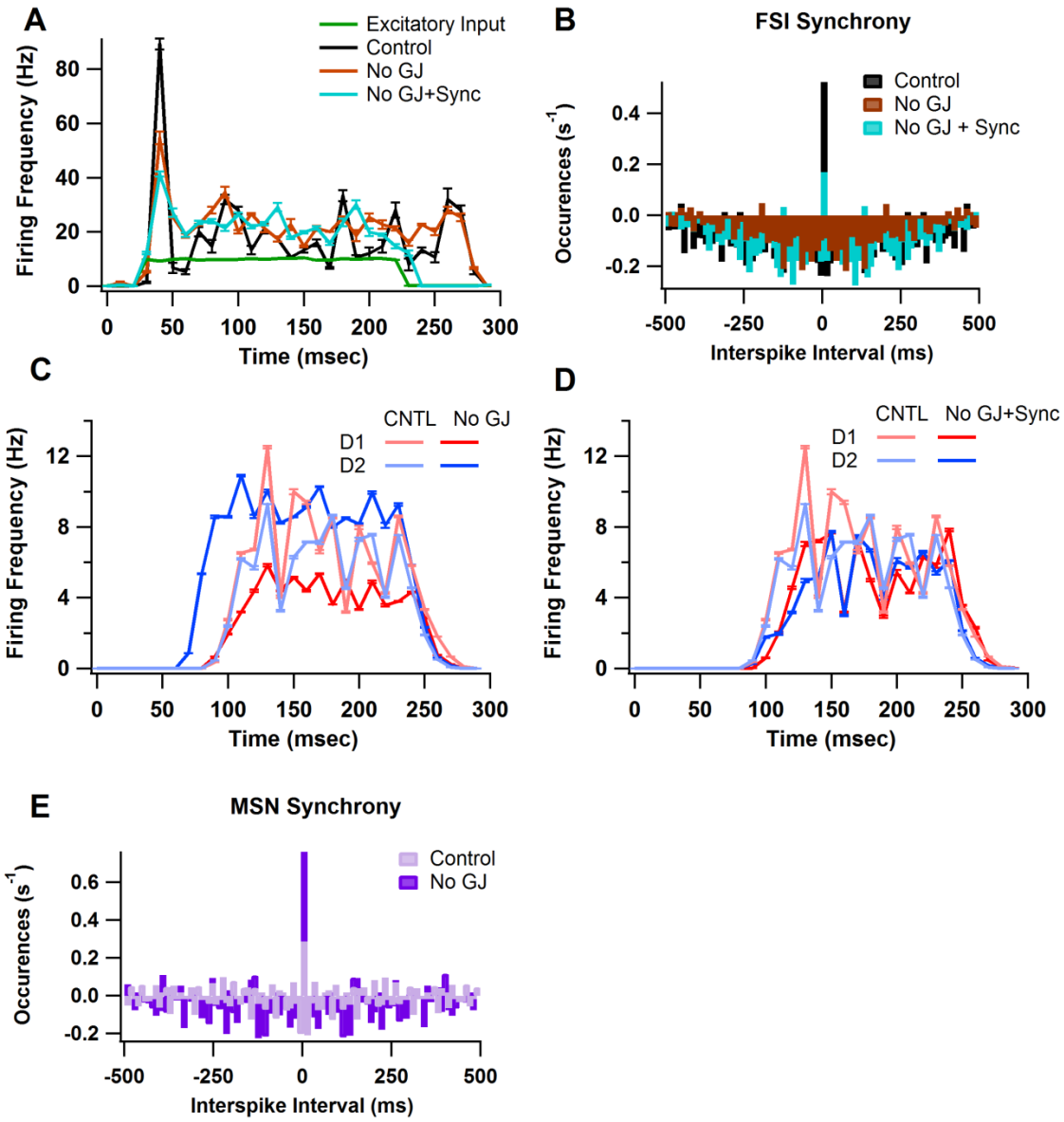

Figure 4. Contributions of FSI-FSI interactions on balance of firing between D1 and D2 MSNs.
A. The mean firing frequency of FSIs is minimally affected by gap junction inputs from other FSIs. Removal of gap junctions (GJ) results in slightly higher firing of the FSIs. Providing synchronous cortical input to FSIs when gap junctions are removed does not produce significant changes to FSI firing frequencies. **B.** Cross correlograms of FSIs during the same conditions as in A show that GJ removal decreases synchrony, and synchronous input restores synchrony though not quite to the same level seen in the intact network. Note that synchrony is calculated between connected FSIs (Hjorth et al., 2009b). Cross-correlogram between non-connected FSIs reveals no synchrony (data not shown). Inset shows cross-correlograms over entire simulation period, and depicts slight oscillatory behavior. **C.** Firing frequencies of D1 and D2 MSNs when gap junctions between FSIs are removed. D2 MSNs fire at a significantly higher frequency as compared to D1 MSNs. **D.** Balance in firing is restored when synchronous cortical input is provided to FSIs during gap junction block. **E**. Cross correlograms of MSNs during control and No FSI conditions. In addition to leading to disruption of balance between D1 and D2 MSN firing, removing FSI results in decreased overall synchrony between MSNs. Inset shows cross-correlogram over entire simulation period.

Synchronization of FSIs by gap junctions is critical for striatal balance

The contribution of FSI-FSI interactions to the balance of firing between D1 and D2 MSNs was investigated next. The FSIs are connected by GABAergic synapses (1 nS; connection probability of 0.58; (Gittis et al., 2010)) and gap junctions (0.5 nS, connection probability of 0.3; (Koós and Tepper, 1999)). Removing the GABAergic synapses did not cause a significant change to overall firing of FSIs (CNTL: 16.89±1.68 Hz; No GABA: 16.45±1.51 Hz; p=0.703) or to the balance in firing between the two MSN classes (D1:10.86±2.75 Hz; D2:9.96±1.812 Hz, p=0.303**)**. In contrast, removing gap junctions induced a differential responses from D1 and D2 MSNs (D1:6.55±1.61 Hz; D2:15.02±3.93 Hz; p<0.01;Fig4C), despite producing a non-significant change in FSI firing frequency (CNTL:16.89±1.68 Hz; No Gap:17.58±1.32Hz; p=0.161; Fig 4A). To confirm that the imbalance was not due to the slight increase in FSI firing, simulations were repeated in the absence of gap junctions with either a weaker cortical input (lower frequencies), or synchronous cortical input (see Methods) to FSIs. Weaker cortical input restored FSI firing to the level that occurs in the presence of gap junctions, but did not restore the balance between D1 and D2 MSN firing (D1:5.14±1.51 Hz; D2:13.82±4.43 Hz)**.** Synchronization of cortical input to FSIs with no gap junctions increased the level of synchronization between FSIs towards the level seen in the intact network (~30% of control; Fig 4B). This increase in synchronization was sufficient to restore the balance between D1 and D2 MSN firing (D1:7.99±1.82 Hz; D2:7.79±1.55 Hz; Fig 4D**)**. Removing FSIs lead to a reduction in overall synchrony of MSNs, suggesting that FSIs possibly modulate MSN synchrony in addition to affecting MSN balance (Fig 4E). GLM

reveals that the differences in D1 and D2 MSN firing for the control, no gap junctions, no gap junctions + weak input, and no gap junctions + synchrony groups were significantly different ($F(3,19)=439.33$, $p<0.05$). Post-hoc tests confirmed that no gap junctions + synchrony did not differ from the control ($P=0.653$), and that both of these cases differed from the other two no gap junctions groups ($p<0.01$). Collectively, these simulations show that input to MSNs from FSIs, which are weakly synchronized by gap junctions, produces balanced firing between D1 and D2 MSNs.

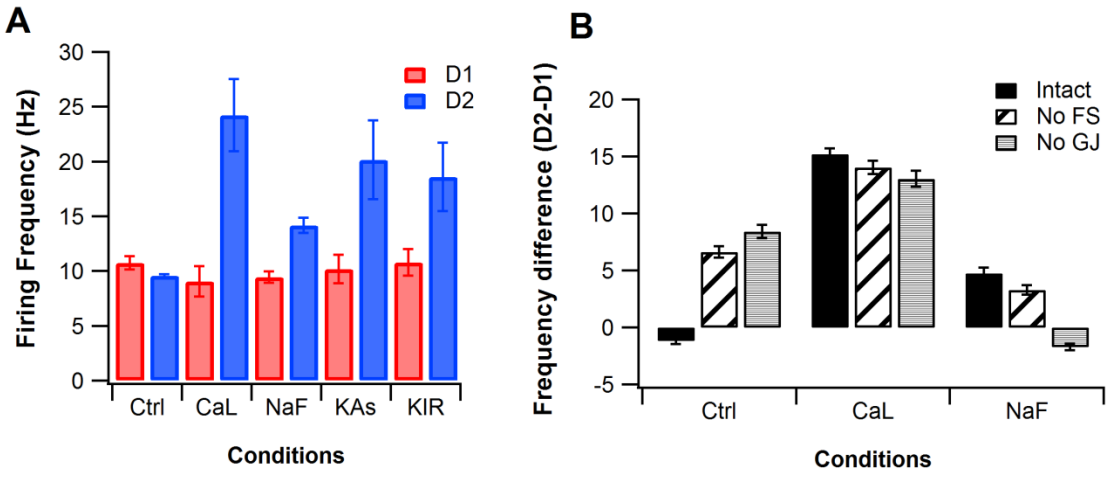

Figure 5. Effects of modulating channel properties and their interaction with inhibitory input on affecting striatal balance.
A. Equalizing CaL, NaF, KAs or KIR produces imbalance between D1 and D2 MSN firing ($p<0.01$ for all conditions). **B.** When CaL or KAs/KIR (data not shown) conductances are equalized between D1 and D2 MSNs, removing FSIs or gap junctions do not affect the imbalance in firing. When NaF properties are equalized, removing gap junctions no longer produces the significant difference in firing between the two MSN classes, restoring balance in firing between D1 and D2 MSNs.

Direct modulation of intrinsic channels is sufficient to disrupt striatal balance

Given that differences in intrinsic channels are required to produce both the observed F-I curves and balanced firing, we investigated the contribution of individual channel

differences between MSN classes on maintaining striatal balance in the intact network. Channel differences were eliminated by changing the maximal conductance of the channels in the D2 MSN to be identical to that of the D1 MSN for four channels: L-type calcium channels (CaL), fast-sodium channels (NaF), inward-rectifying potassium channels (KIR), and slowly inactivating A-type potassium channels (KAs) (Table 2). Removing the differences in conductance of any one of these channels, by setting the D2 conductance equal that of the D1 conductance, was sufficient to produce differential firing between D1 and D2 MSNs, with D2 MSNs firing more than D1 MSNs (Fig 5A; $F(4,24)=210.49$, $p<0.05$). The most profound effect was seen when CaL was made the same between D1 and D2 MSNs, possibly due to the bigger difference in conductance of these channels as compared to the other channels. To further investigate the role of CaL, simulations were repeated with CaL blocked in both D1 and D2 MSNs. Removal of CaL from both MSN classes did indeed disrupt striatal balance in the striatal network mode l (D1:3.7$\pm$1.82 Hz; D2:21.2$\pm$4.25 Hz**)**, which is consistent with a recent *in vitro* study that showed blocking CaL produced imbalanced firing between D1 and D2 MSNs (Flores-Barrera et al., 2011).

The intrinsic channel differences that interact with correlated FSI input in balancing MSN firing were investigated next. Simulations revealed that when the differences of each of CaL (Fig 5B), KAs and KIR were removed in the absence of FSI-MSN synapses or gap junctions, the imbalance was no greater than the effect of removing intrinsic channel differences alone. Curiously, equalizing NaF channels eliminated the difference in firing between D1 and D2 MSNs produced by gap junction removal (Fig

5B). The difference in firing during this condition (NaF equal+ No gap junctions) was significantly different from either No gap junctions or equal NaF alone ($F(2,24)=618.34$, $p<0.05$). This suggests that NaF differences might be critical in allowing differential sensitivity of D1 and D2 MSNs to synchronous inhibitory input.

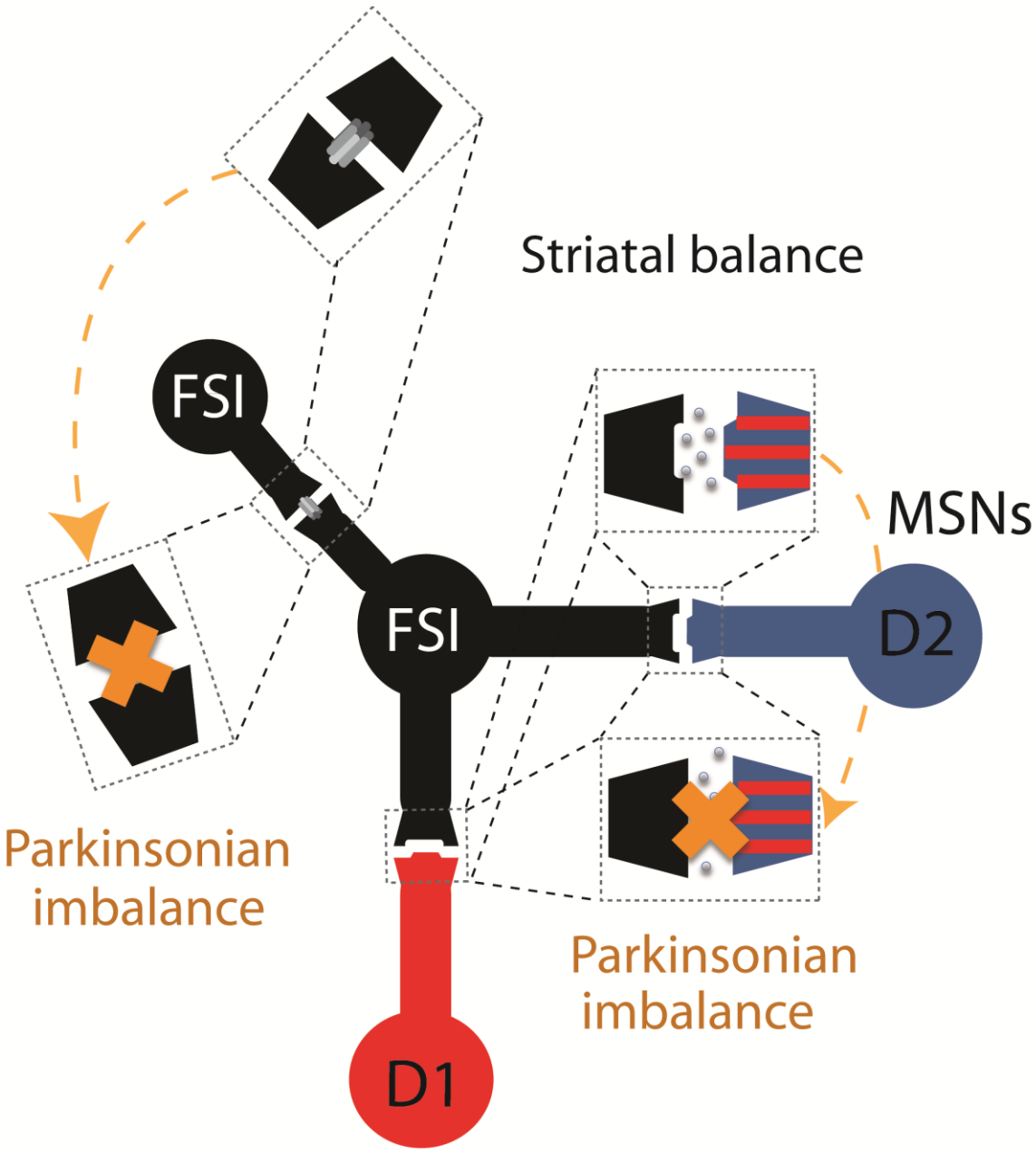

Figure 6. Summary of conditions that produce Parkinsonian imbalance and conditions that restore striatal balance.
This schematic shows the nature of connections between FSI and MSNs and between MSNs, and the effect of removing these connections. When input from FSIs (black) to D1 (red) and D2 (blue) MSNs is removed, D2 MSNs fire more than D1 MSNs. When gap junctions between FSIs are removed D2 MSNs again fire at higher frequencies as compared to D1 MSNs. These two cases have been labeled as Parkinsonian Imbalance. In the latter case, balance is restored when the synchronicity of FSIs is increased by alternative means such as providing highly correlated cortical input to the FSIs. Making NaF the same between D1 and D2 MSNs also restores balance during gap junction block. The network output seen in the control network where the connections are intact is labeled as Striatal balance. Glutamatergic input to both FSIs and MSNs, along with feedback connections between MSNs have been omitted from the schematic to highlight the effect of FSI-MSN connections on striatal balance.

DISCUSSION

Recent studies have evaluated the contributions of differential cortical input (Mallet et al., 2006) and direct channel modulations (Flores-Barrera et al., 2011) on disrupting the balance in firing between D1 and D2 MSNs in the striatum. However, the role of striatal inhibitory circuits in modulating striatal balance is not clear. We constructed a striatal network model of MSNs and FSIs to identify the inhibitory circuits that modulate MSN excitability differently between the two classes. The model was based on a previously published FSI network model (Hjorth et al., 2009b) and MSN single neuron model (Evans et al., 2012b). We found that removing FSI inhibition or reducing the correlation between FSI action potentials by blocking gap junctions produced imbalanced firing between D1 and D2 MSNs (Fig 6). Additionally, intrinsic and synaptic channels of MSNs interact with these inhibitory mechanisms to modulate differences in firing between the two MSN classes.

FSI inhibition produces striatal balance by reducing D2 MSN activity

In our striatal network model, feedforward inhibition from FSIs was found to inhibit D2 MSNs more than D1 MSNs. Since D2 MSNs have a higher intrinsic excitability, the increased inhibition by FSIs brings the level of D2 MSN firing down to that of D1 MSNs. The striatal network model by Humphries et al. (2009) that uses Izhikevich neurons suggests that removing FSIs might alternatively lead to a decrease in overall MSN firing. In their network model they use an FSI-MSN conductance five times stronger than their MSN-MSN conductance. This ratio, lower than that used in our network model, combined with the somatic location of all their MSN synapses, implies that removing FSI synapses eliminates a much smaller fraction of the total inhibitory synaptic current than in our model. Our FSI-MSN:MSN-MSN conductance ratio was estimated based on a recent experimental paper that uses transgenic mice (Gittis et al., 2010) that suggests that the FSI-MSN conductance is closer to 8 nS, which is the value used in this paper.

Selective inhibition of FSIs in the striatum recently was shown to produce dyskinesia in mice (Gittis et al., 2011b) and a mixed effect on MSN firing, with 54% of MSNs having increased firing rates and 38% having reduced firing rates. This is consistent with our results that show that the two populations of MSNs have disparate responses to FSI removal. Though that experimental study did not record from identified D1 and D2 MSNs, our simulations predict that the recorded neurons with reduced firing were D1 MSNs and the neurons with increased firing were D2 MSNs. In that study, block of FSIs produced dyskinesia, and not the hypokinesia typically observed with excess D2 MSN firing (Kravitz et al., 2010), which suggests that the most significant behavioral effect of FSI block may be caused by changes in MSN synchrony, and not an

imbalance in firing. Alternatively, dyskinesia may be caused by changes in synchrony interacting with the modest imbalances in firing produced by selective block of FSI activity, as opposed to the strong imbalance and synchronous firing produced by optogenetic stimulation of D2 MSNs. This hypothesis is consistent with our finding, that removing FSI inhibition results in a reduction in overall MSN synchrony and an imbalance in firing between the two MSN classes.

Though inhibition from FSIs and MSNs constitute a critical part of inhibitory input to MSNs, they are not the only sources of inhibition. MSNs receive inhibitory input from other interneurons in the striatum and also from GABAergic projection neurons in the globus pallidus (Mallet et al., 2008, 2012a), that innervate both MSNs and interneurons. The contributions of these other inhibitory sources to MSN balance must also be explored to form a complete picture of the contribution of inhibitory input on striatal balance.

Desynchronization of FSIs is sufficient to disrupt striatal balance

Reducing the correlation between FSIs by removing gap junctions disrupts the balance in firing between the D1 and D2 MSNs. The strength of FSI inhibition is modulated by the presence of gap junctions that reduce the number of FSI action potentials and increase the level of synchronization between the FSIs (Traub et al., 2001; Hjorth et al., 2009b). Simulations were performed to confirm that the ability of FSIs to balance firing between D1 and D2 MSNs was not dependent on the level of input correlation (data not shown). Direct measures of FSI correlation *in vivo* are problematic due to the low numbers of

FSIs in the striatum; however, the entrainment of FSIs to the striatal gamma rhythm (Berke et al., 2004; Berke, 2009) suggests some degree of correlation among FSIs. The small reduction in FSI correlation due to removal of gap junctions was sufficient to produce striatal imbalance in our network model. That synchronization of FSIs is critical for striatal balance was confirmed when increasing the level of correlation between cortical inputs to FSIs restored the balance. Our finding that a change to correlation between FSIs did not change the mean firing of MSNs in the network is consistent with another computational study that used simplified single neuron models to study the effects of correlated inputs on striatal function (Yim et al., 2011). This implies that even though changes to correlation between FSIs might not affect overall firing frequency of MSNs, they can modulate D1 and D2 MSN firing rates differently. This suggests that changes to FSI synchrony can lead to targeted activation of a population of MSNs without changing the overall activity. Gap junctions can thus act as a key modulator of striatal balance because of their specific role in FSI synchronization.

For the FSI-FSI connections in our network we did not use distance-dependent connections because of the relatively small size of the network. We confirmed that fixed probabilities and distance-dependent probabilities produce similar synchronization levels in our network (data not shown). This is in contrast to the results presented in a recent computational study (Lau et al., 2010) that reports that the synchronous activity of the network is sensitive to the connection type between the neurons (local versus global). We think that this contrast in results might be due to the difference in network architectures

between that study and this present study. Their network model consisted of 200 neurons arranged in a 1D lattice as compared to our 2D, 49 neuron network.

The imbalance produced by gap junctions was altered in our model by modulating NaF. Lowering the conductance of NaF channels in D2 MSNs (to that of D1 MSNs) increased the firing frequency of D2 MSNs, but it also changed their sensitivity to FSI input. With lowered NaF conductance in D2 MSNs, removing FSI inhibition produces a smaller increase in firing frequency than in the control case. This result in the striatum is similar to that reported recently in the globus pallidus. Edgerton et al (2010) found that in the presence of synaptic excitation, the density of fast-sodium channels can alter the sensitivity of globus pallidus neurons to synaptic inhibition. The novel aspect of our result is that eliminating the correlation among FSIs restored the balance when NaF is the same in D1 and D2 MSNs. A possible mechanism is that the synchronized FSI inputs in combination with elevated NaF conductance may enhance NaF inactivation leading to lower firing rates. Either lower NaF conductance or desynchronized FSI inputs avoids this NaF inactivation, permitting higher firing of D2 MSNs. This mechanism is analogous to the enhancement in hippocampal FSI firing produced by Kv3.1 (Erisir et al., 1999). Evaluation of the inactivation gate variable of NaF of D2 MSNs was not different between the different conditions (data not shown), possibly because of the increase in the firing frequency of D2 MSNs in the lower NaF condition. The increase in firing in the D2 MSNs is predicted to increase inactivation which may mask the predicted reduction in inactivation per spike.

Functional Implications of Dopamine

Dopamine may modulate the ability of FSIs to control striatal balance. Dopamine depletion has been shown to reduce the immediate-early gene response of PV+ neurons in the striatum (Trevitt et al., 2005). In addition, FSIs are depolarized by dopamine through D1/D5 receptors (Bracci et al., 2002; Centonze et al., 2003) and thus reduced dopamine can result in lower FSI input to both MSN classes. This makes reduction of FSI input a potential mechanism of disrupting striatal balance during dopamine depletion.

The excitability differences between D1 and D2 MSNs in our model are due to modulation to synaptic and intrinsic channels. Changes to instrinsic channels were sufficient to replicate firing frequency differences between the two MSN classes in response to current injection (Fig 1) measured in identified D1 and D2 MSNs. This implies that the intrinsic excitability of D1 and D2 MSNs in the absence of dopamine should be more similar than in the control condition. This is consistent with recent studies using transgenic mice (Day et al., 2006; Chan et al., 2012), where the current-firing frequency curves of D1 MSNs in the control and dopamine depleted condition was indistinguishable whereas that of the D2 MSN had diminished considerably in the dopamine depleted condition. This reduced firing frequency profile of the D2 MSN during dopamine depletion was much closer to that of the D1 MSN than it was in the control condition (Chan et al., 2012), suggesting that ‘intrinsic’ differences in channel differences might be largely due to basal dopamine in slice preparations.

Modulation of MSN excitability by direct changes to properties of the intrinsic channels can also disrupt balanced striatal firing. In particular, L-type calcium channels have previously been identified as one of the key targets through which dopamine balances excitability in the striatal network (Surmeier et al., 2007; Flores-Barrera et al., 2011). Additionally, L-type calcium channels are located near cortical synaptic inputs (Freund et al., 1984; Higley and Sabatini, 2010) and may be involved in corticostriatal integration. Flores-Barrera et al (2011) showed that blocking CaL produces imbalanced firing of D1 and D2 MSNs in response to synchronous input. Here, we show that striatal imbalance is also produced during block of CaL in response to asynchronous, *in vivo*-like input. Further removal of either FSI inputs or FSI correlation does not enhance the imbalance. This effect is also observed when CaL is increased in the D2 MSNs to match that of D1 MSNs. These results suggest that modulations to FSI inputs and to CaL on MSNs might have similar effects on MSN excitability. However, an alternative explanation for occlusion of the effect of removing FSI inputs is that the difference in firing between D1 and D2 MSNs has reached its maximum in the absence of differential L-type calcium channels. Thus, our simulations suggest that the absence of dopaminergic modulation of L-type calcium channels may be a mechanism whereby dopamine depletion disrupts striatal balance.

An imbalance in firing between D1 and D2 MSNs is not the only striatal mechanism considered to produce pathological globus pallidus activity. Changes to synchrony among MSNs have also been suggested to occur after loss of dopamine (Costa et al., 2006; Burkhardt et al., 2007). Experimental and computational studies have shown

that synchronously firing MSNs dynamically appear after dopamine depletion (Carrillo-Reid et al., 2008; Humphries et al., 2009), with recent large-scale simulations suggesting that the feedback inhibitory connections between MSNs supports the formation and switching between of synchronous assemblies of MSNs (Ponzi and Wickens, 2010). It is not clear whether dopamine also causes a change in FSI correlation, and whether changes to FSI correlation would contribute to the change in MSN synchrony.

A recent *in vivo* study reported that dopamine depletion leads to doubling of FSI input to D2 MSNs (Gittis et al., 2011a). Simulations done in that study predicted that this remodeling of FSI input increased the level of synchronization between MSNs. Doubling FSI input to D2 MSNs did not affect striatal balance in our network model (data not shown), suggesting that different mechanisms might be involved in producing imbalanced versus synchronous firing in the striatum. The link between striatal imbalance and increased correlation of MSNs thus should be explored further.

In summary, using a large-scale network model of heterogeneous, biologically-realistic striatal neurons we have demonstrated a critical role for the synchronization of FSIs through gap junctions in maintaining a balance between the direct and indirect pathway neurons of the striatum. We have also shown that the FSI control of this balance is mediated through channels governing intrinsic excitability differences between the D1 and D2 MSNs, specifically the fast-sodium channels and L-type calcium channels.

GRANTS
This work was supported by ONR grant MURI N00014-10-1-0198 and through the joint NIH-NSF CRCNS program through NIAAA grant RO1AA016022.

Contributions

Conceived of project: Sriraman Damodaran, Kim T. Blackwell

Designed research: Sriraman Damodaran, Kim T. Blackwell

Wrote paper: Sriraman Damodaran, Kim T. Blackwell

Edited paper: Sriraman Damodaran, Kim T. Blackwell, Rebekah C. Evans

Made computational model: Sriraman Damodaran

Ran Simulations: Sriraman Damodaran

Analyzed simulation data: Sriraman Damodaran, Kim T. Blackwell

Performed Experiments: Rebekah C. Evans

Analyzed experimental data: Rebekah C. Evans, Kim T. Blackwell

Citation

Damodaran S, Evans RC, Blackwell, KT. (2014) Synchronized firing of fast-spiking interneurons is critical to maintain balanced firing between direct and indirect pathway neurons of the striatum. *J Neurophysiol* 111:835-848

CHAPTER THREE: DESYNCHRONIZATION OF FAST-SPIKING INTERNEURONS REDUCES BETA BAND OSCILLATIONS AND IMBALANCE IN FIRING IN THE DOPAMINE-DEPLETED STRIATUM

Abstract

Oscillations in the β-band (8-30 Hz) that emerge in the output nuclei of the basal ganglia during Parkinson's disease, along with an imbalanced activation of the direct and indirect pathways, have been linked to the hypokinetic motor output associated with the disease. Though dopamine depletion causes a change in cellular and network properties in the striatum, it is unclear whether abnormal activity measured in the globus pallidus and substantia nigra pars reticulata is caused by abnormal striatal activity. Here we use a computational network model of medium spiny neurons (MSN) – fast spiking interneurons (FSI), based on data from several mammalian species, and find that robust β-band oscillations and imbalanced firing emerge from implementation of changes to cellular and circuit properties caused by dopamine depletion. These changes include a reduction in connections between MSNs, a doubling of FSI inhibition to D2 MSNs, an increase in D2 MSN dendritic excitability and a reduction in D2 MSN somatic excitability. The model reveals that the reduced decorrelation between MSNs due to weakened lateral inhibition enables the strong influence of synchronous FSIs on MSN firing and oscillations. Weakened lateral inhibition also produces an increased sensitivity of MSN output to cortical correlation, a condition relevant to the Parkinsonian striatum.

The oscillations of FSIs, in turn, are strongly modulated by fast electrical transmission between FSIs through gap junctions. These results suggest that pharmaceuticals that desynchronize FSI activity may provide a novel treatment for the enhanced β-band oscillations, imbalanced firing and motor dysfunction in Parkinson's disease.

Introduction

The pathophysiology of Parkinson's disease begins with the depletion of dopamine from the striatum and leads to an increase in oscillations in the globus pallidus and substantia nigra pars reticulata, especially in the 8-30 Hz range (β-band) (Brown and Williams, 2005), and to an imbalance in the activation of the direct and indirect pathways (Albin et al., 1989; Bergman et al., 1990, 1994; Mallet et al., 2006). Studies report synchrony and oscillations within the cortex (Goldberg et al., 2002), the striatum (Courtemanche et al., 2003; Costa et al., 2006; Jáidar et al., 2010; López-Huerta et al., 2013), and between the cortex and striatum (Costa et al., 2006) following dopamine deletion. These observations are consistent with the hypothesis that the striatum is the source of the aberrant activity; however, the closed feedback loop of the basal ganglia could be generating striatal oscillations. Furthermore, observed striatal changes caused by dopamine depletion have not been demonstrated to produce oscillatory activity. Enhanced acetylcholinergic tone in the striatum supports generation of oscillatory activity in both cortex and striatum (McCarthy et al., 2011), but different mechanisms may be operating during dopamine depletion.

Several studies have identified changes in the cellular and circuit properties of the striatum caused by dopamine depletion, but their direct influence on the emergence of abnormal striatal oscillations and firing activity has largely been speculative**.** The cellular changes include increases in Ca^{2+} transients in D2 MSN distal dendrites (Day et al., 2006, 2008b) and a reduction in D2 MSN somatic excitability (Chan et al., 2012). The circuit changes include a drastic reduction in lateral inhibition (LI) (MSN interconnections) (Taverna et al., 2008; Tecuapetla et al., 2009) and increased feedforward inhibition (FFI) from fast-spiking interneurons (FSIs) (Gittis et al., 2011a) to D2 MSNs. The limited knowledge on how these changes propagate through the striatal circuit to produce oscillations and changes to firing is due to the technical difficulty in experimentally isolating the effects of different GABAergic inputs *in vivo*.

We developed a mathematical network model consisting of more than 1000 biophysically realistic MSN and FSI model neurons to answer the following questions : 1) Can the experimentally observed changes in connectivity and intrinsic excitability lead to emergence of β-band oscillations and imbalanced firing in the striatal network and to an increase in striatal susceptibility to cortical correlation? 2) Which cellular or circuit level changes are most important in modulating striatal imbalance and oscillations, and are there potential mechanisms that are suitable to target for pharmacological intervention to restore normal oscillatory activity in the striatum during dopamine depletion? The results indicate that the reduction in decorrelation by weakening of LI is critical in allowing FSI oscillatory activity to drive MSN oscillations in the dopamine-depletion. Weakened LI makes MSNs more sensitive to cortical correlation because FSIs tend to

synchronize in response to high cortical correlation. Our mathematical model further predicts that direct reduction of FSI oscillations through blocking gap junctions between FSIs is a viable mechanism for restoring normal oscillatory and firing activity in the striatum.

Materials and Methods

Striatal network

A previously published striatal network model (Damodaran et al., 2014), consisting of 500 D1 MSNs, 500 D2 MSNs and 49 FSIs, was modified for the present study by changing intrinsic synaptic connections (i.e., GABAergic connections) as described below. The distance between each MSN soma in the model was 25 μm both in the x-axis and the y-axis (Tunstall et al., 2002), resulting in a 775x775 μm^2 grid**.** At each grid location, the assignment of either D1 or D2 MSNs was random with probability=0.5. Each MSN receives input from 55% of striatal FSIs within 100 μm (Tecuapetla et al., 2007), and between 4-27 converge on the same MSN (Koós and Tepper, 1999). Based on these estimates the 49 neuron FSI network corresponded to the FSI network seen by 1000 postsynaptic MSNs. Though the percentage of FSIs is slightly larger than observed experimentally, a smaller number of FSIs would have incorrectly produced homogenous FSI input to each MSN in the network model. The 49 FSIs were evenly distributed in space.

The morphology of both MSN models consisted of 189-compartments with 4 primary dendrites which divide into 8 secondary and then 16 tertiary dendrites. Each

primary dendrite was 20 μm long, secondary dendrites were 24 μm and tertiary dendrites were comprised of 11 compartments, each 36 μm long. Each MSN neuron had the following ionic channels: Fast sodium, fast and slow transient potassium, inward-rectifying potassium, delayed-rectifier potassium, calcium-dependent potassium, L-type calcium, N-type calcium, R-type calcium, T-type calcium. In addition, each MSN had the following synaptic channels: AMPA, NMDA and GABA. D1 and D2 MSN models were created by changing the maximal conductance of intrinsic and synaptic channels (Damodaran et al., 2014) from values used for our previous MSN model (Evans et al., 2012b), based on experimental data measuring the effect of D1 and D2 receptor agonists, as summarized in Nicola et al. (2000) and Moyer et al. (2007). Each FSI in this network consisted of 127 compartments: one soma; 2 primary dendrites, 4 secondary dendrites and 8 tertiary dendrites. The channels incorporated in this model included a fast-sodium channel, Kv3.1, Kv1.3, A-type (transient) potassium channel, AMPA and GABA synaptic channels (Kotaleski et al., 2006b). A heterogeneous network of neurons was generated by changing the A-type (transient) potassium channel conductance (both MSNs and FSIs) and NMDA channel conductance (MSN only) by $\pm$10%. The range of activity of MSNs used in the network, in response to current injections, was within the range of experimentally observed responses (Damodaran et al., 2014).

Intrinsic Synaptic Inputs

MSNs had 227 GABA synapses (1 per isopotential compartment) with a distance-dependent probability of GABAergic connection between MSNs and from FSIs to MSNs. GABAergic synapses on MSNs had a rise time constant of 0.75 ms, decay time constant

of 6.7 ms, and reversal potential of -60 mV (Czubayko and Plenz, 2002; Koos et al., 2004b; Gittis et al., 2010). Synapses from FSIs had a maximal conductance of 3.6 nS (Gittis et al., 2010) whereas the synapses between MSNs had a maximal conductance of 0.75 nS (Koos et al., 2004b). The FSI-MSN synapses also were more proximal than MSN-MSN synapses (Oorschot et al., 2010). The gap junction connections between the FSIs were modeled as resistive elements between the primary dendrites, with a conductance of 0.5 nS, coupling coefficient of 25% and probability of gap junction connection between nearby FSIs (those within 100 μm) of 0.3 (Koós and Tepper, 1999; Tepper et al., 2004; Hjorth et al., 2009b). Each FSI model had 93 GABA synaptic channels with a rise time constant of 1.33 ms, decay time constant of 4 ms, reversal potential of -60 mV, and maximal conductance of 1 nS (Gittis et al., 2010). The probability of chemical synapse connection between FSIs was 0.58 (Gittis et al., 2010) and was independent of the probability of gap junction connection. The difference in feedforward and lateral inhibition connectivity observed between the two MSN types in the control network was implemented for this study. Connection probability from D2 MSNs to either type of MSN was doubled, and strength of connection was doubled from D2 MSNs as compared to connections from D1 MSNs (Taverna et al., 2008). Additionally, FSI connections to D1 MSNs were 15% more probable than were FSI-D2 MSN connections (Gittis et al., 2010). The transmission delays were distance-based using a conduction velocity of 0.8 m/s for both FSI and MSN synapses (Wilson, 1986; Wilson et al., 1990; Tepper and Lee, 2007).

Extrinsic Synaptic Input

Both MSN classes in this model have 360 AMPA and NMDA synaptic channels, and each FSI model has 127 AMPA synaptic channels. Glutamatergic input to all neurons was simulated as Poisson distributed spike trains (generated using MATLAB, version 2007b, MathWorks) where each Poisson train represents activity from more than one cortical neuron, and each synaptic channel represents the population of synapses in a single isopotential compartment. Each excitatory synaptic channel in the MSN model receives an input of 5 Hz (unless otherwise stated) and each excitatory synaptic channel in the FSI model also receives an input of 5 Hz (unless otherwise stated) (Zheng and Wilson, 2002; Blackwell et al., 2003; Humphries et al., 2009). Since this study focuses on the relationship between striatal activity and motor deficits observed during dopamine depletion the distribution of cortical inputs to D1 and D2 MSNs matched the values reported from motor cortices to the MSNs with the D1 MSNs receiving 20% less inputs than D2 MSNs (Wall et al., 2013). Extrinsic GABA input to FSIs (70% of inputs), representing input from either globus pallidus or striatal neurons not included in the network, is provided by Poisson trains of 2 Hz producing a total of 207 GABAergic inputs per second (Kotaleski et al., 2006b).

To introduce correlations within both the MSN and FSI input, each spike from the set of cortical spike trains was assigned to more than one synapse, with probability P=1/n, where $n = N - \sqrt{c(N-1)}$, N=number of synapses, and c=0.5 (Hjorth et al., 2009b). To introduce between-neuron input correlation, an additional shared set of input spikes was generated. The between-neuron input correlation was then adjusted by

changing the fraction of input each neuron received from this shared pool (as opposed to the spike trains that were unique to each neuron). Cortical input correlation values of 0-0.5 were referred to as low levels whereas input correlation values of 0.6-1 were referred to as high levels. For experiments where the contribution of different intrinsic properties to overall β-band power was investigated, cortical input correlation was fixed at 0.3 (to represent low input correlation) and at 0.6 (to represent high input correlation). This was done to evaluate the contribution of intrinsic properties with extrinsic input fixed.

Dopamine depletion – Cellular changes

The response to current injection and the dendritic excitability of MSNs during dopamine depletion were tuned to match experimental observations. The spine reduction in D2 MSNs (Arbuthnott et al., 2000; Stephens et al., 2005; Day et al., 2006) was implemented by increasing the membrane resistance and decreasing membrane capacitance to account for spine loss (Koch and Zador, 1993) since the single neuron models did not have explicit spines. Additionally, transient K^+ channels have been implicated in modulating dendritic excitability in the MSNs during dopamine depletion (Day et al., 2008b) and this was implemented by decreasing KAf channel conductance in D2 distal dendrites.

Dopamine depletion – Circuit changes

MSN-MSN connectivity was modulated differently based on the MSN types. All connections between D1 MSNs were removed, connection probability between D2 MSNs was reduced by 50 %, connection probability between D2 MSNs and D1 MSNs was reduced by 70% (Taverna et al., 2008). The strength of connections between MSNs was reduced by 70%. Connection probability from FSI to D2 MSNs was doubled with no

change to the conductance of FSI-MSN connections, as has been experimentally reported (Gittis et al., 2011a).

Analysis of spikes

The simulation time was 2 s with no downstates, and Python was used to analyze the resulting network spiking activity. To measure synchrony and oscillatory power, cross-correlograms were constructed for each directly coupled neuron pair in the FSI and MSN network, and then averaged over the network (Damodaran et al., 2014). Correlation was corrected for firing frequency by subtracting the shuffled cross-correlograms (Rivlin-Etzion et al., 2006) for the same network condition. The Fourier Transform was used for estimation of the power spectra for the different conditions. All simulations were repeated three times, each with a different random seed controlling intrinsic synaptic connections and extrinsic input. The firing frequency was expressed as mean $\pm$ S.E.M of values obtained from the three different runs of each condition. Error bars in the figures represent S.E.M. Statistical analyses were performed using SAS, with N=3 networks for each condition. When only two groups were being compared, the procedure TTEST was used and $P<0.01$ was considered significant. When more than two groups were compared, analysis of variance was performed using the GLM. Post hoc analyses used Bonferroni correction for multiple comparisons with $P<0.01$ considered significant.

The model was implemented in GENESIS (Bower and Beeman, 2007) and simulations used a time step of 100 μs. The model was based on data from several mammalian species of both sexes. Each network simulation experiment took three weeks to run. The simulation and output processing software along with the files used for the

simulations are freely available from the authors' website:

(http://krasnow.gmu.edu/CENlab/) and modelDB

(http://senselab.med.yale.edu/ModelDB/).

Results

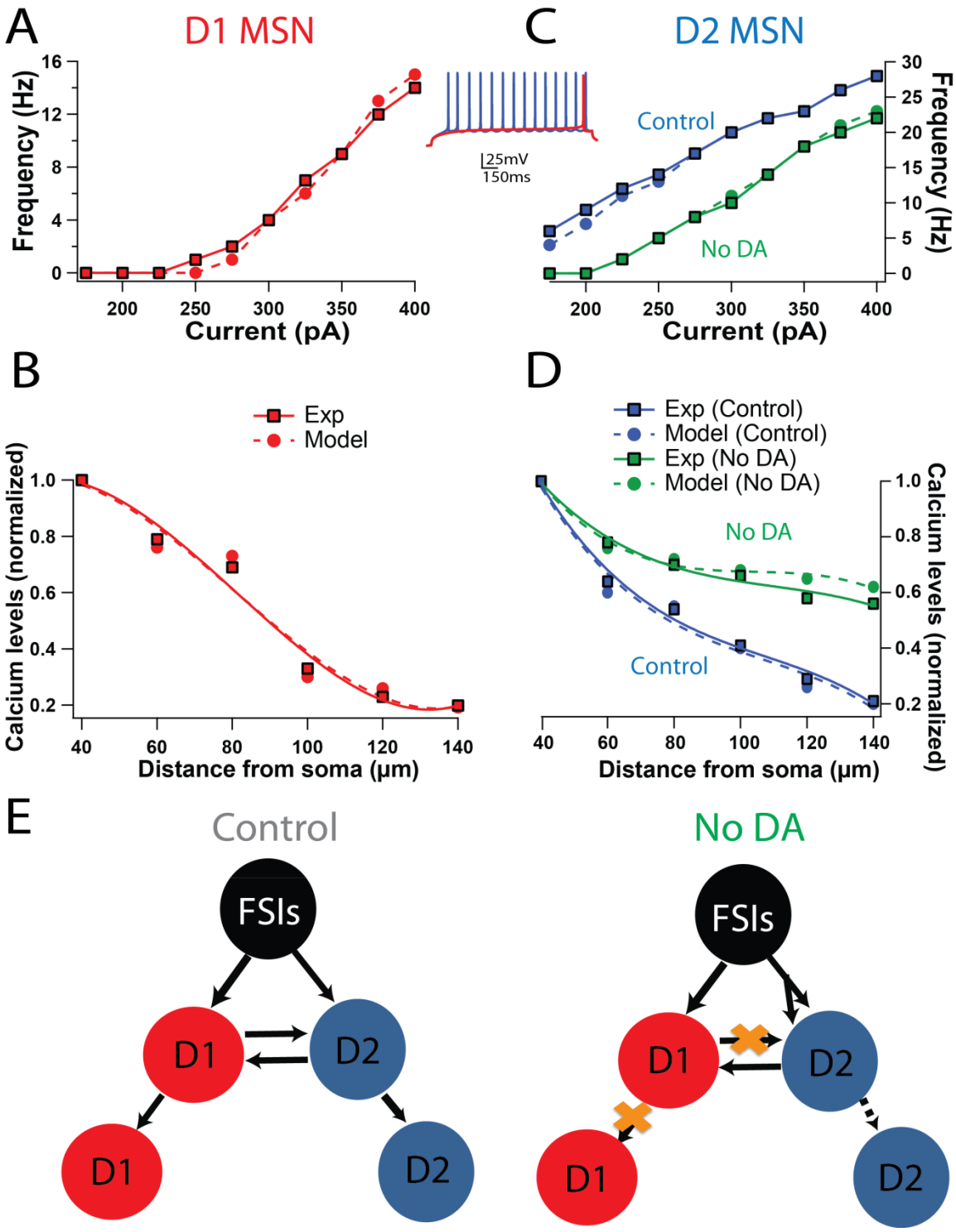
A
D1 MSN
Frequency (Hz)
Current (pA)
25mV
150ms
C
D2 MSN
Control
No DA
Frequency (Hz)
Current (pA)
B
Exp
Model
Calcium levels (normalized)
Distance from soma (μm)
D
Exp (Control)
Model (Control)
Exp (No DA)
Model (No DA)
No DA
Control
Calcium levels (normalized)
Distance from soma (μm)
E
Control
No DA
FSIs
D1
D2
D1
D2
FSIs
D1
D2
D1
D2

Figure 7. **Differences in cellular and circuit properties between control and dopamine depletion conditions.** (**A,C**) Current-Frequency curves for the model neuron with the median parameters (dashed lines) and experiments (solid lines). (**A**) D1 MSN (red), and (**C**) D2 MSN (Control: blue, No DA: green). Experimental data (solid) were replotted from published reports (Gertler et al., 2008b; Chan et al., 2012) for control and dopamine depletion conditions. (**Inset)** Models of D1 and D2 MSNs constructed with differences in intrinsic excitability reproduce electrophysiological dichotomy. The intrinsic channel conductances that differ between D1 and D2 MSNs are the L-type calcium channels, fast-sodium channels, A-type potassium channels and inward-rectifying potassium channels. (**B,D**) Change in amplitude of calcium transients evoked by action potentials versus distance from the soma is calculated by normalizing the distal Ca^{2+} transient to the most proximal transient in D1 (**B**, red, dashed lines) and D2 MSN (**D**, blue, dashed lines). Simulations are from D1 and D2 MSNs with the median parameters. Experimental data (solid lines) were replotted from a published report (Day et al., 2008b) for control (blue) and No DA (green) conditions. The magnitude of the Ca^{2+} transients decrements more in the D1 MSNs vs the D2 MSNs. The distal dendrites of D2 MSNs have enhanced excitability during dopamine depletion vs control. (**E**) Schematic representation of network connections during control and dopamine depletion conditions. During dopamine depletion, increased synaptic connections of D2 MSNs by FSIs have been observed. Additionally, reduced and weaker lateral inhibition between MSNs, specifically an absence of presynaptic connections from D1 MSNs, has also been observed.

Implementation of Dopamine Depletion changes

In order to accurately model the response of the striatal network to changes in cellular and circuit properties, changes in medium spiny neuron excitability and inhibitory connectivity were implemented using biophysically and anatomically realistic compartmental neuron models (Evans et al., 2012b; Damodaran et al., 2014). Dopamine depletion was implemented by changing excitability through modulation of potassium channels in distal dendrites of D2 MSNs (Day et al., 2008b) and reduction of spines in D2 MSNs (see Methods; Arbuthnott et al., 2000; Stephens et al., 2005; Day et al., 2006) to produce firing frequency in response to somatic current injection (Fig. 7A,C, inset) consistent with experimental findings (Day et al., 2008b; Gertler et al., 2008b; Chan et al., 2012). The reduction in amplitude of calcium transients with distance from soma in D1 and D2 MSNs in normal dopamine, along with the increase in calcium transient amplitude in distal D2 MSN dendrites during dopamine depletion (Fig. 7B,D) also were consistent with empirical observations (Day et al., 2008b). In addition, reduction in strength and connectivity of MSNs (Taverna et al., 2008) and a selective increase in FSI-

D2 MSN connectivity (Gittis et al., 2011a) were implemented as per experimental observations (Fig 7E).

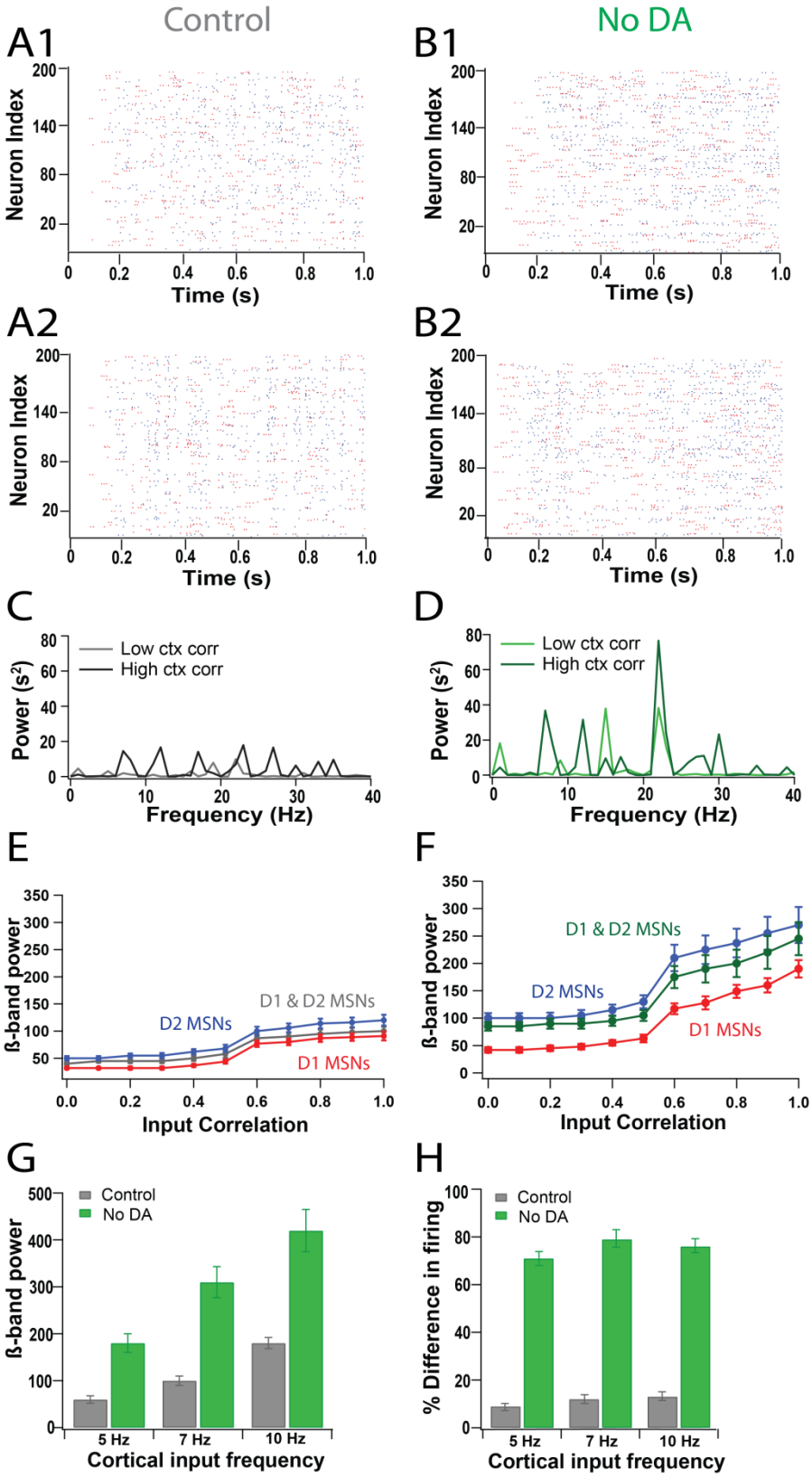
Control
No DA
A1
B1
A2
B2
Neuron Index
Time (s)
C
D
Low ctx corr
High ctx corr
Power (s²)
Frequency (Hz)
E
F
ß-band power
D1 & D2 MSNs
D2 MSNs
D1 MSNs
Input Correlation
G
H
Control
No DA
% Difference in firing
5 Hz
7 Hz
10 Hz
Cortical input frequency

Figure 8. **Emergence of β-band oscillations in dopamine-depleted striatal network model.**
(**A**) Raster plot of 200 MSNs in the normal striatal network (Control) in response to (**A1**) low (0.3) and (**A2**) high (0.6) cortical input correlation. (**B**) Raster plot of 200 MSNs in the dopamine-depleted striatal network in response to (**B1**) low (0.3) and (**B2**) high (0.6) cortical input correlation. Raster plots depict first second of the 2 s simulation, with spikes from D1 MSNs indicated in red, and spikes from D2 MSNs indicated in blue. (**C**) Power spectra of normal striatal network in response to low (0.3) (light gray) and high (0.6) (black) cortical input correlation. The power of α- and β- band oscillations are higher in the network in response to high cortical input correlation. (**D**) Power spectra of dopamine-depleted striatal network in response to low (0.3) (light green) and high (0.6) (dark green) cortical input correlation. Power of α- and β- band oscillations are significantly increased in the dopamine depletion condition as compared to the control condition, especially in response to high cortical input correlation. (**E,F**) Plot of β-band oscillation power vs cortical input correlation for D1 MSNs, D2 MSNs and all MSNs for the (**E**) control and (**F**) dopamine depletion conditions. MSNs have a higher power of β-band oscillations and an increased sensitivity to changes in cortical input correlation in the dopamine depletion condition as compared to control. β-band power of D2 MSNs increases more than that of D1 MSNs in the transition from control to dopamine depletion. (**G**) Higher β-band power of MSNs in the dopamine depletion condition as compared to the control condition in response to different input frequencies (5, 7 and 10 Hz). The effect is robust to changes in input frequency. The cortical input correlation is 0.6. (**H**) % difference in firing between D1 and D2 MSNs in the control and dopamine depletion conditions in response to different input frequencies (5, 7 and 10 Hz). % difference is calculated as difference divided by mean firing of D1 MSNs. The imbalance in firing between the two MSN classes is also robust to changes in input frequency. The cortical input correlation is 0.6. Error bars represent S.E.M.

Table 4: Balance in firing for different network conditions. Cortical input frequency is 5 Hz. Values shown are the mean ± standard error mean, in Hz.

Condition		D1	D2	D1+D2	% Diff
Control	low corr:0.3	3.3 ± 0.1	3.5 ± 0.13	3.4 ± 0.1	6
	high corr:0.6	3.5 ± 0.12	3.8 ± 0.14	3.65 ± 0.13	9
No DA	low corr:0.3	3.9 ± 0.16	5.7 ± 0.19	4.8 ± 0.16	46
	high corr:0.6	3.9 ± 0.15	6.7 ± 0.2	5.3 ± 0.2	71
No DA + No Gaps	low corr:0.3	3.3 ± 0.12	3.5 ± 0.13	3.4 ± 0.13	6
	high corr:0.6	3.4 ± 0.14	3.6 ± 0.13	3.5 ± 0.14	5

Emergent β-band oscillations and striatal imbalance sensitive to level of cortical input correlation

Raster plots of our 1049-neuron striatal model (1000 heterogeneous MSNs, 49 heterogeneous FSIs; see Methods) reveal changes in MSN firing frequency and oscillatory behavior between the control (Fig 8A) and dopamine depletion (Fig 8B)

conditions similar to that observed in experimentally induced Parkinson's Disease. Each excitatory synaptic channel in the MSN and FSI models receives an input of 5 Hz (unless otherwise stated) (Zheng and Wilson, 2002; Blackwell et al., 2003; Humphries et al., 2009). The average firing frequency of MSNs and the imbalance in firing between D1 and D2 MSNs are higher in the dopamine depleted network as compared to the control network (Table 4). The average rate for MSNs in the control condition in response to high cortical input correlation (0.6) is 3.6 $\pm$ 0.13 Hz, consistent with the average MSN spiking rate seen *in vivo* during wakefulness (Mahon et al., 2006), with D1 and D2 MSNs firing at similar rates (Table 4, Fig 8H). MSNs fire at a higher overall rate (5.3 $\pm$ 0.2 Hz) in the dopamine depleted network in response to high cortical input correlation, caused mostly by an increased firing of D2 MSNs (Table 4). The observed increase in MSN firing frequency after dopamine depletion is consistent with some *in vivo* studies (Kish et al., 1999; Tseng et al., 2001) though there is a report of overall decrease in the firing of all striatal neurons (Chang et al., 2006).

The raster plots reveal enhanced oscillations in addition to the altered firing rates. In response to highly correlated cortical input, the power spectra of the entire population peaks at a frequency of 21 $\pm$ 1.8 Hz in the dopamine depleted network whereas the power is more uniform across the different frequencies in the control network (Fig 8C,D). The overall β-band power of MSNs increases with increasing cortical input correlation especially after dopamine depletion (Fig 8E,F). This was confirmed using the GLM procedure with condition and cortical input correlation as the independent variables ($F(3,59)=310.84$, $P<0.001$; $P(\text{condition})<0.001$, $P(\text{correlation})<0.001$,

P(condition*correlation)<0.001). There are also peaks at lower frequencies in the power spectra of the dopamine depleted network, consistent with studies that report both lower and higher frequency of β-band oscillations in the basal ganglia output nuclei after dopamine depletion (Brown and Williams, 2005). The emergence of β-band oscillations (Fig 8G) and firing imbalance between D1 and D2 MSNs (Fig 8H) are independent of the frequency of the input trains confirming that these effects are not unique to a particular cortical firing frequency.

In both the control and dopamine depleted networks, β-band power is higher for D2 MSNs than for D1 MSNS (Fig 8E,F). This was confirmed using the GLM procedure with condition and MSN class as the independent variables at a cortical input correlation of 0.6 ($F(3,11)=46.74$, $P<0.001$; P(condition)<0.001, P(MSN class)<0.001, P(condition*MSN class)<0.001). The cause of this difference in the control network is that D2 MSNs receive less inhibitory inputs than D1 MSNS, as observed experimentally (see Methods; Taverna et al., 2008; Gittis et al., 2010). When D1 and D2 MSNs receive similar inhibitory input under control conditions, they exhibit similar β-band power (data not shown). The asymmetry between D1 MSN and D2 MSN β-band power after dopamine depletion is explained by the differences in network connections that are producing the enhanced β-band power overall, and these are explained in the next section.

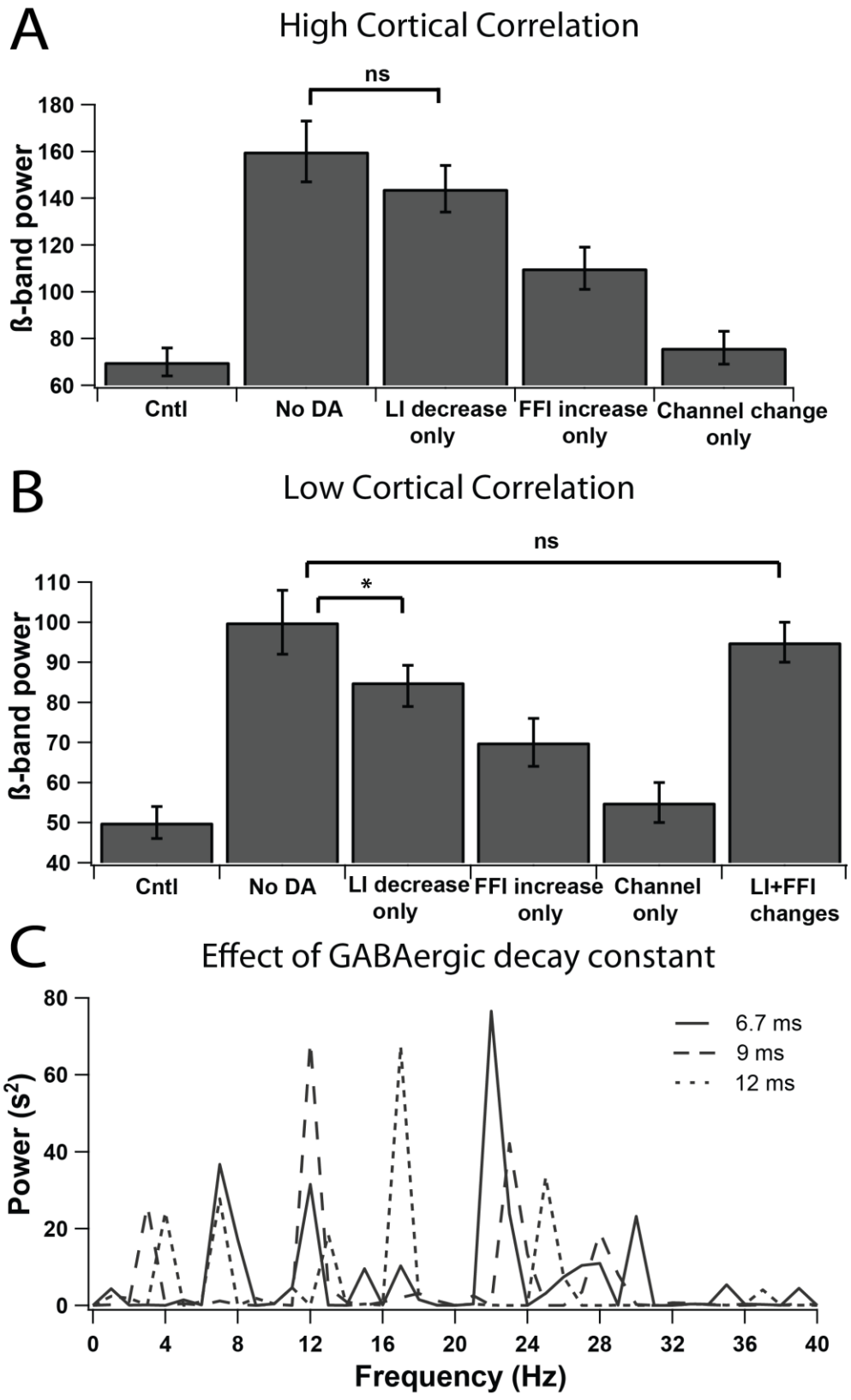
A
High Cortical Correlation
ns
ß-band power
180
160
140
120
100
80
60
Cntl
No DA
LI decrease only
FFI increase only
Channel change only
B
Low Cortical Correlation
ns
*
ß-band power
110
100
90
80
70
60
50
40
Cntl
No DA
LI decrease only
FFI increase only
Channel only
LI+FFI changes
C
Effect of GABAergic decay constant
6.7 ms
9 ms
12 ms
Power (s²)
80
60
40
20
0
0
4
8
12
16
20
24
28
32
36
40
Frequency (Hz)

Figure 9. Contribution of network, cell properties and GABAergic decay constant to power of β-band oscillations.
(A,B) Power of β-band oscillations is significantly increased from control when only LI is decreased or when only FFI is increased. Decreasing LI alone is significantly higher than increasing FFI alone. Changing only cellular properties of MSNs produced small changes to the power of β-band oscillations from the levels seen in control; * indicates $P<0.01$. **(A)** In response to high cortical input correlation decreasing LI alone produces β-band power close to that seen in the dopamine depletion condition. **(B)** In response to low cortical input correlation, both LI and FFI changes together were required to produce β-band power close to that seen in the dopamine depletion condition. **(C)** When the GABAergic decay constant was changed it shifted the peak oscillation frequency of the MSNs though the peak frequency remained with the β-band. The power spectra represented are for the dopamine depletion condition in response to high cortical input correlation (0.6). Error bars represent S.E.M.

Reduction of LI results in largest change in β-band power in response to high cortical input correlation

By isolating the different classes of changes implemented in the dopamine-depleted network, we investigated whether any one specific change was critical in producing the increase in β-band oscillations. The results presented for these experiments are for two values of cortical input correlation (low=0.3 or high=0.6) so as to evaluate the specific roles of cellular and circuit properties of the network, independent of the changes in extrinsic input. Altering the experimentally observed changes to cellular properties but not the changes to circuit properties (only channel changes) resulted in a small increase in β-band power for both input correlation values (Fig 9). We then investigated the distinct contribution of alterations in either FFI or LI to changes in network activity. In response to high cortical input correlation, reducing LI alone was sufficient to increase β-band power close to the levels seen in the dopamine depletion condition whereas increasing FFI connectivity alone raised β-band power significantly less than that produced by reducing LI alone, though it was significantly higher than the power seen in control (Fig 9A). GLM reveals that the β-band power for the control, dopamine depletion, only LI change, only FFI change and only cellular changes groups were significantly different

from each other [$F(4,14) = 89.27$, $P<0.001$]. Post hoc tests (Bonferroni correction for paired comparisons) show that β-band power for dopamine depletion ~= only LI change > only FFI change > only cellular changes ~= control ($P<0.01$). In response to low input correlation, reducing LI alone was not sufficient to increase β-band power to the levels seen in the dopamine depletion condition (Fig 9B), instead changes to both LI and FFI were required to recapitulate the dopamine depletion condition. GLM reveals that the β-band power for the control, dopamine depletion, only LI change, only FFI change and only cellular changes groups were significantly different from each other $F(4,14)=105.20$, $P<0.001$. Post hoc tests (Bonferroni correction for paired comparisons) show that β-band power for dopamine depletion > only LI change > only FFI change > only cellular changes ~= control ($P<0.01$). These results suggest a fundamental role for LI in the striatal network, namely to decorrelate the MSNs from synchronous input. Nonetheless, for decorrelation to play such a significant role during dopamine depletion, there must be sources of highly synchronous input to the network.

We observed that the final frequency at which the MSN network oscillates is due to an interaction between multiple factors: level of inhibition (LI vs FFI) between MSNs, intrinsic excitability of MSNs, and $GABA_A$-receptor decay time constant of MSNs. Changing the GABAergic decay constant shifted the peak oscillation frequency of the MSNs though the peak frequency remained within the β-band, when the constants were within the range of experimentally measured values (Koos et al., 2004; Gittis et al., 2010; Fig 9C). The power spectra shown are for the dopamine depletion condition in response to high cortical input correlation (0.6). The oscillations at β-band in the striatal network

model were thus an emergent property based on parameters constrained by experimentally observed measures.

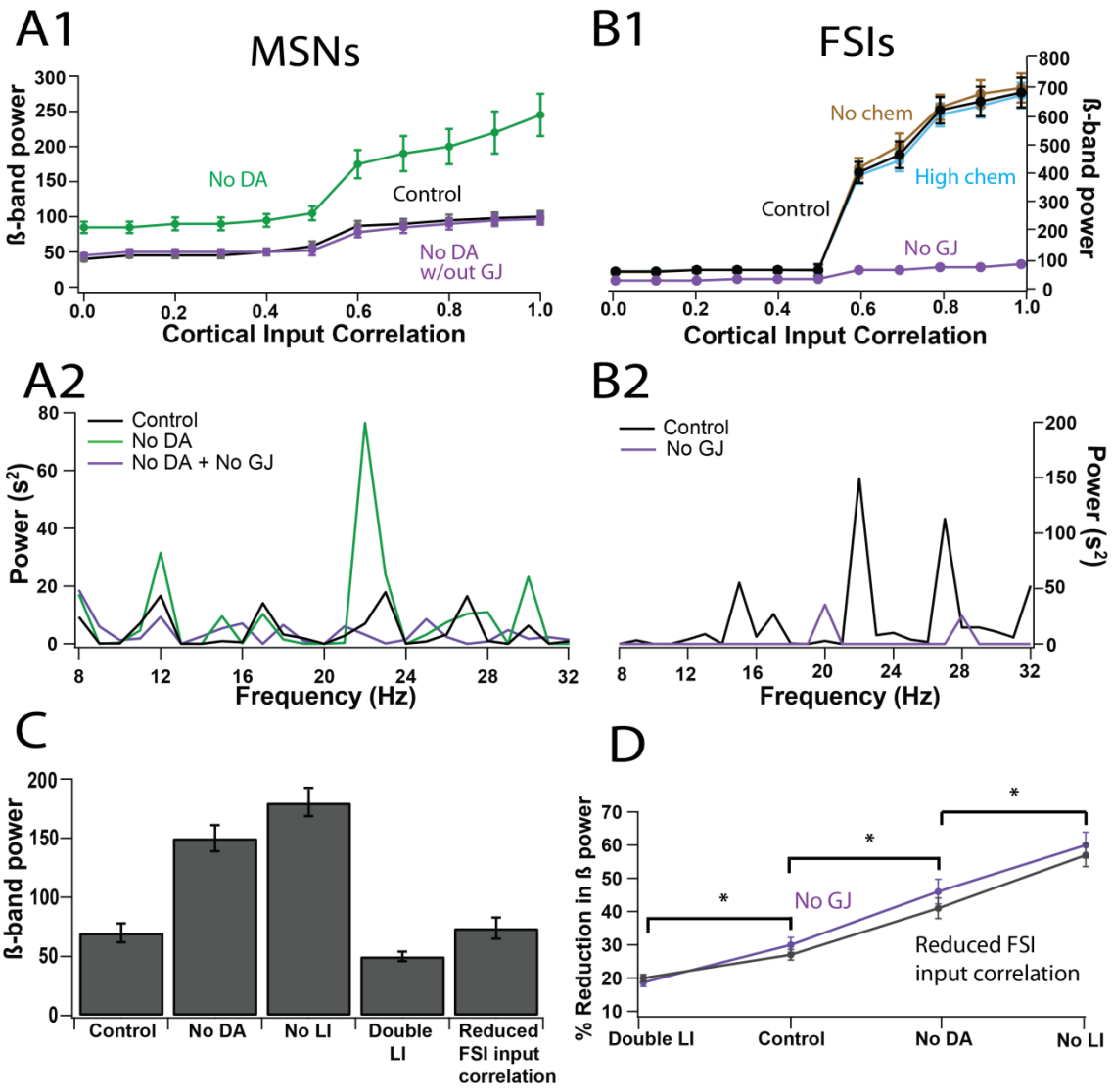

Figure 10. **Blocking gap junctions compensates for weak decorrelation by LI during dopamine depletion.** (**A,B**) Plot of β-band oscillation power vs cortical input correlation and power spectra for MSNs (**A**) and FSIs (**B**). (**A1,B1**) MSNs are more sensitive to higher levels (0.6-1) of cortical input correlation during the dopamine depletion condition (light green) as compared to the control condition (black). FSIs with intact gap junctions (GJ, black) are also more sensitive to higher versus lower cortical input correlation levels, exhibiting a sigmoidal shaped input-output curve under the control condition. Removing gap junctions between FSIs (purple) reduced the FSI correlation, especially in

response to high cortical input correlation. Removing gap junctions between FSIs in the dopamine-depleted network restores sensitivity of MSNs to cortical input correlation (purple), to the sensitivity seen in the control condition. Blocking chemical synapses between FSIs (light brown) or increasing their conductance to equal the strength of GABAergic synapses between MSNs (cyan) did not alter the sensitivity of FSIs to cortical input correlation. Error bars represent S.E.M, and in some cases are smaller than the symbols. (**A2, B2)** Power spectra of MSNs and FSIs for different conditions in response to high cortical input correlation (0.6). **(A2)** The power of β-band oscillations increase drastically for the dopamine-depleted condition (green) as compared to the control condition (black). Blocking gap junctions between FSIs (purple) during the dopamine depletion condition restores the power of the oscillations to control levels. **(B2)** FSIs have higher power of oscillations as compared to the MSNs. FSIs do not undergo any changes in the dopamine-depleted condition in the network and thus they have the same oscillatory power in control and dopamine-depleted networks. Similar to MSNs during dopamine depletion, oscillatory power in the FSIs decreases with gap junction block. (**C**) Blocking all LI resulted in emergent β-band oscillations higher than that seen in dopamine depletion whereas an increase in LI connectivity from control levels lead to a decrease in β-band power. Reducing the cortical input correlation only to FSIs (0.6 to 0.3) was also sufficient to reduce β-band power of MSNs. The values shown are for the MSN network in response to high cortical input correlation (0.6). The control and dopamine depletion bars are the same as the bars depicted in Fig 3 for the respective conditions and were placed in this panel for comparison purposes. (**D**) % of Reduction in β-band power by blocking gap junctions or reducing FSI input correlation for varying levels of intact LI in the MSN network. Lower the level of LI higher the % of reduction in β-band power in response to reduction in FSI correlation.* indicates $P<0.01$. Error bars represent S.E.M.

Blocking gap junctions restores MSN oscillations and firing during dopamine depletion

Two significant feedforward inputs to MSNs are the cortical (excitatory) and FFI input, and their effects on MSN β-band power are investigated next. The power of β-band oscillations of the MSN population increases only slightly with increasing cortical input correlation under the control condition, but increases dramatically during dopamine depletion (Fig. 10A), especially for higher levels of cortical input correlation (0.6-1). Prior research demonstrating that cortical input synchrony is required for gap junctions to correlate FSIs (Hjorth et al., 2009b; Damodaran et al., 2014), prompted us to evaluate the oscillations of the FSI network. The power spectra of the FSI network (Fig 10B) reveals highly oscillatory behavior among the FSIs in the control condition, in response to high levels of cortical input correlation. The sharp increase in FSI β-band power at 0.6 cortical input correlation is due to a threshold effect, at which the influence of gap junctions between FSIs transition from a predominantly shunting effect to a predominantly

synchronizing effect (Hjorth et al., 2009b; Russo et al., 2013). The threshold and the sensitivity of FSIs to cortical input correlation is robust to small changes in gap junction conductance, but can be modified by large changes. Specifically, a change from 0.5 nS to 3 nS reduced the level of cortical input correlation required to significantly increase the power of oscillations of the FSIs to 0.5 instead of 0.6 (data not shown). Though FSIs are connected by GABAergic synapses, these are not sufficient to decorrelate the FSIs, as blocking them did not have an effect on the response of the FSIs to cortical input correlation (Fig 10B).

We separated the contribution of cortical from FSI correlation by altering FSI correlation using several methods. First, providing low cortical input correlation (0.3) to FSIs, independent of the cortical input correlation to MSNs, was sufficient to bring the MSN β-band power to that seen during the control condition (Figure 10C; Control vs reduced FSI: $T(4)=-0.8$, $P=0.48$). Second, electrical synapses have been implicated to be responsible for oscillations of FSIs in other brain regions (Draguhn et al., 1998; Whittington and Traub, 2003). Thus, we reduced the level of FSI correlation independent of its cortical input correlation, by blocking gap junctions. This manipulation drastically reduced the power of β-band oscillations of both FSIs (Fig 10B) and MSNs to control levels (Fig 10A; Control vs no gap junctions: $T(4)=0.5$, $P=0.66$). Blocking gap junctions also restored balanced firing between D1 and D2 MSNs in the dopamine depleted network (Table 4). This effect is independent of the presence of GABAergic synapses between FSIs as blocking or increasing GABAergic conductance between FSIs did not have an effect on the response of the FSIs to cortical correlation (Fig 10B). This is

consistent with a recent study in mouse striatal slices that reported the effect of gap junctions on firing and synchronicity of FSIs being independent of GABAergic synapses (Russo et al., 2013). These results identify a specific and tangible mechanism through which balance and oscillatory power of MSNs can be modulated.

To better understand the contribution of LI towards enhanced β-band oscillations, the interaction between LI manipulation and reduced FSI correlation was evaluated in response to high cortical input correlation. Just eliminating LI in the control network produced highly oscillatory MSN activity in the β-band whereas doubling LI (as compared to control levels) attenuated the existing β-band oscillations in the control network, confirming the robust decorrelation effect of LI (Fig 10C). Additionally, the percentage reduction in MSN β-band power was independent of the method for reducing FSI correlation (either blocking gap junctions or reducing FSI input correlation) but did depend on the level of LI between the MSNs (GLM: $F(7,23) = 104.56$, $P<0.001$, $P(\text{method})=0.3482$; $P(\text{LI})<0.001$; Fig 10D). Specifically, eliminating FSI correlation has a significantly smaller effect on the normal or high LI connection networks. Post-hoc tests show that percentage reduction in β-band power in the MSNs due to reduction of FSI correlation for no LI > dopamine depletion > control > double LI ($P<0.01$). In summary, the reduced decorrelation due to weaker LI connectivity allows MSNs to be controlled by increased FSI correlation and subsequently increased cortical correlation.

Table 5: α-band power for different conditions. Values shown are the mean ± standard error mean, in s^2.

Condition	α-band power
Control (high corr;0.6)	21 ± 1.8
Dopamine depletion (high corr;0.6)	40 ± 3.3
Dopamine depletion + No GJ (high corr;0.6)	16 ± 1.1

The importance of β-band oscillations in Parkinson's disease has been extensively studied but the contribution of oscillations in other bands, specifically α-band, is less clear. Pathological oscillations in the α-band (3-8 Hz) develop in the globus pallidus internal segment and in the subthalamic nucleus of some monkeys after MPTP treatment and of Parkinson's disease patients with tremor at rest (Brown, 2003; Hutchison et al., 2004). Our striatal network model is consistent with this observation and produces a doubling in the power of emergent α-band oscillations, in response to high input correlation, in dopamine depletion as compared to control. Blocking gap junctions between FSIs in the dopamine depleted network results in a reduction in the α-band power to levels slightly lower than the control condition (Table 5). Our network also produces γ-band oscillations though they had lower power and did not change

significantly across conditions. Thus, although dopamine depletion and restorative measures applied to FSIs predominantly affect β-band oscillations, the effect on α- band oscillations is consistent with existing experiments and theories on Parkinson's disease.

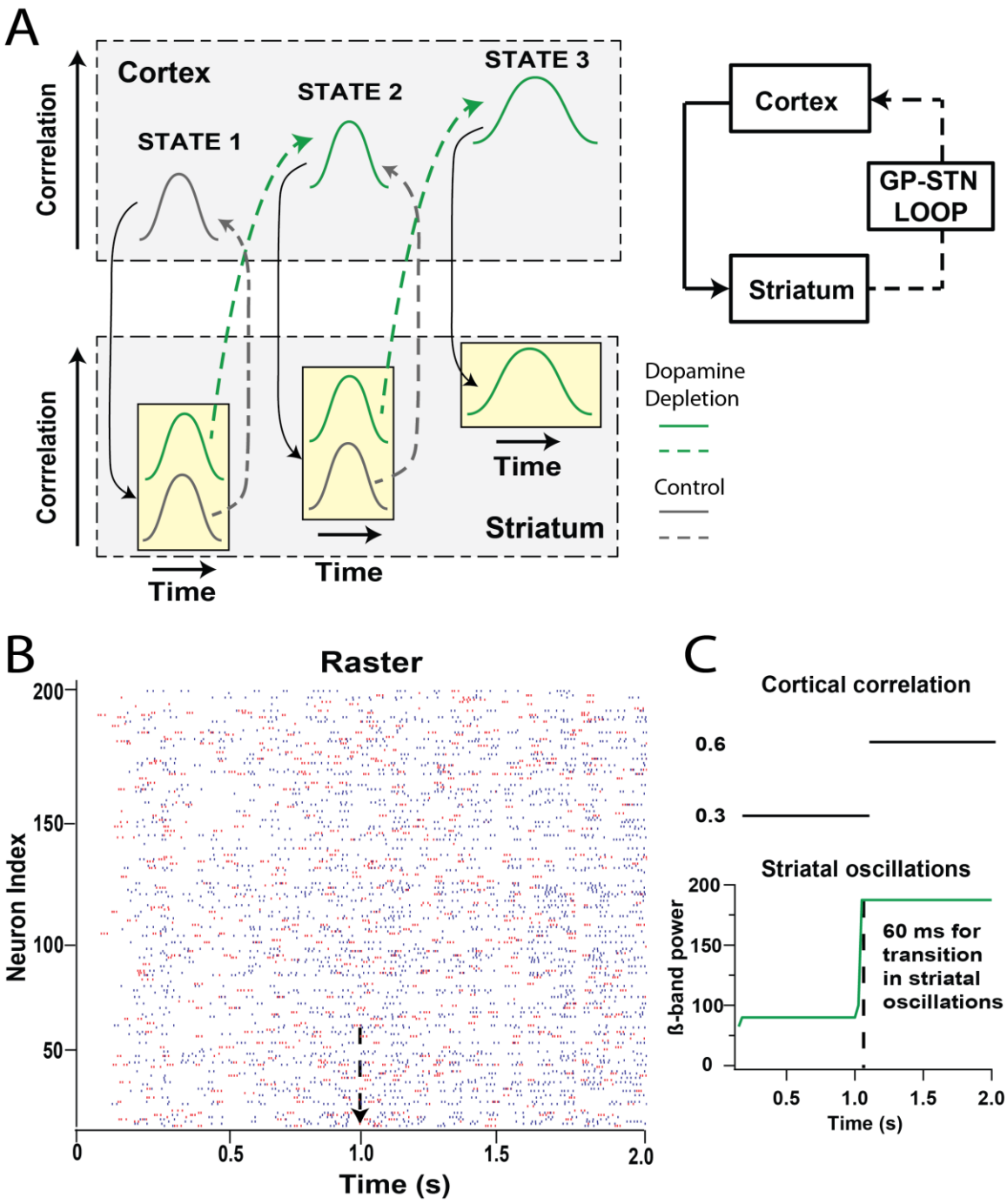

Figure 11. Contribution of striatum to abnormal oscillatory activity experimentally observed in Parkinson's Disease.
(A) Feedback loop amplifies correlation during dopamine depletion. Each column represents a different state, and within each column the x-axis represents time. The tan boxes with gray and green bell-shaped traces represent choice points, where the subsequent state of the cortex-striatum loop depends on whether dopamine is normal (gray) or depleted (green). A normal transient increase in cortical correlation (State 1, gray cortical trace) is decorrelated by the

normal striatum (State 1, striatal gray trace), thus the cortex and striatum remain in the normal state of transient increases in correlation. In the dopamine-depleted striatum (State 1, striatal green trace), the transient increase in cortical correlation leads to a higher striatal correlation, with a subsequent transition into State 2 which has a higher cortical correlation. Feedback from striatum to the cortex through the GP-STN loop contributes towards increased cortical correlation (State 2, cortical green trace). The normal striatum can decorrelate even this elevated cortical correlation (State 2, striatal gray trace), but the dopamine-depleted striatum produces a further increase in correlation (State 2, striatal green trace) with a subsequent transition into State 3 with higher and more prolonged cortical correlation. In State 3, the striatum is unable to decorrelate the cortex, thus no gray, low correlation striatal trace is shown. (B) Raster plot of 200 MSNs in the dopamine-depleted striatal network in response to a switch in cortical input correlation from 0.3 to 0.6 at t= 1s (indicated by arrow). (C) Cortical input correlation (top) and striatal oscillations, measured as power of β-band oscillations (bottom), showing that the dopamine-depleted striatal network takes only ~60 ms to respond to the switch in cortical input correlation. The first 0.1 s was eliminated from the analysis since it represents transient increase as the network transitions from the downstate.

Striatal network responds quickly to increases in cortical correlation

Our simulation results suggest that synchrony and oscillations emerge from the feedback loop from cortex to striatum and ultimately back to the cortex. Small increases in cortical correlation, as observed experimentally (Riehle et al., 1997, 2000; Engelhard et al., 2013), are decorrelated by the normal striatum, but instead are amplified by the dopamine-depleted striatum (Fig 11A). The enhanced striatal synchrony, possibly amplified by globus pallidus and subthalamic nucleus (Plenz and Kital, 1999; Brown, 2007) are transmitted back to the cortex, enhancing its correlation even further. Our simulations show that one second (or longer) of cortical correlation is sufficient to produce striatal synchrony and oscillations, but what if the increases in cortical correlation are briefer than one second? In order for this positive feedback loop of correlation to produce the pathological synchrony and oscillations, the striatum should be able to respond quickly to this transient increase. We tested this hypothesis by measuring the time required for the striatum to increase its correlation following a change in cortical correlation. Results show that the increase in striatal oscillations is detectable within ~60 ms (Fig 11B,C), suggesting that the network does not require a long period of time to

register a change in cortical correlation. This allows the pathological correlation feedback loop to amplify these normal, transient increases in correlation observed during behavior.

Discussion

Our results, using a striatal network model, demonstrate that dopamine depletion produces an increase in striatal oscillations in the β-band, as measured by multi-unit activity. Due to the difficulty in recording simultaneously from multiple units in the striatum, most measurements of synchrony and oscillations in the striatum employ local field recordings (Bergman et al., 1994; Mallet et al., 2006). Our measurements of correlation between MSNs is based on directly coupled pairs of MSNs; whereas measurement of correlation among the entire population reveals no correlations, suggesting that even multi-unit recordings using electrode arrays *in vivo* may not detect such correlations. However, our result is consistent with measurements from dopamine-depleted brain slices that show increases in the number of co-active neurons (Jáidar et al., 2010). The most significant mechanism producing the increased oscillatory activity is a reduction in LI caused by dopamine depletion, making MSNs more sensitive to correlated input from cortex and FSIs.

Firing imbalance between D1 and D2 MSNs accompanies changes to β-band oscillations

The dopamine depleted network also exhibits emergent changes to overall MSN spiking frequency and imbalance in firing between D1 and D2 MSNs. Our network exhibits an

overall increase in firing, caused by a much higher increase in D2 MSNs than in D1 MSNs, resulting in an imbalance in activity between the two classes. This result is consistent with two *in vivo* studies that reported increases in MSN firing in 6-OHDA animals (Kish et al., 1999; Tseng et al., 2001), though another study showed a decrease in overall striatal activity (Chang et al., 2006). The increased firing of D2 MSNs and imbalance between D2 MSNs and D1 MSNs during dopamine depletion also is consistent with *in vivo* studies on 6-OHDA animals with identified MSNs (Mallet et al., 2006).

Interneuron contributions to striatal β-band oscillations

In addition to FFI from FSIs and LI from MSNs, MSNs are modulated by cholinergic interneurons in the striatum (Kreitzer, 2009), whose activity is modulated by dopamine. Changes in cellular and circuit properties of the MSN network in our model are predominantly based on the 6-OHDA experimental model in which acetylcholine levels increase after dopamine depletion (Ikarashi et al., 1997). Therefore, the effects of dopamine mediated changes on cholinergic modulation of the MSN network and consequently on MSN firing are accounted for in the model. A recent study that modeled the effects of cholinergic modulation reported that increased cholinergic modulation results in reduced potassium currents in MSNs, consequently leading to stronger effects of MSN inhibition and the emergence of β-band oscillations in dopamine depletion (McCarthy et al., 2011). In addition, bath application of acetylcholine results in a reduction of FSI-MSN conductance (Koós and Tepper, 2002); however, a recent *in vivo* study has shown that during dopamine depletion FSI-MSN conductance is similar to that

recorded during healthy conditions (Gittis et al., 2011a). This suggests changes in striatal activity caused by dopamine depletion cannot be explained solely by increases in acetylcholinergic tone. Nonetheless, it remains possible that abnormalities in neuromodulators evolve during Parkinson's Disease, with a phase where dopamine depletion produces β-band oscillations in the striatal network, and a phase where increased acetylcholine levels produce β-band oscillations.

Our computational model suggests that, although FFI from FSIs strongly contributes to the high β-band oscillations in the striatum during dopamine depletion, the decrease in LI critically allows the MSNs to be synchronized by the FSIs. Interneurons in other brain regions have been shown to maintain large-scale oscillations at various frequencies (Gray, 1994; Buzsáki and Chrobak, 1995) and FSIs in our network produce strong oscillations in the 20-60 Hz range, consistent with the firing patterns observed *in vivo* (Sciamanna and Wilson, 2011). Though not included in our model, low-threshold spiking interneurons exhibit oscillatory activity at lower frequencies than FSIs (Beatty et al., 2012), and may contribute to MSN synchrony, but are not required to produce β-band oscillations in our model. The oscillations in MSNs emerge at lower frequencies than those of FSIs, indicating that correlation between oscillations and frequency does not imply causation. Despite the strong oscillatory power of FSIs, incorporating *only* the increase in FSI-MSN connectivity leads to an increase in MSN β-band power smaller than that of reducing LI alone. Nonetheless, the increase in β-band power is consistent with results from a simple striatal model showing that increase FFI alone could produce synchrony (Gittis et al., 2011a). In contrast to other brain regions, strong control of MSN

synchrony by FSIs is not observed in the striatum because the effect of oscillatory FFI on the MSNs is opposed by strong LI under control dopamine conditions, but is unmasked when LI is reduced in Parkinson's Disease. The powerful role of LI seems counter-intuitive given the observation of inhibition from MSNs being weaker in strength and more distal as compared to FFI inhibition (Plenz, 2003). On the other hand, our computational result is supported by a recent experimental study showing that LI is strong enough to decrease firing of a subset of MSNs in response to antidromic stimulation from the globus pallidus (López-Huerta et al., 2013). In summary, of the two circuits, changes to the LI circuit produce more widespread changes to MSN oscillations than do changes to the FFI circuit.

Gap junctions as a target to restore basal ganglia oscillations and balance

In order to restore activity to control levels in the Parkinsonian striatum, mechanisms that selectively modulate FSI synchrony were targeted. FSIs are not simple 'integrate and fire' devices as transient activation may activate voltage-dependent conductances, and enable the cell membrane potential to oscillate (Sciamanna and Wilson, 2011). Specifically, interneurons have been demonstrated to maintain population synchrony through gap junctions in the hippocampus and cortex (Michelson and Wong, 1994; Draguhn et al., 1998; Whittington and Traub, 2003; Nimmrich et al., 2005), though not the normal striatum (Berke, 2008; Russo et al., 2013). Accordingly, removing fast electrical transmission between FSIs by blocking gap junctions was sufficient to reduce the power of β-band oscillations in the dopamine-depleted network, specifically in

response to high cortical input correlation. Thus, gap junctions are critical to maintain synchrony and in the modulation of oscillations in the FSI network and consequently in the MSNs.

This action of gap junctions likely is present *in vivo* even though functional coupling between striatal FSIs has not yet been observed *in vivo*. Several reasons may explain why electrical coupling between FSIs has been demonstrated in multiple *in vitro* studies (Koós and Tepper, 1999; Russo et al., 2013), but not *in vivo*. One reason is that the coupling is quite weak and uncorrelated cortical inputs do not produce correlated FSI firing. A second reason is that, even in slice, demonstrating FSI coupling required repetitive action potential initiation in one of a pair of coupled neurons. The high cortical input correlation required to synchronize FSIs does indeed occur transiently during motor activity. Gage et al. (2010) show that large number of FSIs are active around the time of action selection, and motor planning has been suggested to result in increases in cortical spike synchronization (Riehle et al., 1997, 2000). Our model thus makes an important, experimentally testable prediction: selectively inhibiting gap junctions is sufficient to restore striatal firing and β-band oscillatory activity in the Parkinsonian striatum to control levels.

The dopamine-depleted striatum was sensitive to changes in cortical correlation and increased cortical correlation was critical to produce increased striatal oscillations. This suggests that a positive feedback loop, from cortex, to striatum, and ultimately back to cortex is required for the oscillations observed *in vivo*. If the increase in cortical correlation lasts for a long period of time, the striatum has multiple opportunities to

respond to and transmit this increase in cortical correlation. Even if the increase in cortical correlation is transient, as observed during behavior (Averbeck and Lee, 2004; Harris and Thiele, 2011), the striatal network model requires less than 60 ms to respond to a change in cortical correlation. The striatal output reaches the cortex via the globus pallidus; thus the feedback loop will not function if this structure decorrelates striatal output. The increased synchrony in the globus pallidus during dopamine depletion (Brown, 2007) and the oscillatory feedback loop between globus pallidus and subthalamic nucleus (Plenz and Kital, 1999) appears to amplify, rather than reduce, striatal oscillations. Furthermore, the recently discovered feedback connections from globus pallidus to striatum (Mallet et al., 2012b) may be an additional source of synchronizing input to the striatum not yet included in our model. Collectively, our network simulations together with experimental observations suggest that the positive feedback loop of correlation from cortex to stratum and back to the cortex through the globus pallidus can produce the pathological synchrony and oscillations observed in Parkinson's disease. Opening up the feedback loop at any stage should normalize basal ganglia activity, and our model suggests the striatum is a plausible stage since reducing FFI synchrony, by blocking gap junctions of the FSIs, is sufficient to restore sensitivity of the striatum to changes in cortical synchrony to control levels.

GRANTS
This work was supported by ONR grant MURI N00014-10-1-0198 and through the joint NIH-NSF CRCNS program through NIAAA grant RO1AA016022.

Contributions

Conceived of project: Sriraman Damodaran, Kim T. Blackwell

Designed research: Sriraman Damodaran, Kim T. Blackwell

Wrote chapter: Sriraman Damodaran, Kim T. Blackwell

Edited chapter: Sriraman Damodaran, Kim T. Blackwell, John R. Cressman, Zbigniew Jedrzejewski-Szmek

Updated model: Sriraman Damodaran

Ran simulations: Sriraman Damodaran

Analyzed data: Sriraman Damodaran, John R. Cressman, Zbigniew Jedrzejewski-Szmek, Kim T. Blackwell

Citation

Damodaran S, John R. Cressman, Zbigniew Jedrzejewski-Szmek, Blackwell KT. **(in press)** Desynchronization of fast spiking interneurons reduces β-band oscillations and imbalance in firing in the dopamine-depleted striatum. *J Neurosci*

CHAPTER FOUR: CALCIUM DYNAMICS PREDICTS DIRECTION OF SYNAPTIC PLASTICITY IN STRIATAL SPINY PROJECTION NEURONS

Abstract

The striatum is a major site of learning and memory formation for sensorimotor and cognitive association. One of the mechanisms used by the brain for memory storage is synaptic plasticity – the long lasting, activity-dependent change in synaptic strength. All forms of synaptic plasticity require an elevation in intracellular calcium, and a common hypothesis is that the amplitude and duration of calcium transients can determine the direction of synaptic plasticity. The utility of this hypothesis in the striatum is unclear in part because dopamine is required by striatal plasticity and in part because of the diversity in stimulation paradigms. To test whether calcium can predict plasticity direction, we developed a calcium-based plasticity rule using a model MSN with sophisticated calcium dynamics including calcium diffusion, buffering, and pump extrusion. We utilize a spike-timing-dependent plasticity (STDP) induction paradigm, in which post-synaptic potentials are paired with precisely timed action potentials and the timing of such pairing determines whether potentiation or depression will occur. Results show that calcium amplitude and duration are sufficient to predict a wide range of experimental plasticity outcomes.

Introduction

The striatum, the principal input nucleus of the basal ganglia, is a major site of learning and memory formation for sensorimotor and cognitive association. A biophysical mechanism underlying memory storage is activity-dependent plasticity (Magee and Johnston, 1997; Markram et al., 1997; Bi and Poo, 1998; Campanac and Debanne, 2008), which is the change in synaptic strength in response to patterns of synaptic input. Both long term potentiation (LTP) and long term depression (LTD) can be induced with different stimulation patterns at corticostriatal synapses (Calabresi et al., 1996; Mahon et al., 2004; Costa, 2007; Kreitzer and Malenka, 2008; Wickens, 2009; Fino and Venance, 2010), and the change in synaptic plasticity after learning (Hawes et al., *In Press*; Yin et al., 2009) demonstrates its relevance for learning. Additionally, corticostriatal plasticity is significantly modulated in several pathologies affecting the basal ganglia (Calabresi et al., 1996; Kreitzer and Malenka, 2008; Lovinger and Mathur, 2012). Therefore, understanding the mechanisms underlying synaptic plasticity will illuminate mechanisms of memory storage in health and disease.

Though diverse signaling pathways are recruited by different stimulation patterns, all forms of cortico-striatal synaptic plasticity requires an elevation in intracellular calcium concentration. One of the methods of inducing synaptic plasticity is by pairing post-synaptic potentials with precisely timed action potentials, a phenomenon called spike-timing-dependent plasticity (STDP). Pairing of back-propagating action potentials (bAPs) with either glutamate uncaging (Carter and Sabatini, 2004) or naturally occurring upstates (Kerr and Plenz, 2002, 2004) increases the calcium transients produced by

synaptic inputs to MSNs. The increase in calcium transients caused by pairing has the potential to engage STDP mechanisms as was shown by (Shindou et al., 2011), who reported a spine calcium threshold for induction of LTD at corticostriatal synapses in response to STDP protocols. A common hypothesis is that the amplitude and duration of calcium transients can determine the direction of synaptic plasticity (Evans and Blackwell, *In Press*), and a recent computational implementation of this hypothesis Graupner and Brunel (2012) was able to predict a large diversity of STDP curves in the hippocampus and cortex. But it is not clear whether calcium alone can predict striatal synaptic plasticity, in part because dopamine is critical for striatal synaptic plasticity.

We developed a calcium-based plasticity rule using a model MSN with sophisticated calcium dynamics including calcium diffusion, buffering, and pump extrusion to answer the following questions : 1) Can a calcium-based plasticity rule reliably replicate corticostriatal plasticity in both classes of MSNs in response to diverse STDP protocols? 2) Can a calcium-based plasticity rule account for the effects of chronic dopamine on striatal plasticity? The results indicate that calcium amplitude and duration together can predict a wide range of experimental plasticity outcomes.

Materials and Methods

MSN morphology

We modified a previously published MSN model (Evans et al., 2013), which had realistic electrophysiological activity and calcium dynamics, by incorporating spines. The morphology of the MSN model consisted of 189-compartments with 4 primary dendrites

subdivided into 8 secondary and then 16 tertiary dendrites. Each primary dendrite was 12 µm long, secondary dendrites were 14 µm and tertiary dendrites were comprised of 11 contiguous 18-µm-long compartments. Spines, comprised of a 0.5 µm diameter, 0.5 µm length cylindrical head compartment and 0.12 µm diameter, 0.5 µm length cylindrical neck compartment, were added at a density of 0.3 / µm to primary, secondary and tertiary dendrites.

Ionic channels

The ionic channels in this model are similar to our previous model (Evans et al., 2013), with conductance densities adjusted to produce shallow afterhyperpolarizations (AHPs) similar to that measured in dorsal striatum. Briefly, the model contains one fast sodium channel (Naf) (Ogata and Tatebayashi, 1990) and four voltage-gated potassium channels: a fast potassium A channel (Kaf, Kv4.2) (Tkatch et al. 2000), a slow potassium A channel (Kas, Kv1.2) (Shen et al., 2004), a resistant persistent potassium channel (Krp) (Nisenbaum and Wilson, 1995), and an inwardly rectifying potassium channel (Kir) (Steephen and Manchanda, 2009). The model also contains two calcium activated potassium channels: the big conductance BK channel and the small conductance SK channel. All equations governing the kinetics of these channels are described in (Evans et al., 2013).

Calcium dynamics

Five voltage gated calcium channels (VGCCs) are included in this model. High voltage activated channels include CaR (Foehring et al. 2000; Brevi et al. 2001), CaN (Cav2.2) (Kasai and Neher, 1992; Bargas et al., 1994; McNaughton and Randall, 1997), and

CaL1.2 (Cav1.2) (Kasai and Neher, 1992; Bargas et al., 1994; Wolf et al., 2005; Tuckwell, 2012). Low voltage activated channels include CaT (Cav3.3, α1G) (McRory et al., 2001) and CaL1.3 (Cav1.3) (Wolf et al., 2005; Tuckwell, 2012). All of these channels are distributed in the dendrites, whereas only CaR, CaL1.2 and CaL1.3 are included in the spines (Carter and Sabatini, 2004; Olson et al., 2005; Higley and Sabatini, 2010). Calcium channel kinetics and equations are in (Evans et al., 2013). For each calcium channel, the Goldman-Hodgkin-Katz (GHK) formula is applied to accurately compute the driving potential for these channels.

Calcium dynamics were implemented using the calcium *difshell* object in GENESIS, which integrates changes to calcium concentration produced by calcium influx, buffers, pumps and diffusion (Evans et al., 2013). A thin (0.1μm) submembrane shell was created as the outermost shell and concentric shells progressively doubling in thickness were added within the soma and each dendritic electrical compartment. One dimensional calcium diffusion between calcium compartments occurred at a rate of 200μm^2/sec (Allbritton et al.1992). Calcium extrusion was achieved by the addition of two Michaelis-Menten pumps in the spines and submembrane shells: a high affinity pump (K_m=0.3e-3 mM) representing the plasma membrane calcium exchanger, with K_{cat}=85 pmol/(cm^2/s) in the soma, 12 pmol/(cm^2/s) in the dendrites and 7 pmol/(cm^2/s) in the spines; and a low affinity pump (K_m=1e-3 mM) representing the sodium calcium exchanger, with K_{cat}= 30 pmol/(cm^2/s) in the spines. The endogenous calcium buffers calbindin and calmodulin (both N and C terminal binding site) were included using the

difbuffer object in GENESIS, with concentrations and kinetics taken from published models (Evans et al., 2013).

Ca^{2+} dynamics in the dendritic spine and dendritic shaft were tuned to match the response to two-photon uncaging of glutamate, or somatically evoked action potentials (Shindou et al., 2011) (Fig 1). The AMPA and NMDA receptors were located on spine heads, with the NMDA/AMPA ratio for both MSN classes set to 1/1, which falls in the middle of the range reported in the striatum (Logan et al., 2007; Popescu et al., 2007; Ding et al., 2008). The conductance of the AMPA receptor channels and the density of voltage-dependent calcium channels (VDCC) in the spines were adjusted to produce the measured peak calcium concentration in the presence of 300 µM Fluo5F (Shindou et al., 2011). For the cases where the effects of simple calcium dynamics were tested a single time constant of decay was used to model calcium dynamics in the spines, with the calcium in the dendritic shafts still modeled using sophisticated calcium dynamics.

Plasticity rule

To evaluate the ability of calcium dynamics to predict plasticity, we developed a weight change rule based on calcium dynamics (in the absence of Fluo5F) in the post-synaptic density (PSD) region of the spine (Fig 2D). The weight of the cortico-striatal synapse was set to increase if the amplitude of the postsynaptic calcium transient was larger than the higher, potentiation thresholds. The weight was set to decrease if the amplitude of the postsynaptic calcium transient was lower than the potentiation threshold but higher than the lower, depression threshold. No change in weight occurred if the calcium was below the depression threshold.

STDP protocols

The plasticity rule was applied to three different STDP protocols which experimentally blocked $GABA_A$ receptors. This was done because GABA has been reported to reverse STDP in the striatum through modulation of calcium channels (Paille et al., 2013). The first protocol consisted of 4-60 pairings of a single bAP (induced with 4 ms 1 nA somatic current injection) repeated at 0.1 Hz, with the bAP preceded by an EPSP (Pre-Post, Δt =+10 ms) or the bAP followed by an EPSP (negative timing, Δt=-30 ms) (Pawlak and Kerr, 2008). Δt is measured from the onset of the EPSP to the onset of the bAP. The second protocol consisted of 60 pairings repeated at 1 Hz of a single bAP evoked with a longer duration (30 ms) but lower amplitude (0.7 nA) current injection (Fino et al., 2010), with timing between the EPSP and bAP the same as for the previous protocol. The third protocol consisted of trains of five bursts (bursts separated by 200 ms) repeated at 0.1 Hz, with each burst composed of three bAPs (evoked by 5ms of 1nA somatic current injection, repeated at 50 Hz). For Pre-Post pairing, each bAP in the burst was preceded (+5 ms) by a single EPSP, yielding three EPSPs repeated at 50 Hz per burst, whereas for Post-Pre pairing the three bAPs were followed (-10 ms) by a single EPSP (Shen et al., 2008). Although this protocol delivered a different number of EPSPs for forward versus backward pairing, it was implemented since it was the only protocol applied to identified D1 and D2 MSNs and also to the dopamine depleted striatum.

Simulation

The model was implemented in GENESIS (Bower and Beeman, 2007) and simulations used a time step of 100 μs. The model was based on data from several mammalian

species of both sexes. The simulation and output processing software along with the files used for the simulations are freely available from the authors' website: (http://krasnow.gmu.edu/CENlab/) and modelDB (http://senselab.med.yale.edu/ModelDB/).

Results

We created a model of electrical activity and calcium dynamics in D1 and D2 MSNs in order to evaluate whether calcium dynamics could predict the direction of plasticity. Because of the complexity of synaptic plasticity rules and because changes in synaptic strength are likely to depend on spine calcium, calcium dynamics were explicitly controlled by diffusion, several buffers, and membrane pumps, both in the dendrites and in the spines. As in our previous model (Evans et al., 2013), Ca^{2+} transients produced in the dendritic shaft increase from the soma to the proximal tertiary dendrite, and then decrease with distance along the tertiary dendrite (Kerr and Plenz, 2002; Day et al., 2008), due to a decrease in sodium channel density. Prior to developing a calcium-based plasticity rule we adjusted calcium control mechanisms in the spines to replicate experimental measures of calcium dynamics in spines.

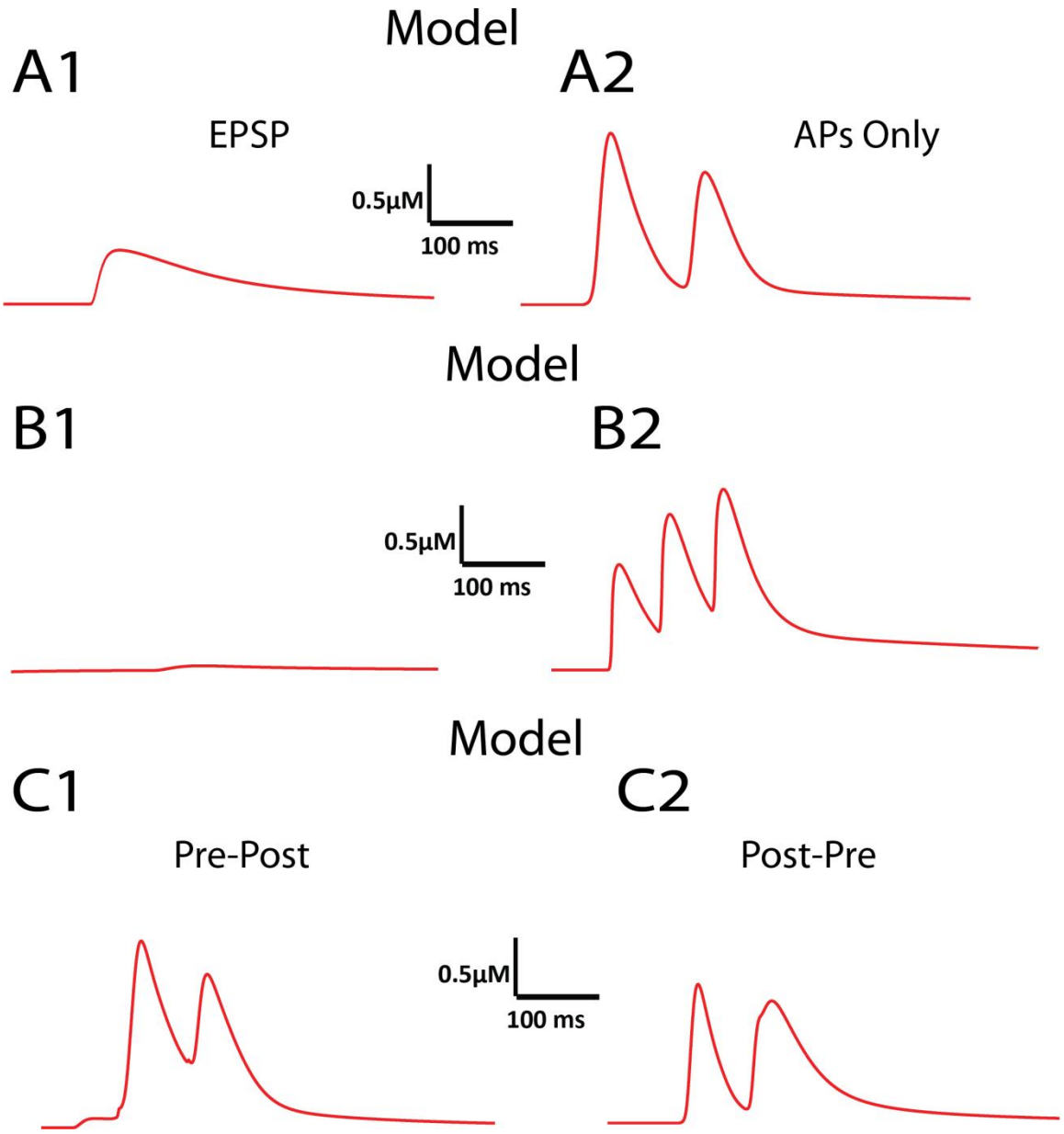

Figure 12. **Validation of calcium response in dendrite and dendritic spine. (A)** Simulated responses of calcium transients (in µM) in dendritic spines in response to EPSP alone (**A1**) and bAPs alone (**A2**). **(B)** Simulated responses of calcium transients (in µM) in dendritic shaft in response to EPSP alone (**B1**) and bAPs alone (**B2**). **(C)** Simulated responses of calcium transients (in µM) in dendritic spine in response to Pre-Post pairing of EPSP and three bAPs (Δt=+10ms) (**C1**) and Post-Pre pairing of EPSP and three bAPs (Δt=-30ms) (**C2**). Experimental traces were adapted from (Shindou et al., 2011). All traces show the calcium bound Fluo5F, converted to calcium concentration using the equation provided in Shindou et al. 2011.

Ca^{2+} transient activity replicates measurements in spines of MSNs

Ca^{2+} dynamics (amplitude and decay time of the calcium bound Fluo5F) in the dendritic spine and dendritic shaft were tuned to match the response to two-photon uncaging of glutamate onto spines (Shindou et al., 2011). In response to stimulation of a spine on the tertiary dendrite of a model neuron, small Ca^{2+} transients were produced in the spine head (0.2 μM; Fig 1A1), because very little NMDA current was activated. Even smaller Ca^{2+} transients were produced in the dendritic shaft (0.05 μM; Fig 1B1), because of low diffusional coupling via the spine neck. Similar transients in dendritic spines are observed at different distances from the soma.

Back-propagating action potentials from the soma also give rise to calcium influx into dendrites and dendritic spines (Day et al., 2006; Shindou et al., 2011). Calcium transients in the dendritic spine in response to bAP induced by somatic current injection in the model neuron also were tuned to match experimental reports (spine : 0.5 μM; Fig 1A2, shaft: 0.55 μM; Fig 1B2; Carter and Sabatini, 2004; Day et al., 2008; Shindou et al., 2011), by adjusting VDCC density and conductance in the spine head. The peak amplitude of the calcium transients in response to the bAP in the spine head is similar to that in the dendritic shaft (in contrast to the different peak concentrations seen with spine stimulation) because the VDCC in both the spine head and shaft are activated by the invasion of the bAPs.

Using the MSN model with calcium tuned to match spine stimulation or back-propagating action potentials alone, the response to paired stimuli was simulated. To verify the calcium dynamics, this pairing simulation experiment employed the protocol of Shindou et al. (2011; see Materials and Methods) . Experimentally, when three action

potentials were evoked after the presynaptic stimulation (Δt = +10ms, Pre-Post), the pairing produced a large calcium transient (1.9 μM; Fig 1C1), whereas when the action potentials were evoked before the presynaptic stimulation (Δt = -30ms, Post-Pre) the pairing resulted in a smaller calcium transient (1.51 μM; Fig 1C2). In the simulation, the Pre-Post calcium transient was close to 20% higher than the Post-Pre calcium transient, similar to that measured experimentally (Shindou et al., 2011). In contrast to the calcium influx seen in the spines, in both simulations and experiments the calcium influx in the dendritic shaft in response to the pairing protocols showed very small differences between the pre-post (0.55 μM) and post-pre (0.53 μM) protocols. This validates the calcium model, and demonstrates that it can accurately replicate the sensitivity of calcium transients in the spine and the dendrite to paired stimuli.

Synaptic weight change in MSNs predicted by Ca^{2+} transient activity for several STDP paradigms

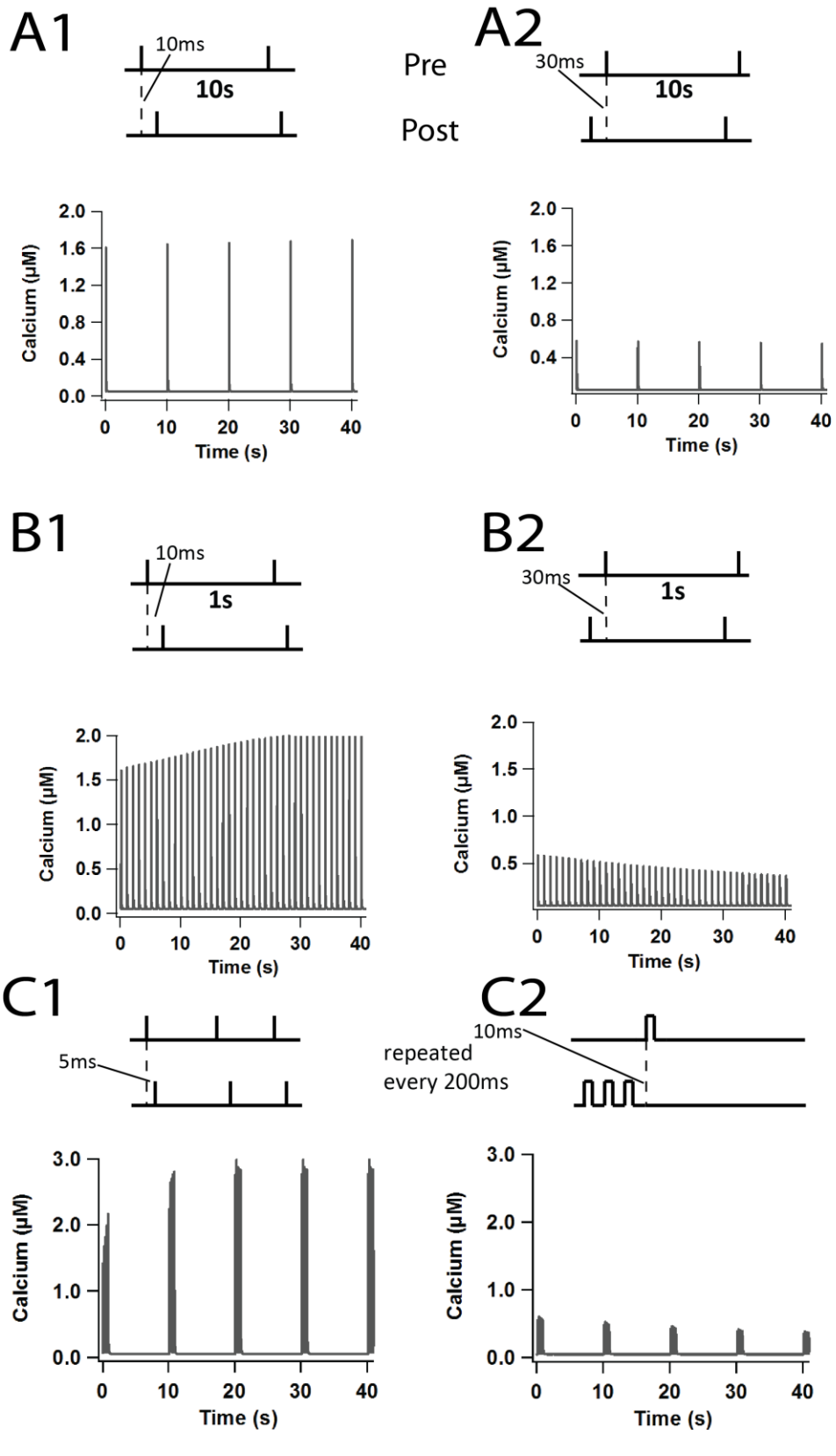
A1
10ms
10s
A2
Pre
Post
30ms
10s
Calcium (µM)
Time (s)
B1
10ms
1s
B2
30ms
1s
C1
5ms
C2
10ms
repeated
every 200ms

Figure 13. **Calcium transients and plasticity rule in response to a single pairing of three different STDP protocols. (A)** A single bAP evoked with a 4ms, 1nA somatic current injection is paired with a single EPSP (Pawlak and Kerr, 2008). The EPSP either preceded the bAP (Pre-Post, Δt =+10 ms; **A1**) or followed the bAP (Post-Pre, Δt =-30 ms; **A2**). The peak calcium transients in the PSD region of the spine head in Pre-Post case were ~ 2.5 times greater than that seen in Post-Pre. **(B)** A single bAP was evoked with a longer duration (30 ms) but lower amplitude (0.7 nA) current injection (Fino et al., 2010). The timing between the EPSP and bAP was similar to **(A).** The difference in peak calcium transients in the spine head was similar to the protocol in **(A)**. **(C)** The protocol of (Shen et al., 2008) consisted of five bursts, with each burst composed of three bAPs (evoked by current injection, 1nA). For Pre-Post, the three EPSPs repeated at 50 Hz (Δt =+5 ms; **C1**) were each followed by a single bAP, whereas for Post-Pre three bAPs repeated at 50 Hz were followed by one EPSP (Δt =-10 ms; **C2**). In response to this protocol the peak calcium transients in the spine head in Pre-Post case were around 6 times greater than that seen in Post-Pre.

Using the validated calcium dynamics model, we first evaluated the calcium transient at the PSD region of the spine head in response to a single pairing of three different protocols in both D1 and D2 MSN models. The first protocol consisted of multiple pairings repeated at 0.1 Hz of a single bAP evoked with a 4ms, 1nA somatic current injection paired with a single EPSP. The EPSP either preceded the bAP (Pre-Post, Δt= +10 ms) or followed the bAP (Post-Pre, Δt =-30 ms) (Pawlak and Kerr, 2008). In response to this protocol the peak calcium transients in the PSD region of the spine head in Pre-Post case were ~ 4 times greater than that seen in Post-Pre (Fig 2A). This suggests that the difference in timing of the paired stimuli is sufficient to produce a difference in the spine calcium transients, which may account for the different direction in plasticity. The second protocol consisted of multiple pairings repeated at 1 Hz of a single bAP evoked with a longer duration (30 ms) but lower amplitude (0.7 nA) current injection (Fino et al., 2010). Otherwise, the timin.g between the EPSP and bAP was similar to the previous protocol. In response to this protocol the difference in peak calcium transients in the spine head was similar to the previous protocol (Fig 2B), again able to account for the difference in plasticity direction. The third protocol consisted of pairing of five bursts repeated at 0.1 Hz, with each burst composed of three bAPs (evoked by 5 ms of 1 nA

somatic current injection). For Pre-Post, the three EPSPs repeated at 50 Hz (each to a separate spine) were each followed by a single bAP (Δt =+5 ms), whereas for Post-Pre three bAPs repeated at 50 Hz were followed by one EPSP (Δt =-10 ms) (Shen et al., 2008). In response to this protocol the peak calcium transients in the spine head in Pre-Post case were around 5 times greater than that seen in Post-Pre (Fig 2C). Note that for all three protocols, the peak calcium in D2 MSNs was greater than that in D1 MSNs, though in all cases pre-post produced greater calcium than post-pre (data not shown).

We then derived a synaptic weight change model based on both amplitude and duration of the calcium transient in the PSD region of the spine head. The goal was to derive a single rule, with a single set of parameters, which could account for plasticity outcomes for all three protocols. At each simulation time step, the calcium concentration was compared to two thresholds, a higher, potentiation threshold and a lower, depression threshold (Fig 3A). The weight of the cortico-striatal synapse was set to increase continually while the amplitude of the postsynaptic calcium transient was larger than the potentiation threshold. The weight was set to decrease continually while the amplitude of the postsynaptic calcium transient was between the potentiation and depression thresholds. No change in weight occurred if the calcium was below the depression threshold. This rule was applied to calcium transients that changed over time and hence the weight change accumulated for the duration that the calcium remained above (or below) the thresholds.

The plasticity rule was first applied to a single pairing of each protocol in order to illustrate the operation of the plasticity rule. Fig 3B shows the change in weight over time

for one of the protocols (Fino et al., 2010). The synaptic weight first increases during the peak of the calcium transient, and then the weight decreases slightly once the calcium drops below the LTP threshold, though the net weight change remains that of potentiation. Despite the variation in calcium for the different protocols, a single weight change rule can explain the change in synaptic weight for all three STDP paradigms. In response to all protocols the cumulative increases and decreases in response to Pre-Post resulted in a net increase in synaptic weight, measured when the calcium returns to basal, whereas Post-Pre produced a reduction in synaptic weight.

Sensitivity of calcium to spike timing

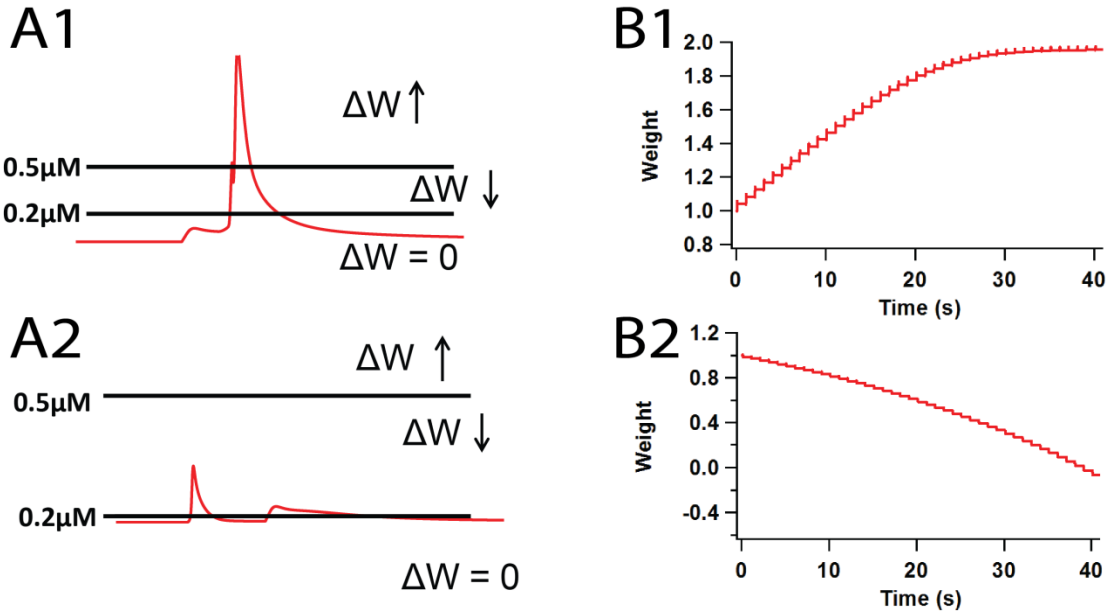

Figure 14. Two threshold plasticity rule and change in synaptic weight over time. (A) The weight of the cortico-striatal synapse was set to increase (upward arrow; **A1**) if the amplitude of the postsynaptic calcium transient was larger than the potentiation threshold (1.8 μM). The weight was set to decrease if the amplitude of the postsynaptic calcium transient was between the potentiation (T_{LTP}) and depression (T_{LTD}) thresholds (**A2**). No change in weight occurred if the calcium was below the depression threshold. **(B)** The change in weight for the Fino et al. 2006 protocol in response to Pre-Post (**B1**) and Post-Pre (**B2**) protocols. The default weight was one with the maximum weight capped at two and minimum capped at zero.

To further validate the calcium dynamics and plasticity rule, the dependence of synaptic plasticity on different calcium sources was evaluated. The source of spine calcium that contributes to LTP is the NMDA receptor (NMDAR) (Calabresi et al., 1992; Kerr and Wickens, 2001; Dan and Poo, 2004; Pawlak and Kerr, 2008; Kreitzer and Malenka, 2008; Di Filippo et al., 2009; Fino and Venance, 2010) and thus the next set of simulations tested the impact of the NMDAR on the calcium output and plasticity outcome in the model. When NMDARs were blocked (by setting conductance to zero) the peak amplitude of the calcium transient in response to Pre-Post was significantly reduced, resulting in similar calcium amplitudes in response to both Pre-Post and Post-Pre timing (Fig 4A). These altered calcium dynamics result in the absence of both LTP and LTD in response to the protocol of Pawlak and Kerr (2008; Fig 4B) and is consistent with their results during NMDAR block. These results suggest that calcium dynamics that accurately model the sensitivity to timing of pre- and postsynaptic activity is sufficient to predict the effect of blocking NMDAR on cortico-striatal plasticity.

The distance-dependent variation in calcium due to the bAP (Kerr and Plenz, 2004; Day et al., 2008) suggests that the plasticity evoked with STDP protocols may be less effective at distal synapses, thus simulations were repeated using spines on primary dendrites and more distal tertiary branches. Stimulation of spines on primary dendritic branches (12 μm from soma) produced similar calcium transients to stimulation of spines on proximal (80 μm from soma) and distal (206 μm from soma) tertiary branches during Pre-Post pairing, but significantly higher calcium transients during Post-Pre pairing (data not shown). This resulted in a smaller difference in transients between Pre-Post and Post-

Pre pairing when spines on more proximal branches, specifically primary branches, were stimulated. These results suggest that stimulating more distal dendrites can possibly result in bigger differences in calcium transients between Pre-Post and Post-Pre pairing.

Calcium-based rule not sufficient to explain all dopamine-depletion changes to cortico-striatal plasticity

Unlike plasticity at hippocampal or cortical synapses, dopamine has been shown to be critical for synaptic plasticity at cortico-striatal synapses. Acute block of dopamine D1 receptors prevents LTP induced by high frequency stimulation (Calabresi et al., 2007), theta burst (Hawes et al., 2013) as well as STDP (Pawlak and Kerr, 2008). Acute block of dopamine D2 receptors produces less consistent changes, with one report of no change to either LTP or LTD induced by STDP (Pawlak and Kerr, 2008) or in response to HFS (Calabresi et al., 1997; Kreitzer and Malenka, 2007). D1R or A2A adenosine receptors are required to produce the cAMP and PKA crucial for synaptic plasticity (Surmeier et al., 1996; Rivera et al., 2002; Spencer and Murphy, 2002), but dopamine also influences calcium dynamics, and its absence could disrupt plasticity through these changes. Therefore, the impact of dopamine-depletion-induced cellular changes to MSNs on the calcium responses to STDP protocols and consequently on synaptic weight change was investigated next.

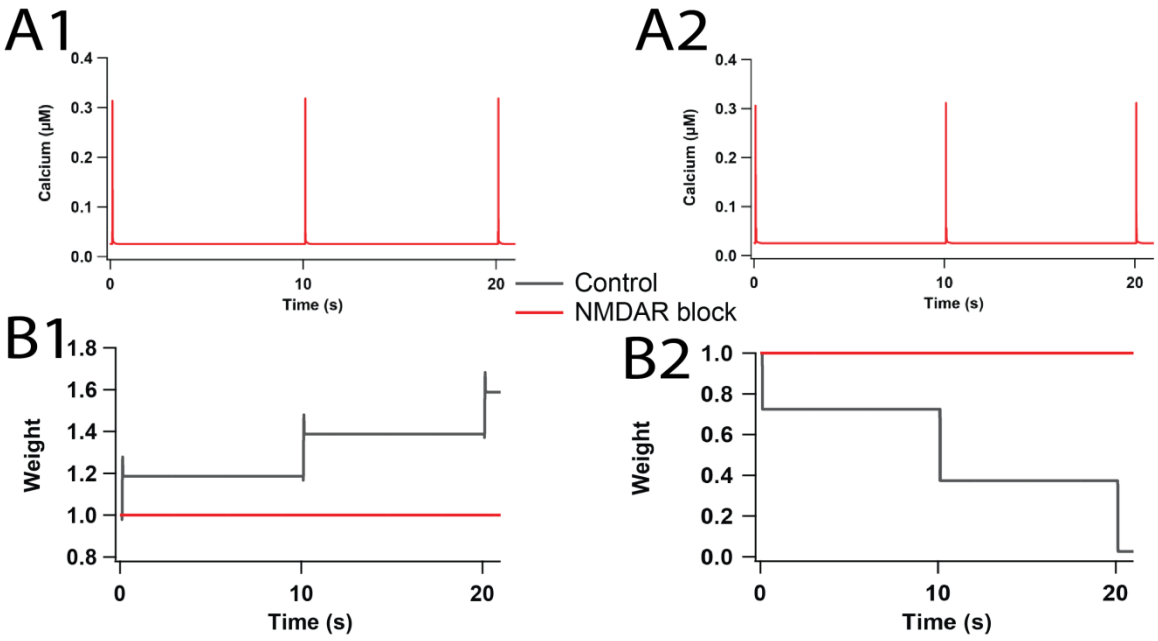

Figure 15. Contribution of NMDARs to corticostriatal STDP. (**A**) When the conductance of NMDAR was set to zero the peak calcium in response to Pre-Post (**A1**) and Post-Pre (**A2**) timing were smaller than that seen in control and was similar to each other in response to the Kerr Protocol. (**B**) The weight of the synapses did not change in both the Pre-Post (**B1**) and Post-Pre (**B2**) protocols when NMDAR conductance was set to zero.

To investigate the change in plasticity we implement the cellular changes reported after dopamine depletion, which include an increase in D2 MSN dendritic excitability (Day et al., 2006, 2008), a reduction in D2 MSN somatic excitability (Chan et al., 2012) and a halving of the NMDA:AMPA ratio to both MSNs (Bagetta et al., 2012). In response to the STDP protocols implemented by Shen et al. (2008) on D2 MSNs, there was a dramatic reduction in the calcium transients in response to Pre-Post timing, and a smaller reduction in the calcium in response to Post-Pre timing resulting in similar calcium transient levels between both timing protocols (Fig 5A). This resulted in the absence of both LTP and LTD (Fig 5B). A similar result was seen in response to the other two protocols (data not shown). Nonetheless, these results disagree with Shen et al. (2008), who reported an induction of only LTD in D1 MSNs in response to both timing

protocols but a presence of only LTP in D2 MSNs. This effect can potentially be accounted for if the potentiation and depression thresholds were reduced as may be expected from homeostatic plasticity mechanisms (Turrigiano, 2012).

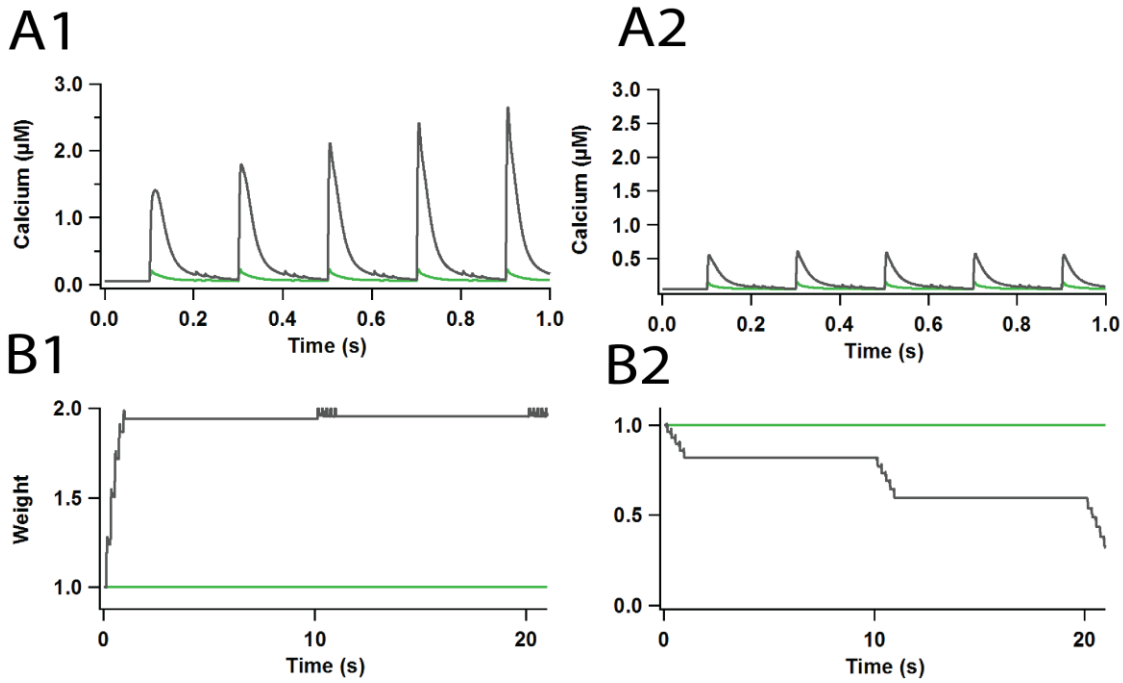

Figure 16. The effect of chronic dopamine depletion on calcium transients and on synaptic weight. (A) In response to the protocols of Shen et al. (2008) D2 MSNs had decreased calcium transients in both Pre-Post (**A1**) and Post-Pre (**A2**) protocols during the dopamine-depleted condition (green) as compared to the control condition (Grey). (**B**) The weight of the synapses did not change in both the Pre-Post (**B1**) and Post-Pre (**B2**) protocols during the dopamine-depleted condition.

Discussion

A mechanistic understanding of how diverse stimulation protocols, working through calcium activated signaling pathways, control corticostriatal plasticity would greatly improve our understanding of mechanisms underlying memory storage (Calabresi et al., 2007; Kreitzer and Malenka, 2007). The change in synaptic strength is hypothesized to be a result of the interaction between cellular processes sensitive to the timing of pre- and

postsynaptic activity, which controls calcium influx through NMDAR and VDCC. Our model evaluated whether calcium dynamics alone can predict the direction of plasticity for a range of STDP protocols. Similar to models accounting for neocortical or hippocampal STDP experiments (Shouval et al., 2002; Kumar and Mehta, 2011; Graupner and Brunel, 2012), we constructed a plasticity rule based on the amplitude and duration of calcium elevation in response to plasticity paradigms. Our model is unique in that it uses sophisticated calcium dynamics, and this allows us to account for plasticity results using several induction paradigms (Pawlak and Kerr, 2008; Shen et al., 2008; Fino et al., 2010) with a single set of model parameters.

Amplitude, duration and location of calcium are critical

As has been discussed previously (summarized in Evans and Blackwell, *In Press*), calcium amplitude alone is not sufficient to predict plasticity direction. Indeed, the calcium in response to Post-Pre for the burst protocol exceeds that of the other Pre-Post protocols; thus the plasticity rule implicitly uses both amplitude and duration of calcium dynamics. The plasticity rule was robust to changes in the two thresholds suggesting that the amplitude and duration of the calcium transients invoked by these three protocols can reliably predict the direction of weight change at the synapses. Though not included in the model, the amplitude and duration of the calcium elevation influences the activation of downstream signaling molecules, such as kinases and phosphatases, as has been shown in several models (Rubin et al., 2005; Carlson and Giordano, 2011). The ability for a two threshold plasticity rule to predict experimental plasticity outcomes suggests that the

different affinities and kinetics of downstream signaling molecules can translate calcium dynamics into potentiation or depression of synapses.

In addition to calcium amplitude and duration, the location or source of the calcium elevation influences the direction of plasticity. In our model, as in experiments, NMDAR was found to be critical in allowing MSNs to be sensitive to pre- and postsynaptic activity. Blocking NMDAR in our model lowered the calcium in response to both Pre-Post and Post-Pre timing, thereby eliminating LTP and LTD. This result is consistent with the only experimental report of blocking NMDARs in the striatum in response to a STDP protocol (Pawlak and Kerr 2008).

Interactions of Dopamine and Calcium in Synaptic Plasticity

Unlike the neocortex and striatum, both calcium and dopamine are critical for cortico-striatal synaptic plasticity. Dopamine acting through D1 receptors is required to produce the cAMP and PKA crucial for synaptic potentiation (Surmeier et al., 1996; Rivera et al., 2002; Spencer and Murphy, 2002; Yagishita et al., 2014). On the other hand, the contribution of D1 receptor signaling to LTD is unclear, and post-synaptic D2 receptors inhibit cAMP and PKA, expected to oppose LTP (Kreitzer and Malenka, 2008). One possibility is that dopamine acting through pre-synaptic D2 receptors are important for release of acetylcholine which is implicated in synaptic plasticity. In particular, muscarinic receptors are required for LTD induced by HFS (Wang et al., 2006) and STDP (Fino et al., 2010). Both calcium and the Gq subtype of GTP binding protein activated by muscarinic M1 receptors interact to produce endocannabinoids required for

LTD. Though our model did not include muscarinic or dopamine receptors, our results do not imply that these metabotropic receptors are unnecessary.

Though most experiments evaluating the role of dopamine in plasticity apply receptor antagonists acutely, chronic depletion of dopamine also produces deficits in synaptic plasticity. In addition to the lack of acutely released dopamine, chronic dopamine depletion produces changes to MSN electrical activity which modifies calcium dynamics. Thus, we evaluated whether the synaptic plasticity deficits observed in dopamine depletion can be predicted by the changes in cell excitability and calcium dynamics. We simulated the calcium elevation and applied the plasticity rule to dopamine depleted D1and D2 MSNs, and observed the absence of plasticity. These results agree with experimental measurements in the striatum in response to higher frequency protocols (Calabresi et al., 2007; Kreitzer and Malenka, 2008) but not the unidirectional plasticity observed in response to a STDP protocol (Shen et al., 2008). Our simulations cannot rule-out that altered plasticity is caused by effects of dopamine on calcium dynamics. One possibility is that additional, but as yet unknown cellular changes affect MSNs after dopamine depletion. Alternatively, the chronic changes in synaptic inputs and excitability may be accompanied by a change in the plasticity thresholds, i.e., homeostatic plasticity as is observed in cortex (Turrigiano, 2012). In other words, chronic dopamine depletion may also be accompanied by changes in the LTP and LTD thresholds for D2 MSNs. If the LTP and LTD thresholds were lowered, these neurons might exhibit LTD or LTP only, depending on the threshold values. A change in threshold could be evaluated experimentally by using weaker plasticity

induction stimuli: model simulations predict that applying either of the single spike protocols to dopamine depleted D2 MSNs would yield LTD.

Contributions

Conceived of project: Sriraman Damodaran, Kim T. Blackwell

Designed research: Sriraman Damodaran, Kim T. Blackwell

Wrote chapter: Sriraman Damodaran, Kim T. Blackwell

Edited chapter: Sriraman Damodaran, Kim T. Blackwell

Updated model: Sriraman Damodaran

Ran simulations: Sriraman Damodaran

Citation

Damodaran S, Blackwell KT. Calcium dynamics predicts direction of synaptic plasticity in striatal spiny projection neurons. *(In Preparation.)*

REFERENCES

Adermark L, Lovinger DM (2007) Combined activation of L-type Ca2+ channels and synaptic transmission is sufficient to induce striatal long-term depression. J Neurosci Off J Soc Neurosci 27:6781–6787.

Albin RL, Young AB, Penney JB (1989) The functional anatomy of basal ganglia disorders. Trends Neurosci 12:366–375.

Alexander ME, Wickens JR (1993) Analysis of striatal dynamics: the existence of two modes of behaviour. J Theor Biol 163:413–438.

Allbritton NL, Meyer T, Stryer L (1992) Range of messenger action of calcium ion and inositol 1,4,5-trisphosphate. Science 258:1812–1815.

Arbuthnott GW, Ingham CA, Wickens JR (2000) Dopamine and synaptic plasticity in the neostriatum. J Anat 196 (Pt 4):587–596.

Averbeck BB, Lee D (2004) Coding and transmission of information by neural ensembles. Trends Neurosci 27:225–230.

Bagetta V, Sgobio C, Pendolino V, Papa GD, Tozzi A, Ghiglieri V, Giampà C, Zianni E, Gardoni F, Calabresi P, Picconi B (2012) Rebalance of Striatal NMDA/AMPA Receptor Ratio Underlies the Reduced Emergence of Dyskinesia During D2-Like Dopamine Agonist Treatment in Experimental Parkinson's Disease. J Neurosci 32:17921–17931.

Bargas J, Howe A, Eberwine J, Cao Y, Surmeier DJ (1994) Cellular and molecular characterization of Ca2+ currents in acutely isolated, adult rat neostriatal neurons. J Neurosci Off J Soc Neurosci 14:6667–6686.

Beatty JA, Sullivan MA, Morikawa H, Wilson CJ (2012) Complex autonomous firing patterns of striatal low-threshold spike interneurons. J Neurophysiol 108:771–781.

Bennett BD, Bolam JP (1994) Synaptic input and output of parvalbumin-immunoreactive neurons in the neostriatum of the rat. Neuroscience 62:707–719.

Bergman H, Wichmann T, DeLong MR (1990) Reversal of experimental parkinsonism by lesions of the subthalamic nucleus. Science 249:1436–1438.

Bergman H, Wichmann T, Karmon B, DeLong MR (1994) The primate subthalamic nucleus. II. Neuronal activity in the MPTP model of parkinsonism. J Neurophysiol 72:507–520.

Berke JD (2008) Uncoordinated firing rate changes of striatal fast-spiking interneurons during behavioral task performance. J Neurosci Off J Soc Neurosci 28:10075–10080.

Berke JD (2009) Fast oscillations in cortical-striatal networks switch frequency following rewarding events and stimulant drugs. Eur J Neurosci 30:848–859.

Berke JD, Okatan M, Skurski J, Eichenbaum HB (2004) Oscillatory entrainment of striatal neurons in freely moving rats. Neuron 43:883–896.

Bi GQ, Poo MM (1998) Synaptic modifications in cultured hippocampal neurons: dependence on spike timing, synaptic strength, and postsynaptic cell type. J Neurosci Off J Soc Neurosci 18:10464–10472.

Blackwell KT, Czubayko U, Plenz D (2003) Quantitative estimate of synaptic inputs to striatal neurons during up and down states in vitro. J Neurosci Off J Soc Neurosci 23:9123–9132.

Bower JM, Beeman D (2007) Constructing realistic neural simulations with GENESIS. Methods Mol Biol Clifton NJ 401:103–125.

Bracci E, Centonze D, Bernardi G, Calabresi P (2002) Dopamine excites fast-spiking interneurons in the striatum. J Neurophysiol 87:2190–2194.

Brevi S, de Curtis M, Magistretti J (2001) Pharmacological and biophysical characterization of voltage-gated calcium currents in the endopiriform nucleus of the guinea pig. J Neurophysiol 85:2076–2087.

Brown P (2003) Oscillatory nature of human basal ganglia activity: relationship to the pathophysiology of Parkinson's disease. Mov Disord Off J Mov Disord Soc 18:357–363.

Brown P (2007) Abnormal oscillatory synchronisation in the motor system leads to impaired movement. Curr Opin Neurobiol 17:656–664.

Brown P, Williams D (2005) Basal ganglia local field potential activity: character and functional significance in the human. Clin Neurophysiol Off J Int Fed Clin Neurophysiol 116:2510–2519.

Burkhardt JM, Constantinidis C, Anstrom KK, Roberts DCS, Woodward DJ (2007) Synchronous oscillations and phase reorganization in the basal ganglia during akinesia induced by high-dose haloperidol. Eur J Neurosci 26:1912–1924.

Buzsáki G, Chrobak JJ (1995) Temporal structure in spatially organized neuronal ensembles: a role for interneuronal networks. Curr Opin Neurobiol 5:504–510.

Calabresi P, Maj R, Pisani A, Mercuri NB, Bernardi G (1992a) Long-term synaptic depression in the striatum: physiological and pharmacological characterization. J Neurosci Off J Soc Neurosci 12:4224–4233.

Calabresi P, Picconi B, Tozzi A, Di Filippo M (2007) Dopamine-mediated regulation of corticostriatal synaptic plasticity. Trends Neurosci 30:211–219.

Calabresi P, Pisani A, Mercuri NB, Bernardi G (1992b) Long-term Potentiation in the Striatum is Unmasked by Removing the Voltage-dependent Magnesium Block of NMDA Receptor Channels. Eur J Neurosci 4:929–935.

Calabresi P, Pisani A, Mercuri NB, Bernardi G (1996) The corticostriatal projection: from synaptic plasticity to dysfunctions of the basal ganglia. Trends Neurosci 19:19–24.

Calabresi P, Saiardi A, Pisani A, Baik JH, Centonze D, Mercuri NB, Bernardi G, Borrelli E (1997) Abnormal synaptic plasticity in the striatum of mice lacking dopamine D2 receptors. J Neurosci Off J Soc Neurosci 17:4536–4544.

Campanac E, Debanne D (2008) Spike timing-dependent plasticity: a learning rule for dendritic integration in rat CA1 pyramidal neurons. J Physiol 586:779–793.

Carlson KD, Giordano N (2011) Interplay of the magnitude and time-course of postsynaptic Ca2+ concentration in producing spike timing-dependent plasticity. J Comput Neurosci 30:747–758.

Carrillo-Reid L, Tecuapetla F, Tapia D, Hernández-Cruz A, Galarraga E, Drucker-Colin R, Bargas J (2008) Encoding network states by striatal cell assemblies. J Neurophysiol 99:1435–1450.

Carter AG, Sabatini BL (2004) State-dependent calcium signaling in dendritic spines of striatal medium spiny neurons. Neuron 44:483–493.

Centonze D, Grande C, Usiello A, Gubellini P, Erbs E, Martin AB, Pisani A, Tognazzi N, Bernardi G, Moratalla R, Borrelli E, Calabresi P (2003) Receptor subtypes involved in the presynaptic and postsynaptic actions of dopamine on striatal interneurons. J Neurosci Off J Soc Neurosci 23:6245–6254.

Chan CS, Peterson JD, Gertler TS, Glajch KE, Quintana RE, Cui Q, Sebel LE, Plotkin JL, Shen W, Heiman M, Heintz N, Greengard P, Surmeier DJ (2012) Strain-specific regulation of striatal phenotype in Drd2-eGFP BAC transgenic mice. J Neurosci Off J Soc Neurosci 32:9124–9132.

Chang J-Y, Shi L-H, Luo F, Woodward DJ (2006) Neural responses in multiple basal ganglia regions following unilateral dopamine depletion in behaving rats performing a treadmill locomotion task. Exp Brain Res 172:193–207.

Choi S, Lovinger DM (1997) Decreased frequency but not amplitude of quantal synaptic responses associated with expression of corticostriatal long-term depression. J Neurosci Off J Soc Neurosci 17:8613–8620.

Costa RM (2007) Plastic corticostriatal circuits for action learning: what's dopamine got to do with it? Ann N Y Acad Sci 1104:172–191.

Costa RM, Lin S-C, Sotnikova TD, Cyr M, Gainetdinov RR, Caron MG, Nicolelis MAL (2006) Rapid alterations in corticostriatal ensemble coordination during acute dopamine-dependent motor dysfunction. Neuron 52:359–369.

Courtemanche R, Fujii N, Graybiel AM (2003) Synchronous, focally modulated beta-band oscillations characterize local field potential activity in the striatum of awake behaving monkeys. J Neurosci Off J Soc Neurosci 23:11741–11752.

Cui G, Jun SB, Jin X, Pham MD, Vogel SS, Lovinger DM, Costa RM (2013) Concurrent activation of striatal direct and indirect pathways during action initiation. Nature 494:238–242.

Czubayko U, Plenz D (2002) Fast synaptic transmission between striatal spiny projection neurons. Proc Natl Acad Sci U S A 99:15764–15769.

Damodaran S, Cressman JR, Jedrzejewski-Szmek Z, Blackwell KT (In Press.) Desynchronization of fast spiking interneurons reduces β-band oscillations and imbalance in firing in the dopamine-depleted striatum. J Neurosci Off J Soc Neurosci.

Damodaran S, Evans RC, Blackwell KT (2014) Synchronized firing of fast-spiking interneurons is critical to maintain balanced firing between direct and indirect pathway neurons of the striatum. J Neurophysiol 111:836–848.

Dan Y, Poo M-M (2004) Spike timing-dependent plasticity of neural circuits. Neuron 44:23–30.

Day M, Wang Z, Ding J, An X, Ingham CA, Shering AF, Wokosin D, Ilijic E, Sun Z, Sampson AR, Mugnaini E, Deutch AY, Sesack SR, Arbuthnott GW, Surmeier DJ

(2006) Selective elimination of glutamatergic synapses on striatopallidal neurons in Parkinson disease models. Nat Neurosci 9:251–259.

Day M, Wokosin D, Plotkin JL, Tian X, Surmeier DJ (2008a) Differential excitability and modulation of striatal medium spiny neuron dendrites. J Neurosci Off J Soc Neurosci 28:11603–11614.

Day M, Wokosin D, Plotkin JL, Tian X, Surmeier DJ (2008b) Differential excitability and modulation of striatal medium spiny neuron dendrites. J Neurosci Off J Soc Neurosci 28:11603–11614.

DeLong MR (1990) Primate models of movement disorders of basal ganglia origin. Trends Neurosci 13:281–285.

Di Filippo M, Picconi B, Tantucci M, Ghiglieri V, Bagetta V, Sgobio C, Tozzi A, Parnetti L, Calabresi P (2009) Short-term and long-term plasticity at corticostriatal synapses: implications for learning and memory. Behav Brain Res 199:108–118.

Ding J, Peterson JD, Surmeier DJ (2008) Corticostriatal and thalamostriatal synapses have distinctive properties. J Neurosci Off J Soc Neurosci 28:6483–6492.

Draguhn A, Traub RD, Schmitz D, Jefferys JG (1998) Electrical coupling underlies high-frequency oscillations in the hippocampus in vitro. Nature 394:189–192.

Edgerton JR, Hanson JE, Günay C, Jaeger D (2010) Dendritic sodium channels regulate network integration in globus pallidus neurons: a modeling study. J Neurosci Off J Soc Neurosci 30:15146–15159.

Engelhard B, Ozeri N, Israel Z, Bergman H, Vaadia E (2013) Inducing Gamma Oscillations and Precise Spike Synchrony by Operant Conditioning via Brain-Machine Interface. Neuron 77:361–375.

Erisir A, Lau D, Rudy B, Leonard CS (1999) Function of specific K(+) channels in sustained high-frequency firing of fast-spiking neocortical interneurons. J Neurophysiol 82:2476–2489.

Evans RC, Blackwell KT (In Press) Calcium Amplitude, Duration, or Location? Biol Bull.

Evans RC, Maniar YM, Blackwell KT (2013) Dynamic modulation of spike timing-dependent calcium influx during corticostriatal upstates. J Neurophysiol 110:1631–1645.

Evans RC, Morera-Herreras T, Cui Y, Du K, Sheehan T, Kotaleski JH, Venance L, Blackwell KT (2012a) The Effects of NMDA Subunit Composition on Calcium Influx and Spike Timing-Dependent Plasticity in Striatal Medium Spiny Neurons. PLoS Comput Biol 8:e1002493.

Evans RC, Morera-Herreras T, Cui Y, Du K, Sheehan T, Kotaleski JH, Venance L, Blackwell KT (2012b) The effects of NMDA subunit composition on calcium influx and spike timing-dependent plasticity in striatal medium spiny neurons. PLoS Comput Biol 8:e1002493.

Fino E, Paille V, Cui Y, Morera-Herreras T, Deniau J-M, Venance L (2010) Distinct coincidence detectors govern the corticostriatal spike timing-dependent plasticity. J Physiol 588:3045–3062.

Fino E, Venance L (2010) Spike-timing dependent plasticity in the striatum. Front Synaptic Neurosci 2:6.

Flores-Barrera E, Laville A, Plata V, Tapia D, Bargas J, Galarraga E (2009) Inhibitory contribution to suprathreshold corticostriatal responses: an experimental and modeling study. Cell Mol Neurobiol 29:719–731.

Flores-Barrera E, Vizcarra-Chacón BJ, Bargas J, Tapia D, Galarraga E (2011) Dopaminergic modulation of corticostriatal responses in medium spiny projection neurons from direct and indirect pathways. Front Syst Neurosci 5:15.

Foehring RC, Mermelstein PG, Song WJ, Ulrich S, Surmeier DJ (2000) Unique properties of R-type calcium currents in neocortical and neostriatal neurons. J Neurophysiol 84:2225–2236.

Freund TF, Powell JF, Smith AD (1984) Tyrosine hydroxylase-immunoreactive boutons in synaptic contact with identified striatonigral neurons, with particular reference to dendritic spines. Neuroscience 13:1189–1215.

Gage GJ, Stoetzner CR, Wiltschko AB, Berke JD (2010) Selective activation of striatal fast-spiking interneurons during choice execution. Neuron 67:466–479.

Galarreta M, Hestrin S (2002) Electrical and chemical synapses among parvalbumin fast-spiking GABAergic interneurons in adult mouse neocortex. Proc Natl Acad Sci U S A 99:12438–12443.

Gertler TS, Chan CS, Surmeier DJ (2008a) Dichotomous anatomical properties of adult striatal medium spiny neurons. J Neurosci Off J Soc Neurosci 28:10814–10824.

Gertler TS, Chan CS, Surmeier DJ (2008b) Dichotomous anatomical properties of adult striatal medium spiny neurons. J Neurosci Off J Soc Neurosci 28:10814–10824.

Gittis AH, Hang GB, LaDow ES, Shoenfeld LR, Atallah BV, Finkbeiner S, Kreitzer AC (2011a) Rapid target-specific remodeling of fast-spiking inhibitory circuits after loss of dopamine. Neuron 71:858–868.

Gittis AH, Leventhal DK, Fensterheim BA, Pettibone JR, Berke JD, Kreitzer AC (2011b) Selective inhibition of striatal fast-spiking interneurons causes dyskinesias. J Neurosci Off J Soc Neurosci 31:15727–15731.

Gittis AH, Nelson AB, Thwin MT, Palop JJ, Kreitzer AC (2010) Distinct roles of GABAergic interneurons in the regulation of striatal output pathways. J Neurosci Off J Soc Neurosci 30:2223–2234.

Goldberg JA, Boraud T, Maraton S, Haber SN, Vaadia E, Bergman H (2002) Enhanced synchrony among primary motor cortex neurons in the 1-methyl-4-phenyl-1,2,3,6-tetrahydropyridine primate model of Parkinson's disease. J Neurosci Off J Soc Neurosci 22:4639–4653.

Goldberg JA, Teagarden MA, Foehring RC, Wilson CJ (2009) Nonequilibrium calcium dynamics regulate the autonomous firing pattern of rat striatal cholinergic interneurons. J Neurosci Off J Soc Neurosci 29:8396–8407.

Graupner M, Brunel N (2012) Calcium-based plasticity model explains sensitivity of synaptic changes to spike pattern, rate, and dendritic location. Proc Natl Acad Sci 109:3991–3996.

Gray CM (1994) Synchronous oscillations in neuronal systems: mechanisms and functions. J Comput Neurosci 1:11–38.

Gruber AJ, Solla SA, Surmeier DJ, Houk JC (2003) Modulation of striatal single units by expected reward: a spiny neuron model displaying dopamine-induced bistability. J Neurophysiol 90:1095–1114.

Harris KD, Thiele A (2011) Cortical state and attention. Nat Rev Neurosci 12:509–523.

Hawes SL, Evans RC, Unruh BA, Benkert EE, Gillani F, Dumas TC, Blackwell KT (In Press) Multi-modal plasticity in dorsal striatum while learning a lateralized navigation task. J Neurosci.

Hawes SL, Gillani F, Evans RC, Benkert EA, Blackwell KT (2013) Sensitivity to theta-burst timing permits LTP in dorsal striatal adult brain slice. J Neurophysiol 110:2027–2036.

Higley MJ, Sabatini BL (2010) Competitive regulation of synaptic Ca2+ influx by D2 dopamine and A2A adenosine receptors. Nat Neurosci 13:958–966.

Hikosaka O, Takikawa Y, Kawagoe R (2000) Role of the basal ganglia in the control of purposive saccadic eye movements. Physiol Rev 80:953–978.

Hjorth J, Blackwell KT, Kotaleski JH (2009a) Gap junctions between striatal fast-spiking interneurons regulate spiking activity and synchronization as a function of cortical activity. J Neurosci Off J Soc Neurosci 29:5276–5286.

Hjorth J, Blackwell KT, Kotaleski JH (2009b) Gap junctions between striatal fast-spiking interneurons regulate spiking activity and synchronization as a function of cortical activity. J Neurosci Off J Soc Neurosci 29:5276–5286.

Humphries MD, Wood R, Gurney K (2009) Dopamine-modulated dynamic cell assemblies generated by the GABAergic striatal microcircuit. Neural Netw Off J Int Neural Netw Soc 22:1174–1188.

Hutchison WD, Dostrovsky JO, Walters JR, Courtemanche R, Boraud T, Goldberg J, Brown P (2004) Neuronal Oscillations in the Basal Ganglia and Movement Disorders: Evidence from Whole Animal and Human Recordings. J Neurosci 24:9240–9243.

Ikarashi Y, Takahashi A, Ishimaru H, Arai T, Maruyama Y (1997) Regulation of Dopamine D1 and D2 Receptors on Striatal Acetylcholine Release in Rats. Brain Res Bull 43:107–115.

Jáidar O, Carrillo-Reid L, Hernández A, Drucker-Colín R, Bargas J, Hernández-Cruz A (2010) Dynamics of the Parkinsonian Striatal Microcircuit: Entrainment into a Dominant Network State. J Neurosci 30:11326–11336.

Jin X, Tecaupetla F, Costa R (2011) Distinct activity in the basal ganglia direct vs. indirect pathways during the learning and performance of ultrafast action sequences. Soc Neurosci Abstr 811.20/RR11.

Kasai H, Neher E (1992) Dihydropyridine-sensitive and omega-conotoxin-sensitive calcium channels in a mammalian neuroblastoma-glioma cell line. J Physiol 448:161–188.

Kerr JND, Plenz D (2002) Dendritic calcium encodes striatal neuron output during up-states. J Neurosci Off J Soc Neurosci 22:1499–1512.

Kerr JND, Plenz D (2004) Action potential timing determines dendritic calcium during striatal up-states. J Neurosci Off J Soc Neurosci 24:877–885.

Kerr JN, Wickens JR (2001) Dopamine D-1/D-5 receptor activation is required for long-term potentiation in the rat neostriatum in vitro. J Neurophysiol 85:117–124.

Kish LJ, Palmer MR, Gerhardt GA (1999) Multiple single-unit recordings in the striatum of freely moving animals: effects of apomorphine and D-amphetamine in normal and unilateral 6-hydroxydopamine-lesioned rats. Brain Res 833:58–70.

Kita H (1996) Glutamatergic and GABAergic postsynaptic responses of striatal spiny neurons to intrastriatal and cortical stimulation recorded in slice preparations. Neuroscience 70:925–940.

Kita H, Kosaka T, Heizmann CW (1990) Parvalbumin-immunoreactive neurons in the rat neostriatum: a light and electron microscopic study. Brain Res 536:1–15.

Koch C, Zador A (1993) The function of dendritic spines: devices subserving biochemical rather than electrical compartmentalization. J Neurosci Off J Soc Neurosci 13:413–422.

Koester HJ, Sakmann B (1998) Calcium dynamics in single spines during coincident pre- and postsynaptic activity depend on relative timing of back-propagating action potentials and subthreshold excitatory postsynaptic potentials. Proc Natl Acad Sci 95:9596–9601.

Koós T, Tepper JM (1999) Inhibitory control of neostriatal projection neurons by GABAergic interneurons. Nat Neurosci 2:467–472.

Koós T, Tepper JM (2002) Dual cholinergic control of fast-spiking interneurons in the neostriatum. J Neurosci Off J Soc Neurosci 22:529–535.

Koos T, Tepper JM, Wilson CJ (2004a) Comparison of IPSCs evoked by spiny and fast-spiking neurons in the neostriatum. J Neurosci Off J Soc Neurosci 24:7916–7922.

Koos T, Tepper JM, Wilson CJ (2004b) Comparison of IPSCs evoked by spiny and fast-spiking neurons in the neostriatum. J Neurosci Off J Soc Neurosci 24:7916–7922.

Kotaleski JH, Plenz D, Blackwell KT (2006a) Using potassium currents to solve signal-to-noise problems in inhibitory feedforward networks of the striatum. J Neurophysiol 95:331–341.

Kotaleski JH, Plenz D, Blackwell KT (2006b) Using potassium currents to solve signal-to-noise problems in inhibitory feedforward networks of the striatum. J Neurophysiol 95:331–341.

Kravitz AV, Freeze BS, Parker PRL, Kay K, Thwin MT, Deisseroth K, Kreitzer AC (2010) Regulation of parkinsonian motor behaviours by optogenetic control of basal ganglia circuitry. Nature 466:622–626.

Kreitzer AC (2009) Physiology and pharmacology of striatal neurons. Annu Rev Neurosci 32:127–147.

Kreitzer AC, Malenka RC (2007) Endocannabinoid-mediated rescue of striatal LTD and motor deficits in Parkinson's disease models. Nature 445:643–647.

Kreitzer AC, Malenka RC (2008) Striatal plasticity and basal ganglia circuit function. Neuron 60:543–554.

Krüger J, Aiple F (1988) Multimicroelectrode investigation of monkey striate cortex: spike train correlations in the infragranular layers. J Neurophysiol 60:798–828.

Kumar A, Mehta MR (2011) Frequency-Dependent Changes in NMDAR-Dependent Synaptic Plasticity. Front Comput Neurosci 5:38.

Lau T, Gage GJ, Berke JD, Zochowski M (2010) Local dynamics of gap-junction-coupled interneuron networks. Phys Biol 7:16015.

Logan SM, Partridge JG, Matta JA, Buonanno A, Vicini S (2007) Long-lasting NMDA receptor-mediated EPSCs in mouse striatal medium spiny neurons. J Neurophysiol 98:2693–2704.

López-Huerta VG, Carrillo-Reid L, Galarraga E, Tapia D, Fiordelisio T, Drucker-Colin R, Bargas J (2013) The Balance of Striatal Feedback Transmission Is Disrupted in a Model of Parkinsonism. J Neurosci 33:4964–4975.

Lovinger DM, Mathur BN (2012) Endocannabinoids in striatal plasticity. Parkinsonism Relat Disord 18 Suppl 1:S132–S134.

Magee JC, Johnston D (1997) A synaptically controlled, associative signal for Hebbian plasticity in hippocampal neurons. Science 275:209–213.

Mahon S, Deniau J-M, Charpier S (2004) Corticostriatal plasticity: life after the depression. Trends Neurosci 27:460–467.

Mahon S, Vautrelle N, Pezard L, Slaght SJ, Deniau J-M, Chouvet G, Charpier S (2006) Distinct Patterns of Striatal Medium Spiny Neuron Activity during the Natural Sleep–Wake Cycle. J Neurosci 26:12587–12595.

Mallet N, Ballion B, Le Moine C, Gonon F (2006) Cortical inputs and GABA interneurons imbalance projection neurons in the striatum of parkinsonian rats. J Neurosci Off J Soc Neurosci 26:3875–3884.

Mallet N, Micklem BR, Henny P, Brown MT, Williams C, Bolam JP, Nakamura KC, Magill PJ (2012a) Dichotomous organization of the external globus pallidus. Neuron 74:1075–1086.

Mallet N, Micklem BR, Henny P, Brown MT, Williams C, Bolam JP, Nakamura KC, Magill PJ (2012b) Dichotomous Organization of the External Globus Pallidus. Neuron 74:1075–1086.

Mallet N, Pogosyan A, Márton LF, Bolam JP, Brown P, Magill PJ (2008) Parkinsonian beta oscillations in the external globus pallidus and their relationship with subthalamic nucleus activity. J Neurosci Off J Soc Neurosci 28:14245–14258.

Markram H, Lübke J, Frotscher M, Sakmann B (1997) Regulation of synaptic efficacy by coincidence of postsynaptic APs and EPSPs. Science 275:213–215.

McCarthy MM, Moore-Kochlacs C, Gu X, Boyden ES, Han X, Kopell N (2011) Striatal origin of the pathologic beta oscillations in Parkinson's disease. Proc Natl Acad Sci 108:11620–11625.

McNaughton NC, Randall AD (1997) Electrophysiological properties of the human N-type Ca2+ channel: I. Channel gating in Ca2+, Ba2+ and Sr2+ containing solutions. Neuropharmacology 36:895–915.

McRory JE, Santi CM, Hamming KS, Mezeyova J, Sutton KG, Baillie DL, Stea A, Snutch TP (2001) Molecular and functional characterization of a family of rat brain T-type calcium channels. J Biol Chem 276:3999–4011.

Mercuri NB, Calabresi P, Stefani A, Stratta F, Bernardi G (1991) GABA depolarizes neurons in the rat striatum: an in vivo study. Synap N Y N 8:38–40.

Michelson HB, Wong RK (1994) Synchronization of inhibitory neurones in the guinea-pig hippocampus in vitro. J Physiol 477 (Pt 1):35–45.

Moyer JT, Wolf JA, Finkel LH (2007a) Effects of dopaminergic modulation on the integrative properties of the ventral striatal medium spiny neuron. J Neurophysiol 98:3731–3748.

Moyer JT, Wolf JA, Finkel LH (2007b) Effects of dopaminergic modulation on the integrative properties of the ventral striatal medium spiny neuron. J Neurophysiol 98:3731–3748.

Neely MD, Schmidt DE, Deutch AY (2007) Cortical regulation of dopamine depletion-induced dendritic spine loss in striatal medium spiny neurons. Neuroscience 149:457–464.

Nicola SM, Surmeier J, Malenka RC (2000) Dopaminergic modulation of neuronal excitability in the striatum and nucleus accumbens. Annu Rev Neurosci 23:185–215.

Nimmrich V, Maier N, Schmitz D, Draguhn A (2005) Induced sharp wave-ripple complexes in the absence of synaptic inhibition in mouse hippocampal slices. J Physiol 563:663–670.

Nisenbaum ES, Wilson CJ (1995) Potassium currents responsible for inward and outward rectification in rat neostriatal spiny projection neurons. J Neurosci Off J Soc Neurosci 15:4449–4463.

Obeso JA, Rodriguez-Oroz M, Marin C, Alonso F, Zamarbide I, Lanciego JL, Rodriguez-Diaz M (2004) The origin of motor fluctuations in Parkinson's disease: importance of dopaminergic innervation and basal ganglia circuits. Neurology 62:S17–S30.

Ogata N, Tatebayashi H (1990) Sodium current kinetics in freshly isolated neostriatal neurones of the adult guinea pig. Pflüg Arch Eur J Physiol 416:594–603.

Olson PA, Tkatch T, Hernandez-Lopez S, Ulrich S, Ilijic E, Mugnaini E, Zhang H, Bezprozvanny I, Surmeier DJ (2005) G-protein-coupled receptor modulation of striatal CaV1.3 L-type Ca2+ channels is dependent on a Shank-binding domain. J Neurosci Off J Soc Neurosci 25:1050–1062.

Oorschot DE, Lin N, Cooper BH, Reynolds JNJ, Sun H, Wickens JR (2010) Local connectivity between rat striatal spiny projection neurons: A three-dimensional ultrastructural study of somal innervation. In, pp 114. New Jersey.

Paille V, Fino E, Du K, Morera-Herreras T, Perez S, Kotaleski JH, Venance L (2013) GABAergic circuits control spike-timing-dependent plasticity. J Neurosci Off J Soc Neurosci 33:9353–9363.

Pawlak V, Kerr JND (2008) Dopamine receptor activation is required for corticostriatal spike-timing-dependent plasticity. J Neurosci Off J Soc Neurosci 28:2435–2446.

Planert H, Szydlowski SN, Hjorth JJJ, Grillner S, Silberberg G (2010) Dynamics of synaptic transmission between fast-spiking interneurons and striatal projection neurons of the direct and indirect pathways. J Neurosci Off J Soc Neurosci 30:3499–3507.

Plenz D (2003) When inhibition goes incognito: feedback interaction between spiny projection neurons in striatal function. Trends Neurosci 26:436–443.

Plenz D, Kitai ST (1998) Regulation of the nigrostriatal pathway by metabotropic glutamate receptors during development. J Neurosci Off J Soc Neurosci 18:4133–4144.

Plenz D, Kital ST (1999) A basal ganglia pacemaker formed by the subthalamic nucleus and external globus pallidus. Nature 400:677–682.

Plotkin JL, Day M, Surmeier DJ (2011) Synaptically driven state transitions in distal dendrites of striatal spiny neurons. Nat Neurosci 14:881–888.

Ponzi A, Wickens J (2010) Sequentially switching cell assemblies in random inhibitory networks of spiking neurons in the striatum. J Neurosci Off J Soc Neurosci 30:5894–5911.

Popescu AT, Saghyan AA, Paré D (2007) NMDA-dependent facilitation of corticostriatal plasticity by the amygdala. Proc Natl Acad Sci 104:341–346.

Ramanathan S, Hanley JJ, Deniau J-M, Bolam JP (2002) Synaptic convergence of motor and somatosensory cortical afferents onto GABAergic interneurons in the rat striatum. J Neurosci Off J Soc Neurosci 22:8158–8169.

Riehle A, Grammont F, Diesmann M, Grün S (2000) Dynamical changes and temporal precision of synchronized spiking activity in monkey motor cortex during movement preparation. J Physiol Paris 94:569–582.

Riehle A, Grün S, Diesmann M, Aertsen A (1997) Spike synchronization and rate modulation differentially involved in motor cortical function. Science 278:1950–1953.

Rivera A, Alberti I, Martín AB, Narváez JA, de la Calle A, Moratalla R (2002) Molecular phenotype of rat striatal neurons expressing the dopamine D5 receptor subtype. Eur J Neurosci 16:2049–2058.

Rivlin-Etzion M, Ritov Y, Heimer G, Bergman H, Bar-Gad I (2006) Local shuffling of spike trains boosts the accuracy of spike train spectral analysis. J Neurophysiol 95:3245–3256.

Rubin JE, Gerkin RC, Bi G-Q, Chow CC (2005) Calcium time course as a signal for spike-timing-dependent plasticity. J Neurophysiol 93:2600–2613.

Russo G, Nieus TR, Maggi S, Taverna S (2013) Dynamics of action potential firing in electrically connected striatal fast-spiking interneurons. Front Cell Neurosci 7 Available at: http://www.ncbi.nlm.nih.gov/pmc/articles/PMC3827583/ [Accessed February 16, 2014].

Sciamanna G, Wilson CJ (2011) The ionic mechanism of gamma resonance in rat striatal fast-spiking neurons. J Neurophysiol 106:2936–2949.

Shen W, Flajolet M, Greengard P, Surmeier DJ (2008) Dichotomous Dopaminergic Control of Striatal Synaptic Plasticity. Science 321:848–851.

Shen W, Hernandez-Lopez S, Tkatch T, Held JE, Surmeier DJ (2004) Kv1.2-containing K+ channels regulate subthreshold excitability of striatal medium spiny neurons. J Neurophysiol 91:1337–1349.

Shindou T, Ochi-Shindou M, Wickens JR (2011) A Ca2+ Threshold for Induction of Spike-Timing-Dependent Depression in the Mouse Striatum. J Neurosci 31:13015–13022.

Shouval HZ, Bear MF, Cooper LN (2002) A unified model of NMDA receptor-dependent bidirectional synaptic plasticity. Proc Natl Acad Sci U S A 99:10831–10836.

Spencer JP, Murphy KPSJ (2002) Activation of cyclic AMP-dependent protein kinase is required for long-term enhancement at corticostriatal synapses in rats. Neurosci Lett 329:217–221.

Spiga S, Lintas A, Migliore M, Diana M (2010) Altered architecture and functional consequences of the mesolimbic dopamine system in cannabis dependence. Addict Biol 15:266–276.

Steephen JE, Manchanda R (2009) Differences in biophysical properties of nucleus accumbens medium spiny neurons emerging from inactivation of inward rectifying potassium currents. J Comput Neurosci 27:453–470.

Stephens B, Mueller AJ, Shering AF, Hood SH, Taggart P, Arbuthnott GW, Bell JE, Kilford L, Kingsbury AE, Daniel SE, Ingham CA (2005) Evidence of a breakdown of corticostriatal connections in Parkinson's disease. Neuroscience 132:741–754.

Stern EA, Jaeger D, Wilson CJ (1998) Membrane potential synchrony of simultaneously recorded striatal spiny neurons in vivo. Nature 394:475–478.

Surmeier DJ, Ding J, Day M, Wang Z, Shen W (2007) D1 and D2 dopamine-receptor modulation of striatal glutamatergic signaling in striatal medium spiny neurons. Trends Neurosci 30:228–235.

Surmeier DJ, Song WJ, Yan Z (1996) Coordinated expression of dopamine receptors in neostriatal medium spiny neurons. J Neurosci Off J Soc Neurosci 16:6579–6591.

Taverna S, Ilijic E, Surmeier DJ (2008) Recurrent collateral connections of striatal medium spiny neurons are disrupted in models of Parkinson's disease. J Neurosci Off J Soc Neurosci 28:5504–5512.

Tecuapetla F, Carrillo-Reid L, Bargas J, Galarraga E (2007) Dopaminergic modulation of short-term synaptic plasticity at striatal inhibitory synapses. Proc Natl Acad Sci U S A 104:10258–10263.

Tecuapetla F, Koós T, Tepper JM, Kabbani N, Yeckel MF (2009) Differential dopaminergic modulation of neostriatal synaptic connections of striatopallidal axon collaterals. J Neurosci Off J Soc Neurosci 29:8977–8990.

Tepper JM, Koós T, Wilson CJ (2004) GABAergic microcircuits in the neostriatum. Trends Neurosci 27:662–669.

Tepper JM, Lee CR (2007) GABAergic control of substantia nigra dopaminergic neurons. In: Progress in Brain Research (James M. Tepper EDA and JPB, ed), pp 189–208. Elsevier. Available at: http://www.sciencedirect.com/science/article/pii/S0079612306600113 [Accessed August 5, 2013].

Tkatch T, Baranauskas G, Surmeier DJ (2000) Kv4.2 mRNA abundance and A-type K(+) current amplitude are linearly related in basal ganglia and basal forebrain neurons. J Neurosci Off J Soc Neurosci 20:579–588.

Traub RD, Kopell N, Bibbig A, Buhl EH, LeBeau FE, Whittington MA (2001) Gap junctions between interneuron dendrites can enhance synchrony of gamma oscillations in distributed networks. J Neurosci Off J Soc Neurosci 21:9478–9486.

Trevitt JT, Morrow J, Marshall JF (2005) Dopamine manipulation alters immediate-early gene response of striatal parvalbumin interneurons to cortical stimulation. Brain Res 1035:41–50.

Tseng KY, Kasanetz F, Kargieman L, Riquelme LA, Murer MG (2001) Cortical Slow Oscillatory Activity Is Reflected in the Membrane Potential and Spike Trains of Striatal Neurons in Rats with Chronic Nigrostriatal Lesions. J Neurosci 21:6430–6439.

Ts'o DY, Gilbert CD (1988) The organization of chromatic and spatial interactions in the primate striate cortex. J Neurosci Off J Soc Neurosci 8:1712–1727.

Tuckwell HC (2012) Quantitative aspects of L-type Ca2+ currents. Prog Neurobiol 96:1–31.

Tunstall MJ, Oorschot DE, Kean A, Wickens JR (2002) Inhibitory interactions between spiny projection neurons in the rat striatum. J Neurophysiol 88:1263–1269.

Turrigiano G (2012) Homeostatic synaptic plasticity: local and global mechanisms for stabilizing neuronal function. Cold Spring Harb Perspect Biol 4:a005736.

Wall NR, De La Parra M, Callaway EM, Kreitzer AC (2013) Differential Innervation of Direct- and Indirect-Pathway Striatal Projection Neurons. Neuron 79:347–360.

Walsh JP (1993) Depression of excitatory synaptic input in rat striatal neurons. Brain Res 608:123–128.

Wang Z, Kai L, Day M, Ronesi J, Yin HH, Ding J, Tkatch T, Lovinger DM, Surmeier DJ (2006) Dopaminergic control of corticostriatal long-term synaptic depression in medium spiny neurons is mediated by cholinergic interneurons. Neuron 50:443–452.

Whittington MA, Traub RD (2003) Interneuron diversity series: inhibitory interneurons and network oscillations in vitro. Trends Neurosci 26:676–682.

Wilson CJ (1986) Postsynaptic potentials evoked in spiny neostriatal projection neurons by stimulation of ipsilateral and contralateral neocortex. Brain Res 367:201–213.

Wilson CJ (2005) The mechanism of intrinsic amplification of hyperpolarizations and spontaneous bursting in striatal cholinergic interneurons. Neuron 45:575–585.

Wilson CJ, Chang HT, Kitai ST (1990) Firing patterns and synaptic potentials of identified giant aspiny interneurons in the rat neostriatum. J Neurosci 10:508–519.

Wilson CJ, Goldberg JA (2006) Origin of the slow afterhyperpolarization and slow rhythmic bursting in striatal cholinergic interneurons. J Neurophysiol 95:196–204.

Wilson CJ, Kawaguchi Y (1996) The origins of two-state spontaneous membrane potential fluctuations of neostriatal spiny neurons. J Neurosci Off J Soc Neurosci 16:2397–2410.

Wolf JA, Moyer JT, Lazarewicz MT, Contreras D, Benoit-Marand M, O'Donnell P, Finkel LH (2005) NMDA/AMPA ratio impacts state transitions and entrainment to oscillations in a computational model of the nucleus accumbens medium spiny projection neuron. J Neurosci Off J Soc Neurosci 25:9080–9095.

Yagishita S, Hayashi-Takagi A, Ellis-Davies GCR, Urakubo H, Ishii S, Kasai H (2014) A critical time window for dopamine actions on the structural plasticity of dendritic spines. Science 345:1616–1620.

Yim MY, Aertsen A, Kumar A (2011) Significance of input correlations in striatal function. PLoS Comput Biol 7:e1002254.

Yin HH, Mulcare SP, Hilário MRF, Clouse E, Holloway T, Davis MI, Hansson AC, Lovinger DM, Costa RM (2009) Dynamic reorganization of striatal circuits during the acquisition and consolidation of a skill. Nat Neurosci 12:333–341.

Zheng T, Wilson CJ (2002) Corticostriatal Combinatorics: The Implications of Corticostriatal Axonal Arborizations. J Neurophysiol 87:1007–1017.

BIOGRAPHY

Sriraman Damodaran graduated from MES Indian School in Doha, Qatar, in June 2004. He received his Bachelor of Science with distinction from Purdue University, West Lafayette, IN in December 2007 with a major in Electrical Engineering (specialization: Nanoelectronics). He started the Ph.D. program in neuroscience in September 2008.

Damodaran S, Evans RC, Blackwell KT (2013) Striatal models: Cellular Detail, *Encyclopedia of Computational Neuroscience*. *SpringerReference*, *ISBN: 978-1-4614-7320-6*. Eds. Dieter Jaeger and Ranu Jung.

Damodaran S, Evans RC, Blackwell KT (2014) Synchronized firing of fast-spiking interneurons is critical for maintaining balance between direct and indirect pathways of striatum. *J. Neurophysiol 111:835-848*

Damodaran S, Cressman JR, Jedrzejewski-Szmek, Blackwell KT (**in press**) Desynchronization of fast-spiking interneurons reduces β-band oscillations and imbalance in firing in the dopamine-depleted striatum. *J. Neurosci*

Damodaran S, Blackwell KT (2014) Calcium dynamics predicts direction of synaptic plasticity in striatal spiny projection neurons. *In preparation*

Damodaran S, Senft S, Ascoli GA (2012) Neuron Atlas: An application for browsing neuronal reconstructions on Neuromorpho.org. http://neuromorpho.org/neuroMorpho/LS_Video.jsp